DESIGN OF WIDE-AREA DAMPING CONTROL SYSTEMS FOR POWER SYSTEM LOW-FREQUENCY INTER-AREA OSCILLATIONS

By

YANG ZHANG

A dissertation submitted in partial fulfillment of
the requirements for the degree of

DOCTOR OF PHILOSOPHY IN ELECTRICAL ENGINEERING

WASHINGTON STATE UNIVERSITY
School of Electrical Engineering and Computer Science

DECEMBER 2007

To the Faculty of Washington State University:

The members of the Committee appointed to examine the dissertation of YANG ZHANG find it satisfactory and recommend that it be accepted.

_____
Chair

_____

_____

ACKNOWLEDGMENT

I would like to express my deepest gratitude to my academic and research advisor Dr. Anjan Bose for his guidance and constant support in helping me to conduct and complete this work. His firm grasps and forte on all diverse areas of power systems ensured a steady stream of ideas that spawns gateways for solving the problems at hand. He has been a great source of inspiration and I am his student forever.

I would also like to express my appreciation to the members of my committee Dr. Kevin Tomsovic, and Dr. Venkatasubramanian Mani for all their supports and useful feedback during my research. Their lectures on the advanced topics of power system laid a solid foundation for my research.

I also want to thank all the power group members. The healthy academic environment provided by the students at the Power Lab always sparks my interest to learn more. Special thanks go to Sanjoy Kumar Sarawgi, Guoping Liu, Hui Yuan, Sudipto Bhowmik, and Dr. Yi Zhang.

I owe my sincere appreciation to my family and relatives who have been a constant support and encouragement. I want to extend my profound appreciation to my wife for her love, affection, invaluable support and sacrifice during my life and studies.

This work was partially supported by the Consortium of Electric Reliability Technology Solutions (CERTS) and the Power Systems Engineering Research Center (PSERC). I sincerely acknowledge the financial support extended to this project by the sponsors.

DESIGN OF WIDE-AREA DAMPING CONTROL SYSTEMS FOR POWER SYSTEM LOW-FREQUENCY INTER-AREA OSCILLATIONS

Abstract

by Yang Zhang, Ph.D.
Washington State University
December 2007

Chair: Anjan Bose

The recently developed robust control theories and wide-area measurement technologies make the wide-area real-time feedback control potentially promising. The objective of this research is to develop a systematic procedure of designing a centralized damping control system for power grid inter-area oscillations by applying wide-area measurement and robust control techniques while putting emphasis on several practical considerations.

The first consideration is the selection of stabilizing signals. Geometric measures of controllability/observability are used to select the most effective stabilizing signals and control sites. Line power flows and currents are found to be the most effective input signals. The second consideration is the effects of time-delay in the communication of input/output signals. Time-delays reduce the efficiency of the damping control system. In some cases, large delays can destabilize the system. Time-delays should be modeled in the controller design procedure so that the resulting controller can handle a range of time-delays. In this work, time-delays are modeled by Padé Approximations and the delay uncertainty is described by Linear Fractional Transformations (LFT). The third

consideration is the controller robustness. The synthesis of the controller is defined as a problem of mixed $H_2/H\infty$ output-feedback control with regional pole placement and is resolved by the Linear Matrix Inequality (LMI) approach. The controller designed by robust control techniques has satisfactory performance in a wide range of operating points. The fourth consideration is the efficiency of the controller designed by linear techniques in realistic nonlinear discrete environments. A tuning process and nonlinear simulations are used to modify the controller parameters to ensure the performance and robustness of the controller designed with linear techniques. The last consideration is the selection of PMU data reporting rates. The performance of controllers designed in the *s*-domain is tested in digital environments and proper PMU data reporting rates are selected with consideration of the effects of time-delay.

The design procedure of wide-area damping systems is illustrated by three study systems. The first study system is a two-area four-machine system. The second one is the New England 39-bus 10-machine system. The last one is a 29-generator 179-bus study system, which is a reduced order model of the Western Electricity Coordinating Council (WECC) system.

Keywords: Damping controller, data reporting rate, $H\infty$ synthesis, LMI, PMU, inter-area oscillations, robust control, time-delay, wide-area.

TABLE OF CONTENTS

Page

LIST OF FIGURES

LIST OF TABLES

Chapter 1. Introduction

1.1 Motivation

Power systems contain many modes of oscillation as a consequence of interactions of its components, as for example one generator rotor swinging relative to another. There are two distinct types of oscillations which have presented problems in power systems, local mode oscillations and inter-area oscillations. Local mode oscillations occur when a generator (or group of generators) under voltage regulator control at a station is swinging against the rest of the system. Inter-area oscillations involve combinations of machines on one part of a system swinging against machines on another part of the system. The characteristic frequency of inter-area modes of oscillation is generally in the range of 0.1 to 1.0 Hz.

Local plant modes, control modes and torsional modes are usually induced by the interaction between the mechanical and electrical modes of a turbine-generator system. Inter-area modes may be caused by either high-gain exciters or heavy power transfers across weak tie-lines [1]. Large power systems typically exhibit multiple dominant inter-area swing modes, which are associated with the dynamics of power transfers and involve groups of machines oscillating relative to each other. When present in a power system, this type of oscillation limits the amount of power transfer on the tie-lines between the regions containing the groups of coherent generators [2]. With the increasing of the interconnections and inter-changes of energy in electrical networks, low-frequency inter-area oscillations become more poorly damped and power system oscillatory stability becomes more and more of concern. Large disturbances tend to induce inter-area

oscillations in major grids throughout the world: at 0.6 Hz in the Hydro-Québec system [44], 0.2 Hz in the western North-American interconnection [45], 0.15-0.25 Hz in Brazil [46] and 0.19-0.36 Hz in the UCTE/CENTREL interconnection in Europe [47]. The recent 2003 blackout in eastern Canada and US was accompanied by severe 0.4-Hz oscillations in several post-contingency stages [48]. Over the years, many incidents of system outage resulting from these oscillations have been reported. Following examples are some of system failures owing to oscillations:

a. In early 1960's, oscillations were observed when the Detroit Edison (DE), Ontario Hydro (OH) and Hydro-Québec (HQ) systems were inter-connected
b. In 1969, oscillations were observed under several operating conditions in the Finland-Sweden (and Norway)-Denmark interconnected system
c. In 1971 and 1972, over 70 incidents of unstable inter-area oscillations occurred in the Mid-Continent Area Power Pool (MAAP) system in North America
d. In 1975, unstable oscillations of 0.6 Hz were encountered on the interconnected power system of New South Wales and Victoria
e. In 1982 and 1983, the State Energy Commission of Western Australia (SECWA) experienced lightly damped system oscillations in the frequency range of 0.2-0.3 Hz
f. On August 10, 1996, the Pacific AC Inter-tie (PACI) in WECC experienced unstable low frequency inter-area oscillations following the outage of four 400 kV lines

The traditional approach to damp out inter-area oscillations is by installing power system stabilizers (PSS) that provide supplementary control action through the excitation system of generators. In recent years, supplementary modulation controllers (SMC) are added to

flexible ac transmission systems (FACTS) devices to damp out the inter-area oscillations. Both PSSs and FACTS SMC are single input single output (SISO) non-coordinated local controllers designed by conventional damping control design synthesis, for example a residue based method which considers a single operating condition of the system. These controllers usually use local inputs and cannot always be effective in easing the problem due to two main shortcomings. First, based on a linearization of the system model in a nominal operating point, conventional local controllers designed by the classical control techniques have their validity restricted to a neighborhood of this point. But power systems constantly experience changes in operating conditions due to variations in generation and load patterns, as well as changes in transmission networks. Even under nominal operating conditions, there is still some uncertainty present due to only an approximate knowledge of the power system parameters, neglected high frequency dynamics, or invalid assumptions made in the model formulation process. Second, local controllers lack global observation of inter-area modes. It has been proved that under certain operating conditions an inter-area mode may be controllable from one area and be observable from another [3]. In such cases, local controllers are not effective for the damping of that mode.

The recently developed wide-area control technologies and robust control theory offer a great potential to overcome the shortcomings of conventional local controllers. Robust control techniques have been applied to design controllers that formally guarantee the system stability with an acceptable performance for a wide range of operating conditions [4]-[7]. With the technology of global positioning system (GPS) based phasor

measurement units (PMU), dynamic data of power systems, such as voltage, current, angle, and frequency can be accurately measured, synchronized and transferred in the range of the whole power system by wide-area measurement systems (WAMS) [8, 9]. This makes possible the construction of wide-area damping control systems. In contrast to conventional local controls, wide-area damping control systems have many benefits. Reference [10] shows that wide-area controls are more efficient than local controls in preventing loss of synchronism and local controls need large gain (from 4 to 20 times more) than wide-area controls [11] to achieve a similar damping effect.

Even though promising simulation results achieved by researchers in applying robust and wide-area techniques into the design of damping control systems for inter-area oscillations, wide-area damping control is still in its infancy due to many difficulties in designing and implementing such systems. This research is motivated by the objectives of finding solutions to the difficulties in the design and implementation of wide-area damping control systems and thus improving the damping of power system low-frequency inter-area oscillations.

1.2 Literature Review on Wide-Area Damping Control for Power Systems

Many researchers achieved promising results from applying wide-area measurements and robust control techniques into wide-area control of power system oscillations.

A research group in Hydro-Québec has done significant work in the field of damping of inter-area oscillations. In reference [12], a decentralized/hierarchical structure with two-loop PSSs is proposed. Wide-area signals based PSS is used to provide additional damping to local ones. A sequential optimization procedure is used to tune the global and local loop of the proposed controller.

Reference [13] uses multi-agents concepts to coordinate several supervisor PSSs (SPSS) based on remote signals and exchanging information with local PSSs to improve power systems stability. The SPSS is designed by H_∞ optimization methods. Rule based fuzzy-logic and robust control techniques are used to deal with uncertainties introduced by nonlinear terms and operating conditions.

Reference [14] proposes a control structure that employs a combination of remote stabilizing signals with diverse modal contents to improve the observability and damping effects. It has shown that an optimum and weighted combination of local and global signals could successfully be used for the control design of PSS and TCSC.

A Remote Feedback Controller (RFC) design methodology using PMU measurements is presented in reference [15]. In a typical implementation, one or more of the generators in

a system are selected as RFC Controllers. The RFC Controller received synchronized phasor measurements from one or more remote phasor sources. The RFC Controller analyzes the phase angles from the multiple sites and determines if an inter-area oscillation exists. If an oscillation exists, a control signal is sent to the generator's voltage regulator that effectively modulates the voltage and effectively damps out the oscillations.

The research group in Washington State University designed a real time control system to enhance the small signal stability of power systems [16]. The proposed controller will initiate specific control actions only when it detects the emergence of poorly damped or negatively damped oscillatory modes in the power system being monitored. The controller is designed for real-time implementation in the large power systems by utilizing the wide-area measurements together with the heuristic control rules developed by offline studies. When the oscillatory instability is detected, the central controller switches the operation of a specific SVC from the normal voltage regulation mode into an aggressive power system damping control (PSDC) mode for damping out the oscillations.

Reference [17] demonstrates the enhancement of inter-area mode damping by multiple FACTS devices. Power system damping control design is formulated as an output disturbance rejection problem. A decentralized H_∞ damping control design based on the mixed-sensitivity formulation in the linear matrix inequality (LMI) framework is proposed.

1.3 Objective and Contributions

Wide-area damping control system is still in its infancy because many issues remain unresolved in the design and implementation of such systems. Some of them are listed as follows:

- Measurement types and locations – what kind of measurements are suitable for stabilizing signals? Where and how can these signals be measured?
- Control devices and locations – what devices should be controlled and what are best control sites?
- Control system structure – which structure is suitable, centralized or decentralized?
- Time-delay – How to design a controller that can handle a range of time-delay?
- System uncertainties – when designing a controller, how to deal with all kinds of uncertainties produced in the system modeling process?
- Digital communication and control techniques – what measurement speed and data-reporting rates are enough? Are digital communication and control techniques suitable for continuous feedback control?
- Measurement processing – error, corruption, loss, noise and aliasing;
- Controller design and implementation – how to design a controller to meet the robust and performance requirements for inter-area oscillations damping? How and where to implement such a controller?

The objective of this research is to propose a systematic procedure of designing a wide-area damping control system for power system inter-area oscillations, with particular

attention to several practical issues like time-delays, digital environment, and controller robustness. The contributions of this dissertation are:

1) Proposed a systematic procedure to design wide-area damping control systems with centralized architectures and shows that it is an effective way to damp out inter-area oscillations by providing remote measurements to the controller and control actions through generator excitation systems supplemental to the action of local PSSs.
2) Demonstrated that geometric measures of modal controllability/observability are effective in evaluating the comparative strength of candidate stabilizing signals of widely differing types with two numerical examples.
3) Demonstrated that mixed H_2/H_∞ output-feedback control with regional pole placement can be applied to the wide-area damping controller synthesis with good results which cannot be obtained by only using either one.
4) Shown the effects of time-delays on wide-area damping control systems and proposed a method to design a wide-area damping controller (WADC) that can handle time-delays.
5) Tested the robustness of the designed controller by evaluating the damping control system performance under different operating conditions and the system response to various disturbances using time domain simulation based on nonlinear power system models.
6) Shown that for the small size systems considered, one stabilizing signal is enough for the input of a wide-area damping controller. Multiple inputs improve the

control performance only slightly for such small systems but are expected to be necessary for acceptable control performance in large systems.

7) Established the effectiveness of controllers designed with continuous and linear techniques by testing in realistic nonlinear environments and with discrete (digital) communication of measurement and control signals.
8) Shown that the data reporting rates of PMUs should be chosen with consideration of time-delay effects.

1.4 Organization of This Dissertation

This dissertation consists of five chapters.

Chapter 1. Introduction describes the motivation, objectives and contributions. A literature review is also given in this chapter that summarizes others' work in the field of wide-area damping control for inter-area oscillations.

Chapter 2. Modeling gives the detailed power system component dynamic models and load models used in this research. Modal analysis of linearized models is outlined.

Chapter 3. Wide-Area Damping Control System Design describes a systematic procedure of designing damping controllers for low-frequency inter-area oscillations. The comparative strength of candidate wide-area measurements and the performance of controllers at different control sites are evaluated by geometric measures of controllability/observability. The synthesis of the robust controller is defined as a problem of mixed H_2/H_∞ output-feedback control with regional pole placement and is resolved by the LMI approach. Practical issues like time delays, digital environments and controller robustness are also discussed.

Chapter 4. Case Studies gives three design examples. The first one is a two-area four-machine system. The second study system is the New England 39-bus 10-machine system. The last one is a 179-bus 29-machine test system that is a reduced order model of the Western Electricity Coordinating Council (WECC) system.

Chapter 5. Conclusions and Future Work summarizes the findings of this research and lists several topics for the future work.

Chapter 2. Modeling

2.1 Power System Component Dynamic Model and Load Model

2.1.1 Synchronous Generator Model

Synchronous generators form the principal source of electric energy in power systems. The power system stability problem is largely one of keeping interconnected synchronous machines in synchronism. Therefore, an understanding of their characteristics and accurate modeling of their dynamic performance are of fundamental importance to the study of power system stability. In this thesis, a fourth-order (two-axis) model, as described in [18] has been used.

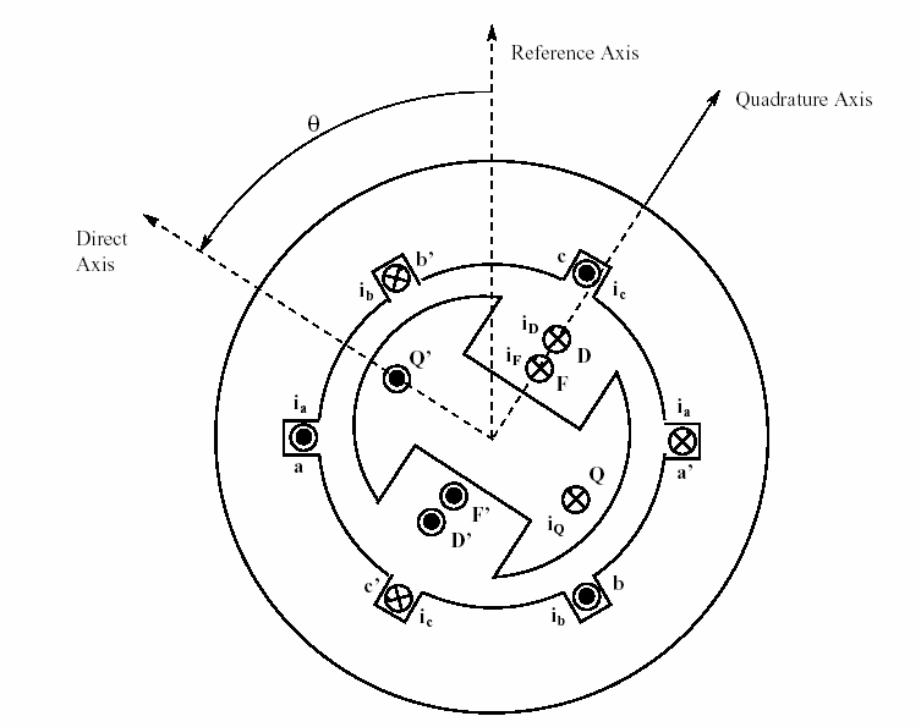

Fig. 2.1 Synchronous generator schematic diagram

The dynamic equations of the synchronous generator, which is shown in Fig.2.1, for the two-axis model can be stated as:

$$\dot{\delta} = (\omega - 1)\omega_s \tag{2.1}$$

$$2H\ \dot{\omega} = P_m - P_g - K_D(\omega - 1) \tag{2.2}$$

$$T'_{do}\ \dot{E}'_q = -E'_q - (x_d - x'_d)I_d + E_{fd} \tag{2.3}$$

$$T'_{qo}\ \dot{E}'_d = -E'_d + (x_q - x'_q)I_q \tag{2.4}$$

where

δ generator rotor angle;

ω generator rotor frequency in per unit;

E'_q internal quadrature-axis voltage;

E'_d internal direct-axis voltage;

E_{fd} exciter output;

H generator inertia constant;

P_m generator input mechanical power;

P_g generator output electrical power;

K_D damping coefficient;

T'_{do}, T'_{qo} direct and quadrature axis transient field winding time constants;

x_d, x'_d direct axis synchronous and transient reactances;

x_q, x'_q quadrature axis synchronous and transient reactances.

The equations relating the external bus quantities and the internal machine transformed (Park's) equations are:

$$V_d = V\sin(\delta - \theta) \tag{2.5}$$

$$V_q = V\cos(\delta - \theta) \tag{2.6}$$

$$P_g = V_d I_d + V_q I_q \tag{2.7}$$

$$Q_g = V_q I_d - V_d I_q \tag{2.8}$$

$$\begin{bmatrix} I_d \\ I_q \end{bmatrix} = \begin{bmatrix} R_a & -x_q' \\ x_d' & R_a \end{bmatrix}^{-1} \begin{bmatrix} E_d' - V\sin(\delta - \theta) \\ E_q' - V\cos(\delta - \theta) \end{bmatrix} \tag{2.9}$$

$$I_g^2 = I_d^2 + I_q^2 \tag{2.10}$$

$$V^2 = V_d^2 + V_q^2 \tag{2.11}$$

where

V, θ external bus voltage magnitude and phase;

P_g, Q_g generator internal real and reactive power injections;

R_a armature resistance;

V_d, V_q internal Park transformed components of terminal bus voltage V;

I_d, I_q internal Park transformed components of terminal bus current I_g.

Park's coordinate frame is rotating synchronously with the rotor. The effect of Park's transformation is simply to transform all stator quantities from phases *a, b* and *c* into new variables, the frame of reference of which moves with the rotor. This leads to great simplification in the mathematical description of the synchronous machine. The

transformation depends on the difference in phase $\delta - \theta$, between the terminal voltage and the internal rotor angle.

2.1.2 Exciter Model

The exciter model used in this study is the standard IEEE type DC1A exciter. Its block diagram is shown in Fig. 2.2.

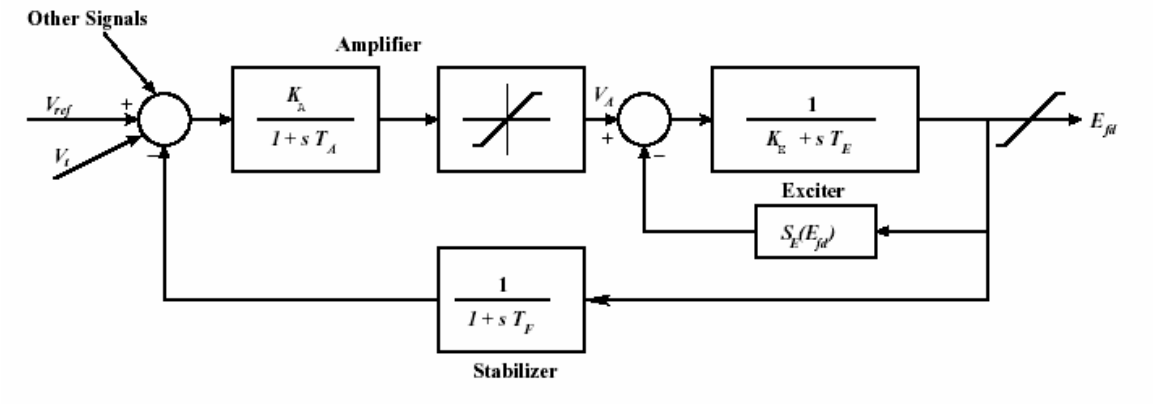

Fig. 2.2 IEEE DC1A exciter block diagram

This model is used to represent field controlled dc commutator exciters with continuously acting voltage regulators (especially the direct-acting rheostatic, rotating amplifier, and magnetic amplifier types). The exciter may be separately excited or self excited, the latter type being more common. When self excited (the voltage regulator operating in buck-boost mode), K_E is selected so that initially V_A=0.5 [1], representing operator action of tracking the voltage regulator by periodically trimming the shunt field rheostat set point. A value of K_E=1 is used to represent a separately excited exciter. The major time constant, T_A, and gain, K_A, associated with the voltage regulator are shown incorporating non-windup limits typical of saturation or amplifier power supply limitations. The

mathematical model representing the dynamics of this exciter is given by the following equations:

$$T_A \dot{V}_A = -V_A + K_A(V_{ref} - V - V_F - V_S) \tag{2.12}$$

$$T_E \dot{E}_{fd} = -K_E E_{fd} + V_A - S_{ex}(E_{fd}) E_{fd} \tag{2.13}$$

$$T_F \dot{V}_F = -V_F + K_F \dot{E}_{fd} \tag{2.14}$$

The term $S_{ex}(E_{fd})$ is a nonlinear function with a value defined at any chosen E_{fd}. The output of this saturation block, is the product of the input, E_{fd}, and the value of the nonlinear function, $S_{ex}(E_{fd})$, at this exciter voltage. V_S is a supplementary stabilizing signal from the power system stabilizer.

2.1.3 Governor Model

The prime mover provides the mechanism for controlling the synchronous machine speed and hence voltage frequency. In order to automatically control speed and frequency, a device must sense either speed or frequency in such a way that comparison with a desired value can be used to create an error signal to take corrective action. The block diagram of such a model for a time constant governor with speed regulation *R* is shown in Fig. 2.3:
The mathematical model of this governor is the following equation:

$$T_G \dot{P}_m = -P_m + P_{ref} - \frac{1}{R}(\omega - 1) \tag{2.15}$$

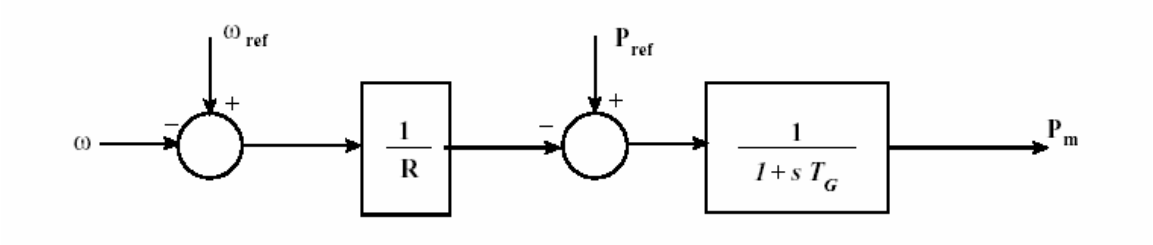

Fig. 2.3 Governor model block diagram

2.1.4 Power System Stabilizer Model

The basic function of a PSS is to add damping to the generator rotor oscillations by controlling its excitation using auxiliary stabilizing signals. A PSS is added to the automatic voltage regulator (AVR), which controls the generator stator terminal voltage. PSS uses stabilizing feedback signals such as shaft speed, terminal frequency and/or power to change the input signal of the AVR. Power system dynamic performance is improved by the damping of system oscillations. To provide damping, PSS must produce a component of electrical torque in phase with the rotor speed deviations. The basic blocks of a typical PSS with two phase compensation are illustrated in Fig. 2.4.

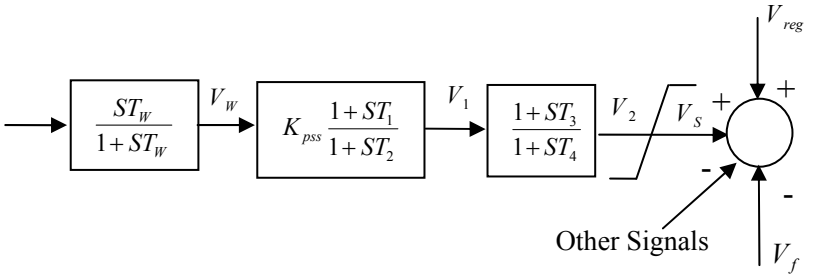

Fig. 2.4 Block diagram of power system stabilizer

The first is the gain block. The stabilizer gain K_{pss} determines the amount of damping introduced by the PSS. Ideally, the gain should be set at a value corresponding to maximum damping; however, it is often limited by other considerations. The second is signal washout block. It serves as a high-pass filter with the time constant T_W high enough to allow signals associated with oscillations in rotor speed to pass unchanged, but does not allow the steady state changes to modify the terminal voltages. It allows the PSS to respond only to changes in speed. The lead/lag phase compensation blocks provides the appreciate phase lead characteristic to compensate for the phase lag between the exciter input and the generator electrical (air-gap) torque. Normally, the frequency range of interest is 0.1 to 2.0 Hz, and the phase-lead network should provide compensation over this entire frequency range. Generally some under-compensation is desirable so that the PSS, in addition to significantly increasing the damping torque, results in a slight increase of the synchronizing torque. The differential equations describing a PSS shown in Fig.2.4 are:

$$T_W \dot{V}_W = -V_W + T_W \dot{\omega} \tag{2.16}$$

$$T_2 \dot{V}_1 = -V_1 + K_{pss}(V_W + T_1 \dot{V}_W) \tag{2.17}$$

$$T_4 \dot{V}_2 = -V_2 + (V_1 + T_3 \dot{V}_1) \tag{2.18}$$

2.1.5 Load Model

The modeling of loads in stability studies is a complex problem due to the unclear nature of aggregated loads (e.g. a mix of fluorescent, compact fluorescent, incandescent lamps,

refrigerators, heater, motor, etc.). Load models are typically classified into two broad categories: static and dynamic. The loads can be modeled using constant impedance, constant current and constant power static load models. Constant impedance load model is a static load model where the real and reactive power is proportional to the square of the voltage magnitude. It is also referred to as constant admittance load model. Constant current load model is a static load model where the real and reactive power is directly proportional to the voltage magnitude. Constant power load model is a static load model where the real and reactive powers have no relation to the voltage magnitude. It is also referred to as constant MVA load model. These load models can be described by the following polynomial equations [19]:

$$P_L = kP_0\left[A_1 + A_2\frac{V}{V_0} + A_3\left(\frac{V}{V_0}\right)^2\right] \tag{2.19}$$

$$Q_L = kQ_0\left[B_1 + B_2\frac{V}{V_0} + B_3\left(\frac{V}{V_0}\right)^2\right] \tag{2.20}$$

where $A_1 + A_2 + A_3 = B_1 + B_2 + B_3 = 1$; P_0 and Q_0, the so-called nominal powers, are the load real and reactive powers consumed under nominal conditions, i.e., at the reference voltage V_0 and the nominal frequency f_0. The actual or consumed load power P_L and Q_L are the powers consumed by the load under current conditions of voltage V and frequency f. Although the actual load in a system is usually frequency dependent, this frequency dependence is ignored in this study for simplicity. The value k is an independent demand variable called loading factor. Such a load model is often referred to as the ZIP load model.

2.2 Linearized State Space Model of Power Systems

The synchronous machine model along with the associated regulating devices thus becomes an eleventh-order model (eleven state variables for each synchronous machine). The dynamic states for this model are:

$$x_d = \begin{bmatrix} \delta & \omega & E_d^{'} & E_q^{'} & V_A & V_F & E_{fd} & V_W & V_1 & V_2 & P_m \end{bmatrix}^T$$

In the design proposed in this research, the control inputs to the system are additional wide-area stabilizing signals added to AVR. Then the control inputs are:

$$u = [u_1 \quad u_2 \quad ... \quad u_{ng}]$$

where *ng* is the number of globally controlled generators.

Thus, for the *i*th machine, the 11 differential equations describing its dynamics are:

$$\dot{\delta}_i = (\omega_i - 1)\omega_s \tag{2.21}$$

$$2H_i \dot{\omega}_i = P_{mi} - P_{gi} - K_{Di}(\omega_i - 1) \tag{2.22}$$

$$T_{doi}^{'} \dot{E}_{qi}^{'} = -E_{qi}^{'} - (x_{di} - x_{di}^{'})I_{di} + E_{fdi} \tag{2.23}$$

$$T_{qoi}^{'} \dot{E}_{di}^{'} = -E_{di}^{'} + (x_{qi} - x_{qi}^{'})I_{qi} \tag{2.24}$$

$$T_{Ai} \dot{V}_{Ai} = -V_{Ai} + K_{Ai}(V_{refi} - V_i - V_{Fi} - V_{Si} + u_i) \tag{2.25}$$

$$T_{Ei} \dot{E}_{fdi} = -K_{Ei}E_{fdi} + V_{Ai} - S_{exi}(E_{fdi})E_{fdi} \tag{2.26}$$

$$T_{Fi} \dot{V}_{Fi} = -V_{Fi} + K_{Fi} \dot{E}_{fdi} \tag{2.27}$$

$$T_{Gi}\dot{P}_{mi} = -P_{mi} + P_{refi} - \frac{1}{R_i}(\omega_i - 1) \tag{2.28}$$

$$T_{Wi}\dot{V}_{Wi} = -V_{Wi} + T_{Wi}\dot{\omega}_i \tag{2.29}$$

$$T_{2i}\dot{V}_{1i} = -V_{1i} + K_{pssi}(V_{Wi} + T_{1i}\dot{V}_{Wi}) \tag{2.30}$$

$$T_{4i}\dot{V}_{2i} = -V_{2i} + (V_{1i} + T_{3i}\dot{V}_{1i}) \tag{2.31}$$

For the bus *i*, the following power flow equations can be derived from (2.5)-(2.11):

$$P_{gi} - P_{Li} - P_i(x_d, x_a) = 0 \tag{2.32}$$

$$Q_{gi} - Q_{Li} - Q_i(x_d, x_a) = 0 \tag{2.33}$$

where x_a are bus voltage magnitudes and phase angles, which are algebraic variables; $P_i(x_d, x_a)$ is the active power injection, $Q_i(x_d, x_a)$ is the reactive power injection, P_{Li} and Q_{Li} are active and reactive loads, which are described with ZIP model. If there is no generators at bus *i*, P_{gi} and Q_{gi} are equal to zero.

Equation (2.21) – (2.31), together with equation (2.32) and (2.33) can be written as differential functions of x_d, x_a and *u* in the following form:

$$\begin{cases} \dot{x}_d = f(x_d, x_a, u) \\ 0 = g(x_d, x_a, u) \end{cases} \tag{2.34}$$

Equation (2.34) is called the DAE model of the power system dynamics.

Therefore, the full dynamic behavior of power system may be described by a set of nonlinear vector valued differential-algebraic equations:

$$\dot{x}_d = f(x_d, x_a, u) \tag{2.35}$$

$$0 = g(x_d, x_a, u) \tag{2.36}$$

$$y = h(x_d, x_a, u) \tag{2.37}$$

where x_d and x_a are the vectors of dynamic and algebraic variables respectively while *u* and *y* are vectors of the input and output variables. Equation (2.35) describes the dynamics of power system and equation (2.36) is in fact the power flow equations. (2.37) are equations of output variables described in terms of state variables and input variables.

According to the small signal theory, the dynamic behavior of power systems around an equilibrium point can be analyzed with a model linearized around this point. The linearized model is valid only in the neighborhood of the equilibrium point, that is, it's only valid for analyzing the dynamics of the system under small disturbances. Suppose the equilibrium point of the system is (x_d^0, x_a^0, u^0, y^0), then small deviations from the linearization point are: $\Delta x_d = x_d - x_d^0$, $\Delta x_a = x_a - x_a^0$, $\Delta u = u - u^0$, $\Delta y = y - y^0$.

A linear DAE model is obtained by partial differentiation of the nonlinear functions *f, g* and *h*:

$$\Delta \dot{x}_d = A_1 \Delta x_d + A_2 \Delta x_a + B_1 \Delta u \tag{2.38}$$

$$0 = A_3 \Delta x_d + A_4 \Delta x_a + B_2 \Delta u \tag{2.39}$$

$$\Delta y = C_1 \Delta x_d + C_2 \Delta x_a + D_1 \Delta u \tag{2.40}$$

where the Jacobian matrices are:

$$A_1 = \left[\frac{\partial f}{\partial x_d}\right],\ A_2 = \left[\frac{\partial f}{\partial x_a}\right],\ A_3 = \left[\frac{\partial g}{\partial x_d}\right],\ A_4 = \left[\frac{\partial g}{\partial x_a}\right],\ B_1 = \left[\frac{\partial f}{\partial u}\right],\ B_2 = \left[\frac{\partial g}{\partial u}\right]$$

$$C_1 = \left[\frac{\partial h}{\partial x_d}\right],\ C_2 = \left[\frac{\partial h}{\partial x_a}\right],\ D_1 = \left[\frac{\partial h}{\partial u}\right]$$

In the following, Δ is omitted as all linear equations use variables that denote deviations from the linearization point. Assuming that A_4 is invertible, then, the algebraic variables can be uniquely determined from (2.39):

$$x_a = -A_4^{-1}(A_3 \Delta x_d + B_2 \Delta u) \tag{2.41}$$

To eliminate algebraic variables in (2.38) and (2.40) by (2.41), we have the general form of linearized state space model of power systems, which is a set of ordinary differential equations (ODE):

$$\dot{x} = Ax + Bu \tag{2.42}$$

$$y = Cx + Du \tag{2.43}$$

Where x is the vector of system state variables, y is the vector of output variables. A is state matrix or the plant matrix, B is input matrix, C is output matrix and D is feedforward matrix.

$$A = A_1 - A_2 A_4^{-1} A_3$$

$$B = B_1 - A_2 A_4^{-1} B_2$$

$$C = C_1 - C_2 A_4^{-1} A_3$$

$$D = D_1 - C_2 A_4^{-1} B_2$$

While both the ODE and DAE descriptions can be considered as state space representations, control design methods known as state space methods predominantly handle only ODE models. An alternative to the state space approach is frequency domain methods based on transfer functions. Starting out from an ODE model, the corresponding set of transfer functions is defined as:

$$G(s) = \frac{Y(s)}{U(s)} = C(sI - A)^{-1} B + D \tag{2.44}$$

where s is the Laplace operator or complex frequency. Transfer functions are well suited for determining transfer function zeroes. An input signal having the frequency of a transfer function zero is blocked and will not affect the output. While being unique for SISO systems, the definition of transfer zeroes for multi-input-multi-output (MIMO) systems is less clear. As a transfer function maps inputs to outputs, it is very convenient when a model is to be based on measurements. Transfer functions carry magnitude and phase information of a signal path as a function of frequency which is used when selecting the proper phase shift of a controller.

2.3 Modal Analysis and Small Signal Stability

Once the state space system for the power system is written in the general form given by (2.42) and (2.43), the small signal stability of the system can be calculated and analyzed. First, the eigenvalues λ_i are calculated for the A matrix. They are the non-trivial solutions of the equation:

$$A\phi = \lambda\phi \tag{2.45}$$

where ϕ is an $n \times 1$ vector. Rearranging (2.45) to solve for λ yields

$$\det(A - \lambda I) = 0 \tag{2.46}$$

The solutions of (2.46) are the eigenvalues of the $n \times n$ matrix A. These eigenvalues are of the form $\sigma \pm j\omega$.The stability of the operating point may be analyzed by studying the eigenvalues. The operating point is stable if all of the eigenvalues are on the left-hand side of the imaginary axis of the complex plane; otherwise it is unstable. If any of the eigenvalues appear on or to the right of this axis, the corresponding modes are said to be unstable, as is the system.

This stability is confirmed by looking at the time dependent characteristic of the oscillatory modes corresponding to each eigenvalue λ_i, given by $e^{t\lambda_i}$. The latter shows that a real eigenvalue corresponds to a nonoscillatory mode. If the real eigenvalue is negative, the mode decays over time. The magnitude is related to the time of decay: the

larger the magnitude, the quicker the decay. If the real eigenvalue is positive, the mode is said to have aperiodic instability.

On the other hand, the conjugate-pair complex eigenvalues ($\sigma \pm j\omega$) each correspond to an oscillatory mode. A pair with a positive σ represents an unstable oscillatory mode since these eigenvalues yield an unstable time response of the system. In contrast, a pair with a negative σ represents a desired stable oscillatory mode. Eigenvalues associated with an unstable or poorly damped oscillatory mode are also called dominant modes since their contribution dominates the time response of the system. It is quite obvious that the desired state of the system is for all of the eigenvalues to be in the left-hand side of the complex plane.

The damped frequency of the oscillation in Hertz and damping ratio are given by:

$$f = \frac{\omega}{2\pi} \tag{2.47}$$

$$\xi = \frac{-\sigma}{\sqrt{\sigma^2 + \omega^2}} \tag{2.48}$$

In a linear system, the dynamics can be described as a collection of modes. A mode is characterized by its frequency and damping and the activity pattern of the system states. If the damping is low, which is the case for electro-mechanical modes or swing modes in power systems, they can be thought of as resonances. The mode concept is based on a change of coordinates by diagonalization. As in many engineering areas an adequate choice of coordinates can decouple complex relations. This is particularly true with

modal coordinates, which offer a convenient simplification of the system while being valid for the full system.

The system matrix A can be diagonalized by the square right modal matrix ϕ:

$$\phi^{-1} A \phi = \Lambda \tag{2.49}$$

The columns of ϕ are the right eigenvectors ϕ_i to A, while the diagonal elements of the diagonal matrix Λ are the eigenvalues λ_i of A. Similarly the left modal matrix ψ holds the left eigenvectors ψ_i as rows and also diagonalizes A:

$$\psi A \psi^{-1} = \Lambda \tag{2.50}$$

For convenience, the right and left modal matrix are normalized so that:

$$\psi \phi = I \tag{2.51}$$

(2.51) is conveniently guaranteed by computing ψ as the inverse of ϕ. If there are eigenvalues at the origin, ϕ can however not be inverted. ψ_i and ϕ_i corresponding to such an eigenvalue are orthogonal and their product is zero. In practice eigenvalues are unlikely to exactly equal zero. Instead they take a very small value, leading to an ill-conditioned matrix. The inverse of ψ can then be computed, but its validity depends on the numerical accuracy that is used. It is therefore necessary to verify that the product of associated left and right eigenvectors of interest is one.

Provided that ψ and ϕ are available, the ODE system can be transformed into modal coordinates z through a transformation $x = \phi z$:

$$\dot{z} = \Lambda z + \psi B u \tag{2.52}$$

$$y = C\phi z + Du \tag{2.53}$$

After such transformation, the dynamics now are governed by uncoupled first order differential equations – the modes. Once the state equations are decoupled through this transformation, the response of a particular state variable, say Δx_k, may be examined in each *i*th mode in the right eigenvector ϕ. This response is called the mode shape of the particular oscillatory mode.

Sometimes it's useful to quantify how important a dynamic state is to the mode. Conveniently, this is done by computing the participation factors [20]. A matrix called the participation matrix, denoted by *P*, provides a measure of association between the state variables and the oscillatory modes. It is defined as:

$$P = [p_1 \quad p_2 \quad \ldots \quad p_n] \tag{2.54}$$

with

$$p_i = \begin{bmatrix} p_{1i} \\ \vdots \\ p_{ni} \end{bmatrix} = \begin{bmatrix} \phi_{1i}\psi_{i1} \\ \vdots \\ \phi_{ni}\psi_{in} \end{bmatrix} \tag{2.55}$$

The element $p_{ki} = \phi_{ki}\psi_{ik}$ is called the participation factor, and gives a measure of the participation of the *k*th state variable in the *i*th mode.

As seen in (2.52), the input u_j affects the mode *i* through element *(i,j)* of the mode

controllability matrix ψB [21]. As a result, if the *i*th row is zero, the inputs have no effect on that mode and the mode is considered to be uncontrollable.

Analogously mode *j* appears in the output y_i to an extent that is determined by element *(i,j)* of the mode observability matrix $C\phi$. If the *i*th column is zero, the outputs do not contribute to that mode and the mode is considered to be unobservable.

For a SISO system input matrix *B* and output matrix *C* are column and row matrices respectively. The controllability of mode *k* from the *i*th input is given by:

$$cont_{ki} = \psi_k B_i \tag{2.56}$$

The observability of mode *k* from the *j*th output is given by:

$$obsv_{kj} = C_j \phi_k \tag{2.57}$$

The *D* matrix in the power system described by (2.42) and (2.43) is usually a zero matrix. Thus, we can rewrite (2.44) as follows:

$$\begin{aligned} G(s) = \frac{Y(s)}{U(s)} &= C(sI - A)^{-1} B \\ &= C\phi[sI - \Lambda^{-1}]\psi B \end{aligned} \tag{2.58}$$

G(s) can be expanded in partial fractions as:

$$G(s) = \frac{Y(s)}{U(s)} = \sum_{k=1}^{n} \frac{R_k}{s - \lambda_k} \tag{2.59}$$

where R_k is the residue of the *G(s)* at the eigenvalue or pole λ_k.

For a SISO system, *G(s)* can be expanded in partial fractions of the Laplace transform of *y* in terms of input, output matrices and the right and left eigenvectors as:

$$G(s) = \sum_{k=1}^{n} \frac{R_k}{s - \lambda_k} = \sum_{k=1}^{n} \frac{C\phi(:,k)\psi(k,:)B}{(s - \lambda_k)} \tag{2.60}$$

The residue R_k can be said to quantify the participation of mode *k* in the dynamics as seen

between the input and the output. The residue R_k of a particular mode k gives the measure of that mode's sensitivity to a feedback between the output and the input. It is the product of the mode's observability and controllability [22, 23]:

$$R_k = C\phi_k\psi_k B \tag{2.61}$$

Chapter 3. Wide-area Damping Control System Design

3.1 General Design Procedure

The design of wide-area damping controllers for inter-area oscillations includes the following steps:

1) Get the full-order nonlinear model of the studied system: The multi-machine dynamic model of the test system is calculated by Matlab [24]. All generators are represented by the detailed model, i.e. two-axis model with exciter, governor and conventional PSS.

2) Model linearization and small signal analysis: The full-order nonlinear model is linearized around a chosen operating point. Then, small signal analysis is conducted with this linear model. The eigenvalues and eigenvectors are calculated to get the frequencies, shapes and damping ratios of local and inter-area modes.

3) Selection of measurements and control sites: The measurements that can be easily obtained, synchronized and have the highest observability of critical inter-area modes are good candidates for stabilizing signals. Geometric measures of joint Controllability/Observability[28] are used to evaluate the comparative strength of candidate signals and the performance of controllers at different locations with respect to a given inter-area mode.

4) Linear model reduction: The controller obtained by LMI approach is of full order, that is, the same size as the design model including weighting functions. A middle size system usually has several hundreds of states. To design a controller with such a high order model is neither practical nor necessary. Therefore, model reduction is often applied to obtain a lower order model for controller design. The reduced order model should be assured to have the same global characteristics as the original system [25]. In this research, the balanced model reduction via the Schur method provided by the robust control toolbox in Matlab [26] is used for the model reduction task.

5) Controller synthesis: An LMI approach to the mixed H_2/H_∞ output-feedback control with regional pole placement is applied to design a wide-area damping controller for inter-area oscillations. The designed controller should meet the requirements of robust stability, robust performance and acceptable transient response. Time-delays should be modeled in the controller synthesis problem so that the designed controller can handle time-delays. Sometimes the order of obtained controller needs to be reduced for easy implementation. In this case, the balanced model reduction is applied again.

6) Closed-loop verification and nonlinear time domain simulation: The performance of the controller and its digital counterpart are evaluated in the closed-loop system with the full-order linear model using Matlab. Since the controller is designed

with liner techniques, it's necessary to tune the controller parameters and verify its effectiveness with nonlinear simulations. PMU data reporting rates selected with consideration of the effects of time-delays. The controller performance in the nonlinear power system model is evaluated by time domain simulation with the help of Transient Security Assessment Tool (TSAT) [27].

3.2 Wide-area Damping Control System Architecture

Generally speaking, there are two classes of solutions to design damping controllers, the decentralized approach and the centralized approach. The main advantage of the first approach comes from the fact that it is based on local measurements hence additional telecommunication equipments are not needed. But, it is less clear that decentralized/local control alone will suffice to economically and efficiently satisfy the damping needs of the heavily stressed networks of the future [11]. On the contrary, centralized wide-area damping control provides a more efficient solution due to the availability of a large amount of system wide dynamic data and better observations of inter-area modes. Wide-area controls include any control that requires some communication link to either gather the input or to send out control signals [29]. It is found that if remote signals are applied to the controller, the system dynamic performance can be enhanced with respect to inter-area oscillations [3], [15], [30]. Even though additional telecommunication equipment is needed for the realization of such a centralized wide-area damping control system, it still turns out to be more cost-effective than installing new control devices.

In most power systems, local oscillation modes are often well damped due to the installation of local PSS, while inter-area modes are often lightly damped because the control inputs used by those PSS are local signals and often lack good observations of some significant inter-area modes. This suggests that a wide-area controller, which uses wide-area measurements as its inputs to create control signals supplement to local PSSs,

may help to improve the damping of inter-area oscillations. A centralized control system structure is thus proposed and shown in Fig. 3.1.

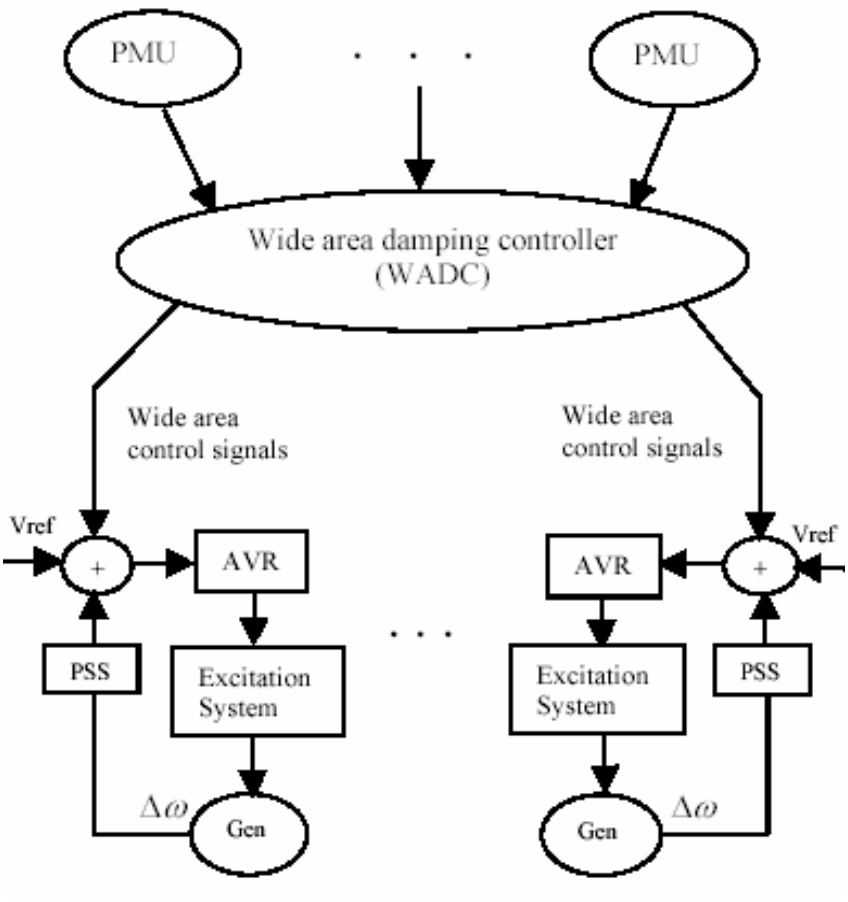

Fig. 3.1 Architecture of wide-area damping control systems

In the proposed wide-area damping control system, selected stabilizing signals are measured by PMUs and sent to the controller through dedicated communication links. The wide-area damping controller calculates modulation signals and sends them to the selected generator exciters. This control scheme is a centralized architecture because every measurement is fed back through central controller to every controller/control device. In practice, there are two ways to implement the proposed wide-area damping

controller. The first way is to install a centralized controller in the control center. The controller collects all measurements, calculates the control signals and sends them to control locations. Another way is to install one controller at each globally controlled generator. Thus, a completely peer-to-peer architecture can be applied to achieve the same function.

In this design, all local PSSs are still conventional controllers designed by classical methods. They are modeled in the open loop state-state representation, on which the design of the WADC is based. The whole damping system includes two levels. The first level is fully decentralized and consists of conventional local PSSs. The second level is centralized and provides supplemental damping actions in addition to the first level for lightly damped inter-area oscillations.

3.3 Selection of Measurements and Control Locations

The selection of appropriate stabilizing signals and locations of control sites is an important consideration in the design of wide-area damping control systems. For FACTS devices, the most often used input signals are line current, line active power and generator angular speed. Reference [2] concluded that the most suitable auxiliary input signal for the SVC for damping improvement is the locally measured transmission line-current magnitude. References [32, 38] select locally measured active power as input signal and references [42, 43] use generator angular speed as input signals. Reference [91] shows that for high stress conditions, current magnitude is a better input signal for the modulation of the parallel Pacific HVDC Intertie to damp Pacific AC Intertie (PACI) oscillations. For PSS, shaft speed, integral of power and terminal frequency are among the commonly used input signals [1]. For local mode oscillations, the largest residue is associated with a local signal (e.g., generator rotor speed signal for a PSS). This means that local signals always have the highest observabily and thus the most effective damping effects for local modes. But for inter-area modes, local signals may not have the maximum observability. The signal with maximum observability for a particular mode may be derived from a remote location or as a combination of signals from several locations. It has been proved that under certain operating conditions an inter-area mode may be controllable from one area and be observable from another [3, 49].

The remote stabilizing signals are often referred to as “global signals” to illustrate that they contain information about overall network dynamics as opposed to local control signals which lack adequate observability of some of the significant inter-area modes.

The recent advances in WAMS technologies using PMUs make it possible to deliver synchronous phasors and control signals at a high speed (e.g., at a 60-Hz sample rate). It is also possible to deploy PMUs at strategic locations on the grid and obtain a coherent picture of the entire network in real time [50].

Methods developed to select feedback signals and control sites resulting in the maximum damping effects can be classified into two categories: controllability/observability analysis and damping torque analysis. Controllability/observability analysis is derived from modal control theory of linear time-invariant system [31, 32]. With this method, measures of modal controllability and observability are calculated to resolve problems of the best control sites and the selection of the stabilizing signals for PSS and FACTS devices [33-37]. Damping torque analysis [38-40] gives more physical meanings to the criteria of selection of control sites and stabilizing signals. But, as pointed out in [41], residue analysis is equivalent to damping torque analysis.

The linearized state-space MIMO model of the studied system can be written as:

$$\dot{x} = Ax + Bu \tag{3.1}$$

$$y = Cx \tag{3.2}$$

where x is the $n \times 1$ state vector, u is the $m \times 1$ input vector and y the $p \times 1$ measured output vector; A $(n \times n)$, B $(n \times m)$ and C $(p \times n)$ are state, input and output matrices respectively. Suppose matrix A has n distinct eigenvalues ($\lambda_k, k = 1,...n$) and the corresponding matrices of right and left eigenvectors respectively ϕ and ψ.

Residue R_k can be said to quantify the participation of mode k in the dynamics as seen between inputs and outputs. Residue matrix R_k associated with the kth natural mode is a $p \times m$ matrix and defined as the product of the mode's observability and controllability:

$$R_k = C\phi_k\psi_k B \tag{3.3}$$

The residue-based measures of controllability $m_{ci}(k)$ and observability $m_{oj}(k)$ associated with mode k can be derived in a normalized form as follows [11]:

$$m_{ci}(k) = \frac{\|R_k(:,i)\|}{\| R_k \|} \qquad (i = 1,...,m) \tag{3.4}$$

$$m_{oj}(k) = \frac{\|R_k(j,:)\|}{\|R_k\|} \qquad (j = 1,..., p) \tag{3.5}$$

If $m_{ci}(k) = 0$, then mode k is uncontrollable from input i. If $m_{oj}(k) = 0$, then mode k is unobservable from output j. With the above definitions, the strength of a signal or the performance of a controller with respect to a given mode can be assessed using relative controllability and observability measures for the ith input and jth output.

In the design of SISO controller, the selection of input signals can't be only based on the measures of observability and the selection of control device locations can't be only based on the measures of controllability. Input and output signals are always simultaneously selected when designing a control loop. This is explained by considering the sensitivity of the kth eigenvalue to the gain K of a proportional feedback controller:

$$\frac{\partial \lambda_k}{\partial K} = \| C\phi_k \psi_k B \| = \|R_k\| = \sigma_k \tag{3.6}$$

In this case, the residue is the modal sensitivity of the constant gain controller. Therefore, the amount of damping that can be added to a given mode *k* by shifting it towards the left on the Laplace plane is proportional to the residue. When $R_k(j,i)$ vanished, the control input *i* has no influence on mode *k* response if the feedback is based on the measured output signal *j*. Even though large feedback gains can still keep the system observable/controllable, there are lots of detrimental effects such as increased sensitivity to noise, control saturation during large disturbances and gain and phase margin limitations [22, 52]. Therefore, when choosing control loops or input/put pairs, large residues or joint controllability/observability measures are desirable. Conventionally, the joint controllability/observability measure is defined by [53]:

$$m_{cok}(i,j) = m_{ci}(k) m_{oj}(k) \tag{3.7}$$

The joint controllability/observability measure m_{cok} is a good index for the SISO control loop selection. Nonzero $m_{cok}(i,j)$ means that mode *k* can be damped using input *i* and output *j*. The input/output pairs with maximum m_{cok} are the most efficient control loops. If maximum $m_{cok}(i,j)$ is achieved with *i* and *j* in the same location, local control is the best choice for damping mode *k*. Otherwise, wide-area control should be considered for better damping of mode *k*.

The limit of residue based modal controllability/observability measures is that they are only valid for the signals of the same type. When signals of a widely differing physical

significance, such as power flow in a tie-line (MW), bus frequency (Hz), shaft speed (rad/s), angle shift (deg.), etc. are involved in the output matrix simultaneously, the residue approach suffers a scaling problem. The validity of the relative measure can be ensured only when all outputs are of the same type [12]. To overcome this shortcoming, geometric measures introduced by Hamdan [28] are used to evaluate the comparative strength of a signal and a control site with respect to a given model. The geometric measures of controllability $gm_{ci}(k)$ and observability $gm_{oj}(k)$ associated with the mode k are:

$$gm_{ci}(k) = \cos(\alpha(\psi_k, b_i)) = \frac{|\psi_k b_i|}{\|\psi_k\| \|b_i\|} \tag{3.8}$$

$$gm_{oj}(k) = \cos(\theta(\phi_k, c_j^T)) = \frac{|c_j \phi_k|}{\|\phi_k\| \|c_j\|} \tag{3.9}$$

with b_i the ith column of input matrix B (corresponding to the ith input) and c_j the jth row of output matrix C (corresponding to the jth output). $|z|$ and $\|z\|$ are the modulus and Euclidean norm of z respectively; $\alpha(\psi_k, b_i)$ is the geometrical angle between the input vector i and the kth left eigenvector, while $\theta(\phi_k, c_j^T)$ is the geometrical angle between the output vector j and the kth right eigenvector. These equations show that the controllability measure is related to the angle between the left eigenvectors and the columns of the input matrix B and that the observability measure is related to the angle between the right eigenvectors and the rows of the output matrix C.

If $gm_{ci}(k) = 0$, then the mode k is uncontrollable from input i. If $gm_{oj}(k) = 0$, then the mode k is unobservable from the output j. Being based on directional properties of the underlying column vectors in the system matrices, the geometrical measures remain effective classifiers, even for inputs and outputs of widely differing types.

3.4 Design of Local PSSs

In the proposed design of wide-area damping control systems, the first level of damping is provided by conventional PSSs for local modes and the damping for inter-area modes are provided by the second level. To implement such a wide-area damping control system, local PSSs need to be redesigned for local modes. The design method for local SISO controller used in this research is the conventional residue-based method. The design procedure is as follows:

Suppose we design a SISO feedback damping controller. The closed loop system is shown in Fig. 3.2, where *G(s)* represents the plant model (which is the open loop transfer function between measurements *y(s)* and reference input u_{ref}, and *H(s)* is the transfer function of the damping controller.

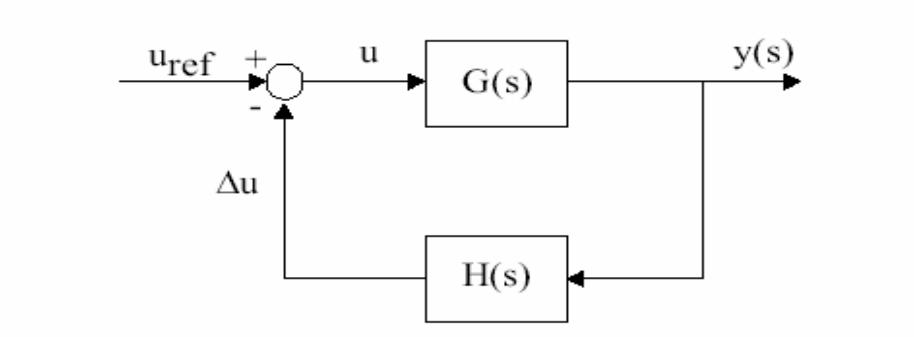

Fig. 3.2 Closed loop system with damping controller

The eigenvalue sensitivity is expressed by [54]:

$$\frac{\partial \lambda_i}{\partial K} = R_i \frac{\partial (K \cdot H(s))}{\partial K} = R_i H(s) \tag{3.10}$$

where, R_i / λ_i is the residue/eigenvalue associated with the *i*th mode, and *K* is the gain of

the damping controller. The small change in the *i*th eigenvalue $\Delta\lambda_i$ caused by the changes of feedback gain ΔK is given by:

$$\Delta\lambda_i = R_i H(s) \cdot \Delta K \tag{3.11}$$

From equation (3.11), it's clear that with the same gain of the feedback loop, a larger residue will result in a larger change of the corresponding oscillation mode. Therefore, the best feedback loop is the one with the largest residue for the considered oscillation mode. The effect of the controller transfer function in the feedback path is to modify the sensitivity of the eigenvalue of the original system by the value of the controller transfer function evaluated at the original eigenvalue. A desired controller is to move the loci of the inter-area modes to the left half of the complex plane as they depart from the open loop poles. This can be done by shaping the phase of controller transfer function *H(s)* using phase lead compensation.

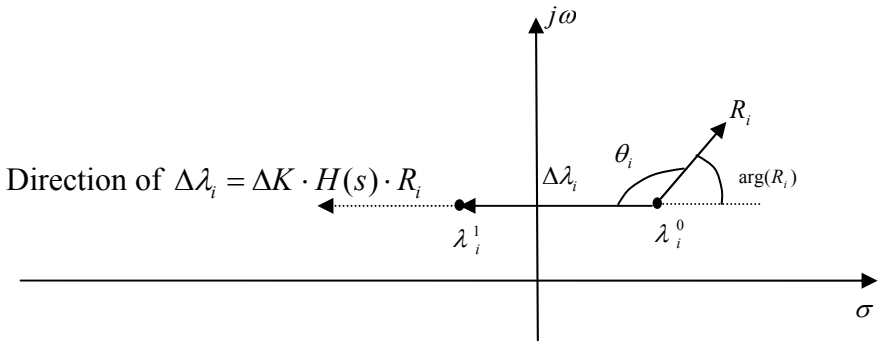

Fig. 3.3 Shift of *i*th mode/eigenvalue with the damping controller

Fig. 3.3 shows the compensation angle needed to move the eigenvalue direct to the left parallel with the real axis θ_i, which is given by [55]:

$$\theta_i = 180^o - \arg(R_i) \tag{3.12}$$

If *H(s)* is a static gain, i.e. *H(s)* = *K*, then

$$\Delta\lambda_i = \Delta\sigma_i + j\Delta\omega_i = K \cdot [\mathrm{Re}(R_i) + j\,\mathrm{Im}(R_i)] \tag{3.13}$$

Equation (3.13) shows that the change of damping and frequency of the *i*th mode, due to the static feedback gain, is proportional to the real and imaginary parts of the residue respectively.

The controller designed is made up of washout filter and lead-lag blocks, with the transfer function:

$$H(s) = K\frac{sT_w}{1+sT_w}\left(\frac{1+sT_1}{1+sT_2}\right)^n \tag{3.14}$$

where T_w is the washout filter time constant and its value can be taken as a number between 1 and 20 seconds. Since the limit of phase compensation of the lead-lag block is about 60^o [56], the number of the lead-lag blocks (n) can be determined by taking the nearest larger number of $\theta/60$. The time constant T_1 and T_2 are calculated from:

$$\alpha = \frac{T_1}{T_2} = \frac{1-\sin\left(\frac{\theta_i}{n}\right)}{1+\sin\left(\frac{\theta_i}{n}\right)}$$

$$T_2 = \alpha T_1, \quad T_1 = \frac{1}{\omega_i\sqrt{\alpha}} \tag{3.15}$$

where ω_i is the frequency of *i*th mode, n is the number of lead-lag blocks.

The controller gain K is computed as a function of the desired eigenvalue location λ_i^{des} :

$$K = \left|\frac{\lambda_i^{des} - \lambda_i}{R_i H(s)}\right| \tag{3.16}$$

3.5 Robust Controller Design Based on H_∞ Technique

3.5.1 Introduction

The power system stabilizer adds damping to generator rotor oscillations by adjusting the generator excitation so that it provides a component of electrical torque in phase with rotor speed deviations. The conventional and most popular method to design a PSS is the residue-based method and the controller is single input and single output. A SISO controller designed by conventional residue-based method has several shortcomings. One of the biggest problems inherent to the classical linear controller design for electric power systems comes from the fact that the controller performance depends strongly on the system operating point, and the system operating conditions usually have significant variations along the day. This system characteristic hinders the achievement of a required performance for the controllers designed by the classical control techniques, given that such techniques are based on a linearization of the system model at a nominal operating point, thus having its validity restricted to a neighborhood of this point [57]. For example, a PSS designed to provide damping for a system with weak tie line by means of phase compensation at the rotor oscillation frequency will not provide adequate phase compensation for another situation, say a strong tie line situation. This is because the increase in reactance with a strong tie line will increase the synchronizing torque thereby increasing the natural frequency of oscillation and also the phase lead compensation requirement. Therefore a PSS, well tuned for a particular operating situation is unable to provide the same sort of performance for another operating condition.

Robust controllers were designed using advanced multi-variable control techniques like LQ, LQG, H_2 and H_∞ in the last decade. The main objective of these robust control methods is to design controllers that are capable of handling modeling errors and uncertainties and produce control actions that stabilize the plant. Additionally, the controller designed should ensure stability and meet performance specifications for all possible plant behavior defined by an uncertainty. These two requirements of the closed loop system are called robust stability and robust performance. Among the various multi-variable control methods the H_∞ based optimization technique is popular. H_∞ [63] is a space of functions on the complex plane that are analytic and bounded in the right half plane. The relevance of H_∞ theory to robust stabilization was provided in the work of Glover in 1986 [64]. The H_∞ based optimization technique provides the design engineer the freedom to formulate his demands using frequency domain based weighting functions, unlike the LQ and H_2 theory which have a purely time domain based performance criterion. The H_∞ design method is based on minimizing the H_∞ norm of a cost function specified to reflect robust stability and robust performance. H_∞ based controllers have been designed successfully for servo applications, flight control applications, process control etc. as shown in a number of published literatures. There have been a few attempts at applying H_∞ based controllers in the area of power system control [58-62], but the design process proved very complex with limitations in the controllers designed.

3.5.2 Definitions of Norms

H_∞ methods of control design, broadly speaking, works by minimizing the H_∞ norm of a certain closed loop transfer function specified to reflect robust stability and robust

performance. The norm denotes a measure of the performance of the system by the size of signals, transfer functions and uncertainties.

In the *s*-domain, the output signal vector *y(s),* of a system modeled by the transfer function matrix, $G(s)$, to any input signal vector, *u(s),* is defined as $Y(s) = G(s)U(s)$.

The performance of this system can be measured by the size of signals *u(t), y(t)* in the time domain and the size of the transfer function matrix $G(s)$, and its uncertainty. These are mathematically denoted as the 'norms' of the signal and function. The L_2 and L_∞ norms have particular significance in the control system design. The L_2 norm is given as $\|u(t)\|_2 = \sqrt{\int_{-\infty}^{\infty} u^T(t)u(t)dt}$. The L_∞ norm, which is the least upper bound on the signal absolute value is given as $\|u(t)\|_\infty = \sup_{t\geq 0} \max_{r=1,2,...,n} |u_r(t)|$; where $u(t) = [u_1(t), u_2(t), ..., u_n(t)]$.

The performance of SISO systems with feedback is influenced strongly by the variation of the open loop gain with frequency. The disturbance rejection and accuracy of tracking also depend on the open loop gain. In the multivariable case the concept of gain is replaced by the singular value of the transfer function matrix. They are also called 'principal gains'. Similar to Bode plots of SISO systems, the singular values are plotted with frequency for a multivariable system.

The transfer function matrix *G(s)* can be characterised by a non-negative number using the H_2 norm and H_∞ norm. To define these norms, let's first define singular value. Singular values of a matrix are good measures of the "size" of the matrix and the

corresponding singular vectors are good indications of strong/weak input or output directions [65].

For a matrix $A \in F^{m\times n}$, there exist unitary matrices $U = [u_1, u_2, ..., u_m] \in F^{m\times m}$ and $V = [v_1, v_2, ..., v_n] \in F^{n\times n}$ such that $A = U\Sigma V^*$, $\Sigma = \begin{bmatrix} \Sigma_1 & 0 \\ 0 & 0 \end{bmatrix}$,

Where $\Sigma_1 = \begin{bmatrix} \sigma_1 & 0 & \cdots & 0 \\ 0 & \sigma_2 & \cdots & 0 \\ \vdots & \vdots & \ddots & \vdots \\ 0 & 0 & \cdots & \sigma_p \end{bmatrix}$, and $\sigma_1 \geq \sigma_2 \geq \cdots \geq \sigma_p \geq 0, p = \min\{m, n\}$.

Then σ_i is the *i*th singular value of *A*, and the vectors u_i and v_j are, respectively, the *i*th left singular vector and the *j*th right singular vector. The following notations for singular values are often adopted:

$\overline{\sigma}(A) = \sigma_{\max}(A) = \sigma_1 =$ the largest singular value of *A*;

$\underline{\sigma}(A) = \sigma_{\min}(A) = \sigma_p =$ the smallest singular value of *A*.

The H_2 norm can be interpreted as an average system gain taken over all frequencies. In fact, the squared H_2 norm of system transfer function coincides with the total 'output energy' in the impulse response of the system. Another nice characteristic of H_2 norm is that it has an interpretation in terms of the asymptotic output variance of the system when it is excited by white noise input signals. This characteristic makes H_2 performance particularly useful in handling stochastic aspects such as noise attenuation and random undisturbance rejection.

H_2 norm is given as

$$\left\|G(j\omega)\right\|_2 = \sqrt{\frac{1}{2\pi}\int_{-\infty}^{\infty} tr\left\{G(j\omega)G^T(-j\omega)\right\}d\omega} = \sqrt{\frac{1}{2\pi}\int_{-\infty}^{\infty}\sum_{r=1}^{n}\sigma_r^2(G(j\omega))d\omega} \tag{3.17}$$

where tr{.} denotes the trace of the matrix; $\sigma_1(.),\sigma_2(.),\cdots,\sigma_n(.)$ denotes the singular values.

H_∞ norm provides a measure of a worst-case system gain. Consider a stable SISO linear system with transfer function $G(s)$. The H_∞ norm is defined as $\left\|G(s)\right\|_\infty = \sup_{u(t)\neq 0}\frac{\left\|y(t)\right\|_2}{\left\|u(t)\right\|_2}$, where *y(t)* and *u(t)* are the system output and input signals, respectively. For stable systems this definition has the form:

$$\left\|G(j\omega)\right\|_\infty = \sup_{\omega}\left|G(j\omega)\right| \tag{3.18}$$

The value of this norm corresponds to the peak on the magnitude Bode plot for the system.

For a multivariable (MIMO) system the H_∞ norm is defined as

$$\left\|G(j\omega)\right\|_\infty = \sup_{\omega}\bar{\sigma}(G(j\omega)) \tag{3.19}$$

$\left|G(j\omega)\right|$ is the factor by which the amplitude of a sinusoidal input with angular frequency ω is magnified by the system. It is seen that the H_∞ norm is simply a measure of the largest factor by which any sinusoid is magnified by the system. The value of this norm corresponds to the peak on the magnitude Bode plot for the system.

The value of $\|G(j\omega)\|_\infty$ can be read off from a frequency response plot of the largest singular value $\bar{\sigma}(G(j\omega))$. The H_∞ norm is the maximum factor by which the magnitude of any vector-valued sinusoidal input is magnified by the system.

3.5.3 Performance and Stability Requirements

The controller *K(s)* which stabilizes the nominal plant $G(s)$, is required to ensure stability and meet performance specifications for all possible plants defined by an uncertainty. This behaviour of the closed loop system is called robust stability and robust performance. These concepts are explained for a multivariable closed loop system whose block diagram is shown in Fig. 3.4. $G(s)$ is the plant transfer function matrix and *K(s)* is the controller transfer function matrix; *y(t), r(t), d(t), n(t)* and *e(t)* denotes the output, reference, disturbance, measurement noise and tracking error signal vectors, respectively.

Using Laplace transforms,

$$Y = (I + GK)^{-1} GK[r - n] + (I + GK)^{-1} d \tag{3.20}$$

The first term in the expression, $(I + GK)^{-1} GK$ is the closed loop transfer function denoted as the complementary sensitivity function, T.

The second term $(I + GK)^{-1}$ is called the sensitivity function, *S*. The closed loop performance requirements of the multivariable feedback system can be expressed in terms of their principal gains:

- to reduce the influence of disturbances on the output signal, the sensitivity function

measured as $\bar{\sigma}(S(j\omega))$ should be as small as possible over the frequency band of the disturbances;

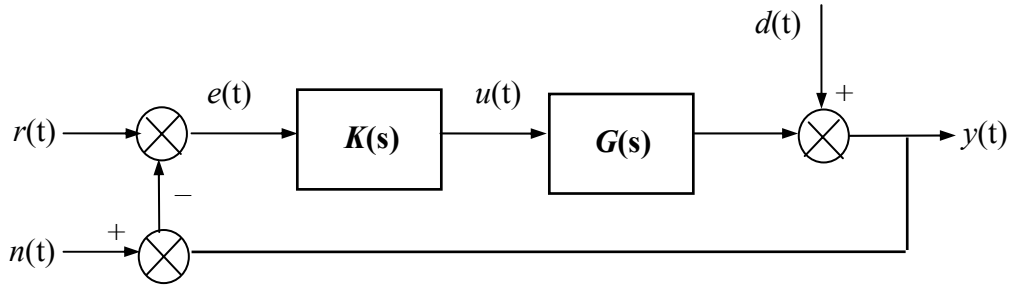

Fig. 3.4 Multivariable closed loop

- to reduce the influence of measurement noise on the output signal, the complementary sensitivity function measured as $\bar{\sigma}(T(j\omega))$ should be as small as possible over the frequency band of the measurement noise.

These control objectives can be reformulated using frequency dependent bounds on the sensitivity and complementary sensitivity functions, and norms. Bounds are approximated by gains of transfer functions $W_1(s)$ and $W_3(s)$ that are chosen in an arbitrary manner. The sensitivity and complementary sensitivity functions performance are represented as

$$\bar{\sigma}(W_1(j\omega)S(j\omega)) \le 1, \tag{3.21}$$

$$\bar{\sigma}(W_3(j\omega)T(j\omega)) \le 1 \tag{3.22}$$

For a multivariable system, the frequency dependent bounds are defined by matrices $W_1(s)$ and $W_3(s)$.

Conditions for robust stability of a multivariable system can be derived from a multivariable version of the small gain theorem. The small gain theorem is a modification of Nyquist stability criterion. It states that the closed loop system will remain stable if a gain measure of the product of all transfer function matrices constituting the feedback path is less than unity [65].

Dealing with, and understanding the effects of uncertainty are important. Reducing the effect of some forms of uncertainty (initial conditions, low frequency disturbances) without catastrophically increasing the effect of other dominant forms (sensor noise, model uncertainty) is the primary job of the feedback control system. Over the years, precise and fixed linear control schemes have been used extensively in many engineering applications. These kinds of designs do not take into account the uncertainties that could be encountered in both the plant and controller models. The uncertainty may have several origins [66].

1) There are many parameters in the linear model, which are only known approximately or are simply in error.
2) The parameters in the linear model may vary due to changes in the operating conditions.
3) Measurement devices cause errors.
4) There are neglected dynamics when simplifying the system model.
5) Uncertainties can be caused by the controller model reduction or by implementation inaccuracies.

The two dominant forms of model uncertainty are: Uncertainty in parameters of the underlying differential equation models, and frequency-domain uncertainty, which often quantifies model uncertainty by describing absolute or relative uncertainty in the process's frequency response. When the plant modeling uncertainty is not too big, we can design high-gain, high-performance feedback controllers. High loop gains significantly larger than one in magnitude can attenuate the effects of plant model uncertainty and reduce the overall sensitivity of the system to plant noise. But if the plant model uncertainty is so large that the sign of the plant gain is not known, then it's not possible to use large feedback gains without the risk that the system will become unstable. Thus, plant model uncertainty can be a fundamental limiting factor in determining what can be achieved with feedback.

The first step of the robust control methodology is to model and bound the above uncertainties in an appropriate way. The next step is to try to design a controller that is insensitive to the difference between the actual system and the model of the system; i.e., a controller that can handle the worst-case perturbations.

Uncertainty is normally classified into two categories [65], the structured uncertainty, which is represented by bounds or ranges on system parameters; unstructured uncertainty, which is given by bounds on the frequency response of the system. The unstructured uncertainty is more important than the structured one because all models include uncertainty to take care of un-modeled dynamics.

The unstructured uncertainty is modeled in the control system design as

- the additive uncertainty $\Delta_a(s)$ which is used to model errors due to high frequency dynamics

$$\Delta_a(s) = \tilde{G}(s) - G(s) \tag{3.23}$$

where $\tilde{G}(s)$ represents the actual model of the plant.

- the multiplicative uncertainty $\Delta_m(s)$ which is used to represent the relative error in the models

$$\Delta_m(s) = \frac{\tilde{G}(s) - G(s)}{G(s)} \tag{3.24}$$

The multiplicative uncertainty which is also represented as $\tilde{G}(s) = (I + \Delta_m(s))G(s)$, is used to model the dynamics of sensors. The two models of uncertainty are shown in Fig. 3.5.

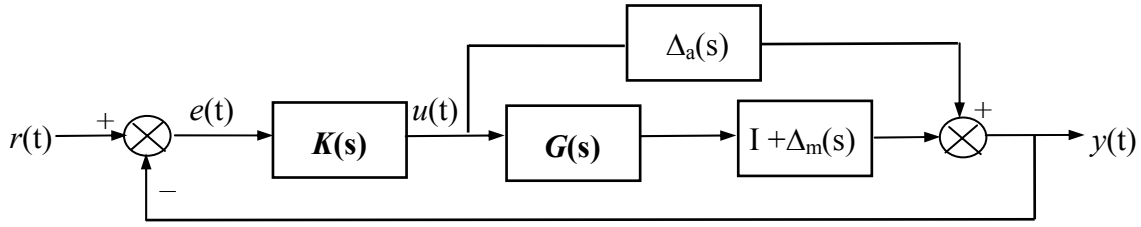

Fig. 3.5 Additive/Multiplicative Uncertainty.

In the case of SISO plants, the frequency at which there are uncertain variations in the plant of size $|\Delta_m|=2$ marks a critical threshold beyond which there is insufficient information about the plant to reliably design a feedback controller. With such a 200% model uncertainty, the model provides no indication of the phase angle of the true plant, which means that the only way to reliably stabilize the plant is to ensure that the loop gain is less than one. Allowing for an additional factor of 2 margin for error, the control

system bandwidth is essentially limited to the frequency range over which multiplicative plant uncertainty Δm has gain magnitude $|\Delta m|<1$.

For stable additive and multiplicative uncertainty transfer functions $\Delta_a(s)$ and $\Delta_m(s)$ under the small gain theorem, the closed loop system shown in Fig. 3.5 will remain robustly stable if for all frequencies ω, the uncertainty models satisfy the following conditions:

additive uncertainty, $|\Delta_a(j\omega)| < \dfrac{1}{|K(j\omega)S(j\omega)|}$;

multiplicative uncertainty, $|\Delta_m(j\omega)| < \dfrac{1}{|T(j\omega)|}$.

Using the H_∞ norm these inequalities are expressed as

$$\bar{\sigma}(S(j\omega)K(j\omega)\Delta_a(j\omega)) < 1 \tag{3.25}$$

and $$\bar{\sigma}(T(j\omega)\Delta_m(j\omega)) < 1 \tag{3.26}$$

As a consequence of this it is common to specify the stability margins of control systems via singular value inequalities,

$$\bar{\sigma}(S(j\omega)K(j\omega)) \le |W_2^{-1}(j\omega)| \tag{3.27}$$

and $$\bar{\sigma}(T(j\omega)) \le |W_3^{-1}(j\omega)| \tag{3.28}$$

These inequalities imply that the smaller the H_∞ norm of the complementary sensitivity function, T, the better the robust stability of the system. From Fig. 3.5, it is seen that $[S(j\omega)K(j\omega)]$ is the transfer function from $d(t)$ to $u(t)$. Thus the robust stability constraint (eqn. 3.27) also limits the maximal control input energy.

3.5.4 Standard H_∞ Optimization Problem

In its abstract "standard" formulation, the H_∞ control problem is one of disturbance rejection. Specifically, it consists of minimizing the closed-loop random-mean-squares (RMS, the largest gain over all square-integrable inputs) gain from *w* to *z* in the control loop of Fig. 3.6. This can be interpreted as minimizing the effect of the worst-case disturbance *w* on the output *z*. Fig. 3.6 consists of a modified plant *G(s)* which includes the weighting functions and a controller *K(s)* which is to be obtained by H_∞ optimization. The plant inputs are grouped into:

- *u*, the vector of control input signals;
- *w*, the vector of exogenous input signals.

The plant outputs are divided into two vectors:

- *y*, the vector which consists of signals that are measured and used as the input vector of the controller to produce the control signal *u*;
- *z*, the vector which consists of a set of signals used in measures of the closed loop system performance.

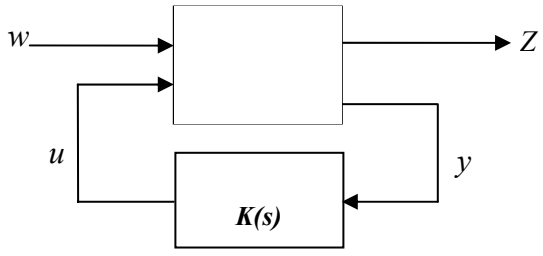

Fig. 3.6 Two-port block diagram of the control

The modified plant *G*(s) may be partitioned as

$$G(s)=\begin{bmatrix} G_{11}(s) & G_{12}(s) \\ G_{21}(s) & G_{22}(s) \end{bmatrix} \tag{3.29}$$

So that the two port system equations are given as

$$Z(s)=G_{11}(s)W(s)+G_{12}(s)U(s) \tag{3.30}$$

$$Y(s)=G_{21}(s)W(s)+G_{22}(s)U(s) \tag{3.31}$$

$$U(s)=K(s)Y(s) \tag{3.32}$$

From these equations the closed loop transfer function relating vectors *z(t)* and *w(t)*, $Z(s)=[F_L(G(s),K(s))]W(s)$

Where, $F_L(G(s),K(s))=G_{11}(s)+G_{12}(s)K(s)(I-G_{22}(s)K(s))^{-1}G_{21}(s)$ (3.33)

is called the linear fractional transformation.

A suitable definition of the signals *w(t)* and *z(t)* or equivalently the corresponding transfer function matrix *G(s)* allows many control system design problems to be cast into the two-port representations. Different measures of $F_L(G(s),K(s))$ can be used to describe the desired control system performance.

The plant *G(s)* can also be represented in the state-space form as

$$\dot{x}(t)=Ax(t)+B_1w(t)+B_2u(t) \tag{3.34a}$$

$$z(t)=C_1x(t)+D_{11}w(t)+D_{12}u(t) \tag{3.34b}$$

$$y(t)=C_2x(t)+D_{21}w(t)+D_{22}u(t) \tag{3.34c}$$

resulting in a packed form notation of,

$$G(s) = \left[\begin{array}{c|cc} A & B_1 & B_2 \\ \hline C_1 & D_{11} & D_{12} \\ C_2 & D_{21} & D_{22} \end{array}\right] \tag{3.35}$$

From the above representation, the standard H_∞ control problem can be stated as follows; "Find an internally stabilizing and realizable controller *K(s)* for a given plant *G(s)* such that the H_∞ norm of the linear fractional transformation matrix $F_L(G(s), K(s))$ is below a given level γ".

i.e. $\|F_L(G(s), K(s))\|_\infty < \gamma$; with $\gamma \in \Re$ and $\gamma > 0$

3.5.5 Formulation of Weighted Mixed Sensitivity Problem

For the closed-loop system shown in Fig. 3.4, we distinguish various 'closed-loop' transfer functions:

- The sensitivity $S = (I + GK)^{-1}$, which maps the reference signal *r* to the (real) tracking error *r - y* and the disturbance *d* to *y*.
- The complementary sensitivity $T = (I + GK)^{-1} GK = I - S$, which maps the reference signal *r* to the output *y* and the sensor noise *n* to *y*.
- The control sensitivity $R = (I + GK)^{-1} K = SK$, which maps the reference signal *r*, the disturbance *d* and the measurement noise *n* to the control input *u*.

Good reference signal tracking, i.e., a small error $e=r-y$, is achieved if the sensitivity function S is small. On the other hand, suppression of measurement noise n requires the complementary sensitivity function T to be small. In the mean time, we also want the control sensitivity function R to be small to avoid actuator saturation. However, due to the relation $S+T=I$, both S and T cannot be small simultaneously. Hence there is necessarily a trade-off between reference signal tracking and sensitivity to measurement noise. Fortunately, the frequency contents of the tracking signal r and the noise signal n are usually concentrated to different frequency ranges: r consists typically of low-frequency components, whereas the noise n is important at higher frequencies. Therefore, controllers with both good (low-frequency) tracking properties and (high-frequency) noise suppression can be designed by making S small at low frequencies and T small at higher frequencies. To have a trade-off between these quantities, the 'weighted mixed sensitivity problem' was formulated [67]. This is the most commonly used configuration since it captures many different practical and physical features and reflects different performance and robustness specifications.

The cost function, $F_L(G(s),K(s))$, whose H_∞ norm is to be minimized is given by $\left\| \begin{matrix} W_1 S \\ W_3 T \\ W_2 SK \end{matrix} \right\|_\infty$, where $G(s)$ is the plant, K is the controller to be designed. W_1 is the weighting on tracking error, W_2 is the weighting on the control signal, W_3 is the weighting on the plant output as shown in Fig. 3.7

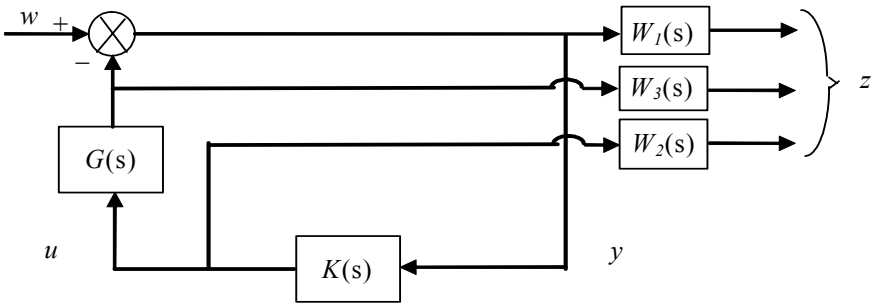

Fig. 3.7 Weighted Mixed Sensitivity Problem

It is seen from Fig. 3.7 that the weighted mixed sensitivity problem is exactly in the same form as the standard problem, therefore for the above given cost function, using the expressions for S and T and comparing with general form of eqn. 3.35 results in a modified plant given by,

$$G(s) = \left[\begin{array}{c|c} W_1(s) & -W_1(s)G_o(s) \\ 0 & W_3(s)G_o(s) \\ 0 & W_2(s) \\ \hline I & -G_o(s) \end{array}\right] \tag{3.36}$$

where I denotes identity matrix.

It is not necessary that all the specifications are considered for one problem; hence all the three weighting functions need not be specified for a problem. In this research, the following mixed sensitivity (S/R) design objective is adopted:

$$\left\| \begin{matrix} W_1 S \\ W_2 R \end{matrix} \right\|_\infty \leq \gamma \tag{3.37}$$

where γ is the bound on H_∞ norm.

This design would minimize a weighted mix of the sensitivity function S that ensures disturbance rejection and good tracking and control sensitivity function R that handles the robustness issues and constrains the controller effort.

Selection of the weighting matrices $W_1(s)$, $W_2(s)$ and $W_3(s)$ is the most important part of the design process since a proper choice of the weighting functions based on knowledge of the plant is required to meet the design requirements. Choosing the weighting functions is based on the knowledge of the plant and design constraints (stability and performance requirements). There are no systematic procedures available for the selection of the weighting functions. Generally speaking, the weight filters should be large on frequency ranges where it is important to constrain the magnitudes of the associated closed-loop transfer functions, and small at other frequencies. The weight filters which are used to achieve the required closed-loop behavior are typically low-pass, high-pass, or band-pass filters.

3.5.6 Mixed H_2/H_∞ Output-Feedback Control

Robust control techniques are introduced into power system damping controller design in the last decade to handle modeling errors and uncertainties. The most often used approach is the single objective synthesis, in which all control requirements are weighted and formulated in a single objective. But in many real-world applications, standard H_∞ synthesis cannot adequately capture all design specifications. For instance, noise attenuation and regulation against random disturbances are more naturally expressed in LQG terms (H_2 norm). Similarly, pure H_∞ synthesis only enforces closed-loop stability and does not allow for direct placement of the closed-loop poles in more specific regions

of the left-half plane. Since the pole location is related to the time response and transient behavior of the feedback system, it is often desirable to impose additional damping and clustering constraints on the closed-loop dynamics. This makes multi-objective synthesis highly desirable in practice. It's well known that each robust method is mainly useful to capture a set of special specifications [68]. H_∞ control maintains good robust performance in presence of model uncertainties. But it is mainly concerned with frequency-domain performance and does not guarantee good transient behaviors for the closed-loop system. H_2 control gives more suitable performance on system transient behaviors and is often applied to meet performance specifications and impulsive disturbance rejection while guaranteeing closed-loop stability.

In many practical applications, the trade-off between conflicting requirements has to be made so that a single norm can represent all design requirements. In this case, minimizing this performance index is not very effective because the resulting controller is often conservative and the achievable closed-loop performance is limited. What's more, the selection of weighting function to meet the trade-off between conflicting requirements is hard and time consuming [25].

To overcome these limitations of a single objective synthesis technique, the multi-objective synthesis technique, which can incorporate various design specifications easily, is naturally considered. By multi-objective control, we refer to synthesis problems with a mix of time- and frequency- domain specifications ranging from H_2 and H_∞ performance to regional pole placement constraints. The H_∞ performance is convenient to enforce robustness to model uncertainty and to express frequency domain specifications such as

bandwidth, low-frequency gain, and roll-off; whereas the H_2 performance is useful to handle stochastic aspects such as measurement noise and random disturbance. In addition, direct placement of the closed-loop poles in specific regions of the left-half plane ensures acceptable transient response in terms of decay and damping ratio.

The configuration of the multi-objective damping controller synthesis is shown in Fig. 3.8. The output channel z_∞ is associated with the H_∞ performance and the channel z_2 is associated with H_2 performance. $\boldsymbol{W_1(s)}$ is a low-pass filter in the H_2 performance channel for output disturbance rejection. $\boldsymbol{W_2(s)}$ is a high-pass filter or some small constant in H_2 performance channel that is used to reduce the control effort. $\boldsymbol{W_3(s)}$ is a high-pass filter in the H_∞ performance channel to ensure robustness against model uncertainties.

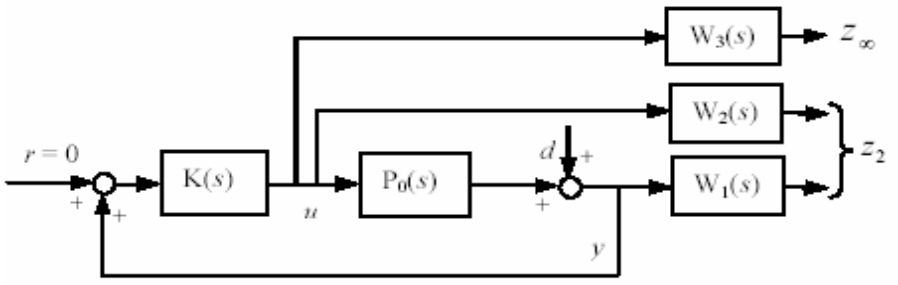

Fig. 3.8 Multi-objective damping controller synthesis configuration

In single objective H_∞ synthesis approach, the H_∞ performance is used to evaluate all design specifications like disturbance rejection, robustness and control efforts. In contrast, in this multi-objective synthesis approach, the H_∞ performance is only used to measure robustness against dynamic uncertainty. The H_2 performance is used to measure control efforts and output disturbance rejection because H_2 control gives more suitable

performance on system transient behaviors and control cost can be more realistically captured by H_2 norm [69]. Since our aim is to damp out inter-area oscillations, the center-of-inertia (COI) differences between areas are selected as controlled output associated with H_2 performance.

3.6 LMI Approach to H_∞ Controller Design

The solution to the H_∞ control problem has been attempted by many researchers. The state space approach was developed in the late 1980's [70]. The characterization involves the solution of two algebraic Riccati equations, of the same order as the modified plant. The solution to the H_∞ control design problem based on the Riccati equation approach generally produces a controller that suffers from pole-zero cancellations between the plant and the controller [71]. Furthermore, some of the specifications in the time domain, such as settling time, peak overshoot (closed-loop damping ratio) cannot be captured in a straight forward manner in Riccati-based design [72]. Riccati-based design depends heavily on the proper selection of weights for conditioning the plant. There is no clear procedure for weight selection in power system damping design.

Recently, LMI techniques have been used to provide a solution to the H_∞ synthesis problem. These LMIs correspond to the inequality counterpart of the usual H_∞ Riccati equations. The numerical approach to solution through a LMI formulation has several distinct advantages. First, the resulting controllers do not in general suffer from the problem of pole-zero cancellation [73]. Second, because LMI's intrinsically reflect constraints rather than optimality, they tend to offer more flexibility for combining several constraints on the closed-loop system or objectives in a numerically tractable manner, even where the analytical solution is not possible [74, 75]. By definition, the LMI solution, if it exists, is robust and optimal. Last, The LMI approach is well-adapted to the power system controller problem since a posteriori determination of the optimality or robustness requires many long, time-consuming simulations. Several researchers have

investigated the use of LMI techniques for H_∞ based power system damping controller design [15, 72, 76-78]. Reference [68] gives a detailed description of an LMI approach to such a complex problem of mixed H_2/ H_∞ output-feedback control with regional pole placement.

3.6.1 Introduction to LMI

A linear matrix inequality is any constraint of the form

$$A(x) := A_0 + x_1 A_1 + ... + x_N A_N < 0 \tag{3.38}$$

where

- $x = (x_1,...,x_N)$ is a vector of unknown scalars (the decision or optimization variables)
- $A_0, A_1,..., A_N$ are given symmetric matrices
- < 0 stands for "negative definite," i.e., the largest eigenvalue of $A(x)$ is negative

The LMI (3.38) is a convex constraint on x and finding a solution x to (3.38), if any, is a convex optimization problem.

LMI techniques are applicable to three general types of control problems: feasibility (3.39), linear objective minimization (3.40) and generalized eigenvalue minimization (3.41) problems. These problems are respectively expressed as follows:

Finding a solution x to $A(x)<0$ (3.39)

Minimizing $C^T x$ subject to $A(x)<0$ (3.40)

$$\text{Minimizing } \lambda \text{ subject to } \begin{cases} A(x) < \lambda B(x) \\ B(x) > 0 \\ C(x) < 0 \end{cases} \tag{3.41}$$

To formulate the LMI problem for a linear time-invariant system, the following state-space representation is used:

$$\begin{aligned} E\frac{dx}{dt} &= Ax(t) + Bu(t) \\ y(t) &= Cx(t) + Du(t) \end{aligned} \tag{3.42}$$

where *A, B, C, D* and *E* are real matrices and *E* is invertible. This formulation is useful for specifying parameter-dependent systems. Recalling the traditional state-space system used for power systems, it's convenient that the LMI method is developed in the same general form.

3.6.2 LMI formulation for Multi-Objective Synthesis

The control problem is sketched in Fig. 3.9. The output channel z_∞ is associated with the H_∞ performance while the channel z_2 is associated with the LQG aspects (H_2 performance). Denoting by $T_\infty(s)$ and $T_2(s)$ the closed-loop transfer functions from *w* to z_∞ and z_2, respectively, we consider the following multi-objective synthesis problem:

Design a dynamic output-feedback controller *u = K(s)y* that

• Maintains the H_∞ norm of $T_\infty(s)$ (RMS gain) below some prescribed value $\gamma_0 > 0$

• Maintains the H_2 norm of $T_2(s)$ (LQG cost) below some prescribed value $\nu_0 > 0$

• Minimizes a trade-off criterion of the form

$\alpha\|T_\infty\|_\infty^2 + \beta\|T_2\|_2^2$, with $\alpha > 0$ and $\beta > 0$

• Places the closed-loop poles in some prescribed LMI region D

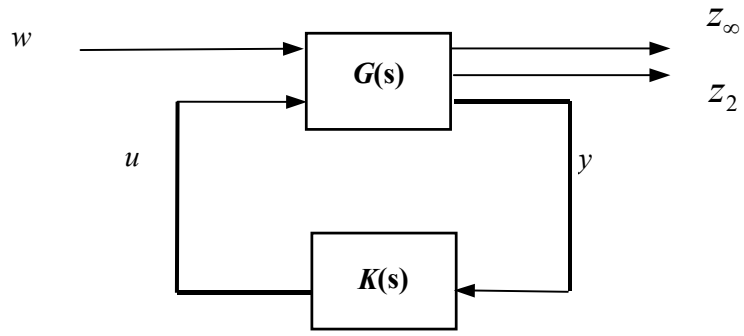

Fig. 3.9 Multi-objective H_∞ synthesis problem

Let

$$\dot{x} = Ax + B_1 w + B_2 u \tag{3.43a}$$

$$z_\infty = C_\infty x + D_{\infty 1} w + D_{\infty 2} u \tag{3.43b}$$

$$z_2 = C_2 x + D_{21} w + D_{22} u \tag{3.43c}$$

$$y = C_y x + D_{y1} w \tag{3.43d}$$

and

$$\dot{x}_k = A_k x_k + B_k y \tag{3.44a}$$

$$u = C_k x_k + D_k y \tag{3.44b}$$

be state-space realizations of the plant *G(s)* and controller *K(s)*, respectively, and let

$$\dot{x} = A_{cl} x_{cl} + B_{cl} w \tag{3.45a}$$

$$z_\infty = C_{cl1}x_{cl} + D_{cl1}w \tag{3.45b}$$

$$z_2 = C_{cl2}x_{cl} + D_{cl2}w \tag{3.45c}$$

be the corresponding closed-loop state-space equations.

The three design objectives can be expressed as follows:

• H_∞ performance: the closed-loop RMS gain from w to z_∞ does not exceed γ if and only if there exists a positive definite symmetric matrix χ_∞ such that

$$\begin{pmatrix} A_{cl}\chi_\infty + \chi_\infty A_{cl}^T & B_{cl} & \chi_\infty C_{cl1}^T \\ B_{cl}^T & -I & D_{cl1}^T \\ C_{cl1}\chi_\infty & D_{cl1} & -\gamma^2 I \end{pmatrix} < 0 \tag{3.46}$$

• H_2 performance: the H_2 norm of the closed-loop transfer function from w to z_2 does not exceed ν if and only if $D_{cl2} = 0$ and there exist two symmetric matrices χ_2 and Q such that

$$\begin{pmatrix} A_{cl}\chi_2 + \chi_2 A_{cl}^T & B_{cl} \\ B_{cl}^T & -I \end{pmatrix} < 0 \tag{3.47}$$

$$\begin{pmatrix} Q & C_{cl2}\chi_2 \\ \chi_2 C_{cl2}^T & \chi_2 \end{pmatrix} > 0 \tag{3.48}$$

$$\text{Trace}(Q) < \nu^2 \tag{3.49}$$

• Pole placement: the closed-loop poles lie in the LMI region

$$D = \{z \in C : L + Mz + M^T\bar{z} < 0\} \tag{3.50}$$

with $L = L^T = \{\lambda_{ij}\}_{1\le i,j\le m}$ and $M = [\mu_{ij}]_{1\le i,j\le m}$ if and only if there exists a positive definite symmetric matrix χ_{pol} satisfying

$$[\lambda_{ij}\chi_{pol} + \mu_{ij}A_{cl}\chi_{pol} + \mu_{ij}\chi_{pol}A_{cl}^T]_{1\le i,j\le m} < 0 \tag{3.51}$$

For tractability in the LMI framework, we must seek a single Lyapunov matrix

$\chi := \chi_\infty = \chi_2 = \chi_{pol}$ that enforces all three sets of constraints. Find matrices *M, N,* $R = R^T$ and $S = S^T$ to factorize χ as

$$\chi = \chi_1\chi_2^{-1},\ \chi_1 := \begin{pmatrix} R & I \\ M^T & 0 \end{pmatrix},\ \chi_2 := \begin{pmatrix} 0 & S \\ I & N^T \end{pmatrix}$$

and introducing the change of controller variables [79]:

$$B_K := NB_K + SB_2D_K \tag{3.52}$$

$$C_K := C_KM^T + D_KC_yR \tag{3.53}$$

$$A_K := NA_KM^T + NB_KC_yR + SB_2C_KM^T + S(A + B_2D_KC_y)R \tag{3.54}$$

The inequality constraints on χ are readily turned into LMI constraints in the variable *R*, *S, Q,* A_K, B_K, C_K and D_K. This leads to the following suboptimal LMI formulation of the multi-objective synthesis problem:

Minimize $\alpha\gamma^2 + \beta Trace(Q)$ over *R, S, Q,* A_K, B_K, C_K, D_K and γ^2 satisfying:

$$\begin{pmatrix} AR + RA^T + B_2C_K + C_K^TB_2^T & A_K^T + A + B_2D_KC_y & B_1 + B_2D_KD_{y1} & (C_\infty R + D_{\infty 2}C_K)^T \\ A_K + (A + B_2D_KC_y)^T & A^TS + SA + B_K + C_y^TB_K^T & SB_1 + B_KD_{y1} & C_\infty^T + C_y^TD_K^TD_{\infty 2}^T \\ (B_1 + B_2D_KD_{y1})^T & SB_1 + B_KD_{y1} & -I & (D_{\infty 1} + D_{\infty 2}D_KD_{y1})^T \\ C_\infty R + D_{\infty 2}C_K & C_\infty + D_{\infty 2}D_KC_y & D_{\infty 1} + D_{\infty 2}D_KD_{y1} & -\gamma^2 I \end{pmatrix} < 0 \tag{3.55}$$

$$\begin{pmatrix} Q & C_2R + D_{22}C_K & C_2 + D_{22}D_KC_y \\ (C_2R + D_{22}C_K)^T & R & I \\ (C_2 + D_{22}D_KC_y)^T & I & S \end{pmatrix} > 0 \tag{3.56}$$

$$\left[\lambda_{ij} \begin{pmatrix} R & I \\ I & S \end{pmatrix} + \mu_{ij} \begin{pmatrix} AR + B_2C_K & A + B_2D_KC_2 \\ A_K & SA + B_KC_2 \end{pmatrix} + \mu_{ji} \begin{pmatrix} RA^T + C_K^TB_2^T & A_K^T \\ (A + B_2D_KC_2)^T & (SA + B_KC_2)^T \end{pmatrix} \right]_{1 \le i,j \le m} < 0 \tag{3.57}$$

$$\text{Trace}(Q) \ < \ \nu_0^2 \tag{3.58}$$

$$\gamma^2 < \gamma_0^2 \tag{3.59}$$

$$D_{21} + D_{22}D_KD_{y1} = 0 \tag{3.60}$$

Given optimal solutions γ^*, Q^* of this LMI problem, the closed-loop H_∞ and H_2 performances are bounded by

$$\|T_\infty\|_\infty \le \gamma^* \tag{3.61}$$

$$\|T_2\|_2 \le \sqrt{Trace(Q^*)} \tag{3.62}$$

3.6.3 LMI Region for Pole Placement Objective

The transient response of a linear system is related to the location of its poles. Good transient response can be achieved by placing all closed-loop poles in a prescribed region. It is often desirable to enforce some minimum decay rate or closed-loop damping via regional pole assignment. In addition, pole constraints are useful to avoid fast dynamics

and high-frequency gain in the controller, which in turn facilitate its digital implementation. While achieving acceptable damping ratio and decay rate, excessively large controller gains should be avoided, since they could lead to controller output saturation and a poor large disturbance response of the system. Thus an unnecessarily large shift of the system poles into the left half plane should be avoided, since this would be accompanied by large feedback gains. Imposition of additional constraints on the closed loop poles restricting their real parts to be greater than a suitable negative number inhibits such excessive shifting of the system poles due to the feedback [80].

The concept of LMI region is useful to formulate pole placement objectives in LMI terms. LMI regions are convex subsets D of the complex plane characterized by

$$D = \{z \in C : f_D(z) < 0\} \tag{3.63}$$

where $f_D(z) = \alpha + \beta z + \beta^T \bar{z} = [\alpha_{kl} + \beta_{kl} z + \beta_{lk} \bar{z}]_{1 \le k,l \le m}$ is called the characteristic function of D. $\alpha = [\alpha_{kl}] \in R^{m \times m}$ and $\beta = [\beta_{kl}] \in R^{m \times m}$ are symmetric matrix. A dynamical system $\dot{x} = Ax$ is called D-stable if all its poles lie in D. The matrix is D-stable if and only if there exits a symmetric matrix X such that

$$M_D(A, X) < 0, X > 0 \tag{3.64}$$

where $M_D(A, X) := \alpha \otimes X + \beta \otimes (AX) + \beta^T \otimes (AX)^T$ and $\otimes$ denotes the Kronecker production of matrices.

Many convex regions in the complex plane which are symmetric with respect to the real axis including half planes, horizontal strips, circles and sectors can be expressed as LMI regions. The intersection of a number of LMI regions is also an LMI region. Some typical LMI regions are:

1) Half-plane Re(z) < $-\alpha$: $f_D(z) = z + \bar{z} + 2\alpha < 0$

2) Conic sector with apex at the origin and inner angle $2\theta(S(0,0,\theta))$:

$$f_D(z) = \begin{bmatrix} \sin\theta(z+\bar{z}) & -\cos\theta(z-\bar{z}) \\ \cos\theta(z-\bar{z}) & \sin\theta(z+\bar{z}) \end{bmatrix} < 0$$

One region for all the control purposes discussed above is shown in Fig. 3.10. When the closed-loop poles are in this region, it ensures minimum damping ratio $\xi = \cos\theta$, minimum rate of decay σ , a maximum undamped natural frequency ω and acceptable controller gains. This in turn bounds the maximum overshoot, the frequency of oscillatory modes, the decay time, the rise time, settling time and maximum gains.

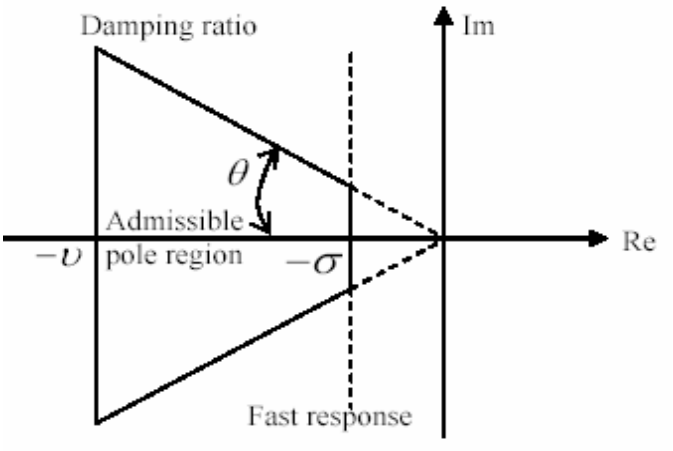

Fig. 3.10 LMI region for pole placement

3.7 Time-Delay

3.7.1 Introduction

With the proposal of wide-area damping control systems, the impact of time-delays received more and more concerns because it reduces the effectiveness of control system damping or destabilizes the system in some cases [82]. In wide-area damping control systems, time-delays are caused by measurements processing, transmission, synchronization and control signals calculation and transmission. Usually, the time-delay between the instant of measurements being taken and that of the control devices receiving control signals is usually considered to be in the order of 100 ms [15]. In the cases of fiber optic communication links used for PMU measurements and control signals transmission, the total time-delay in a feedback loop is in the range of 150 – 300 ms [81].

It is often possible to design a control system taking time-delay effects into account for fixed time-delay communication links [14]. References [83, 84] proposed a procedure based on the unified Smith predictor (USP) approach to design a centralized power system damping controller for FACTS devices like SVC and TCSC. Only fixed time-delays were considered in their approach. But in practice, the value of time-delay is a random variable with a large standard deviation so that time-delay becomes a significant limitation in the design and operation of wide-area damping control systems [12]. This requires that the designed damping controller should be robust not only for different operating conditions, but also for the uncertainty in time-delays. Reference [82] proposed a design of supervisory power system stabilizer (SPSS) that can handle the time-delay uncertainty by using a technique based on H_∞ gain scheduling theory.

The biggest part of time-delay in a wide-area damping control system is data latency. Data latency is the time it takes from measuring the synchrophasor at the PMU to delivering the synchrophasor to the application. It is determined by the PMU processing, intermediate device reprocessing, network bandwidth, collecting and synchronizing all system PMU data and serving the data to applications. The system data latency will be defined by the slowest synchrophasor (of those measured at the same instant) delivered to applications. Data latency is not generally critical for system monitoring and post event analysis. However, it is crucial for real-time continuous damping controls. Time-delays are caused by the following factors:

- Transducer delays
- Window size of the DFT
- Processing time of PMU
- Data size of the PMU output
- Multiplexing and transitions
- Communication link involved
- Data processing and synchronizations

Delay includes two parts:

- Fixed delay
  - Delay due to processing, DFT, multiplexing and data processing and synchronizations
  - Independent of communication medium used
  - Estimated to be around 75 ms [81]
- Propagation delay

- Function of the communication link and physical separation
- Ranges from 20 ms in case of fiber-optic cables to 200 ms in case of low earth orbiting (LEO) satellites

The total time-delays for different communication links, from the instant of data measured by PMUs to the instant that control signals arrive at control locations, are shown in Table 3-1 [81].

Table 3.1: Time-delays for different communication links

Communication link	Associated delay (milliseconds)
Fiber-optic cables	~ 100-150
Microwave links	~ 100-150
Power line (PLC)	~ 150-350
Telephone lines	~ 200-300
Satellite link	~ 500-700

3.7.2 Controller Design Considering Time-delay Uncertainty

The closed-loop feedback control system with time-delays is shown in the Fig. 3.11. The time-delay can be roughly separated into two parts. The first part T_{in} is the time used for measurement processing, synchronization and transmission from PMUs to the centralized controller; the second part T_{out} is the time used for control signal calculations and transmission from the controller to control sites. If fiber-optic cables are used for

communication links, T_{in} is usually in the range of [75 - 200] ms and T_{out} is usually in the range of [50 - 150] ms.

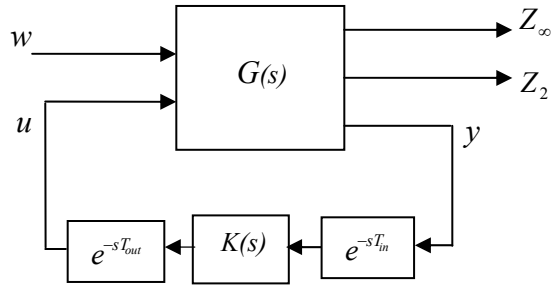

Fig. 3.11 Controller design with time-delay

In Matlab, time-delays are expressed in the exponential form (e^{-sT}) in the Laplace domain. It can be replaced by a first-order Padé Approximation [88]:

$$e^{-sT} \approx \frac{-\frac{1}{2}sT + 1}{\frac{1}{2}sT + 1} \tag{3.65}$$

Time-delay uncertainty can be described in a state space realization called a Linear Fractional Transformation (LFT).

Let time-delay be given by:

$$\tau_d = a + b\delta_t, \qquad \delta_t \in [-1,1] \tag{3.66}$$

Where both *a* and *b* are constants.

If the time-delay block is approximated by the first order Padé Approximation in (3.65), the state expression for the delay is then derived as:

$$\dot{x} = -\frac{2}{\tau_d}x + \frac{4}{\tau_d}u \tag{3.67a}$$

$$y = x - u \tag{3.67b}$$

The LFT of $\frac{1}{\tau_d}$ is shown in the Fig. 3.12:

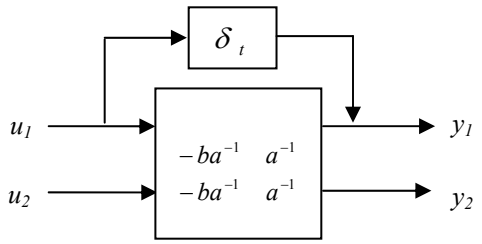

Fig. 3.12 LFT representation of time-delay.

The term $\frac{1}{\tau_d}$ can be represented by a constant matrix and an uncertainty matrix:

$$\frac{1}{\tau_d} = F_u\left(\begin{bmatrix} -ba^{-1} & a^{-1} \\ -ba^{-1} & a^{-1} \end{bmatrix}, \quad \delta_t\right) \tag{3.68}$$

$T_{in} = 0.125(1+0.6\,\delta_t)$. This covers an uncertain time-delay from 75ms to 200ms.

$T_{out} = 0.1(1+0.5\,\delta_t)$. This covers an uncertain time-delay from 50ms to 150ms.

The total time-delay is in the range of [125 – 350] ms.

Fig 3.13 gives a delay-free system without the controller connected with a time-delay block.

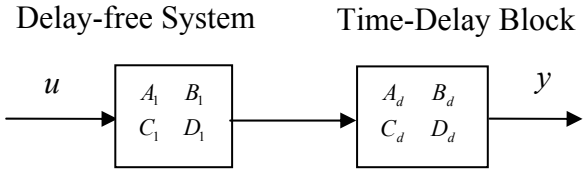

Fig. 3.13 Delay-free system connected with time-delay block

The state-spaces of these two systems are represented mathematically as:

$$\begin{aligned} \dot{X}_1 &= A_1 X_1 + B_1 U_1 \\ Y_1 &= C_1 X_1 + D_1 U_1 \end{aligned} \tag{3.69}$$

$$\begin{aligned} \dot{X}_d &= A_d X_d + B_d U_d \\ Y_d &= C_d X_d + D_d U_d \end{aligned} \tag{3.70}$$

Since $U_2=Y_1$, we have:

$$\begin{aligned} \begin{bmatrix} \dot{X}_1 \\ \dot{X}_d \end{bmatrix} &= \begin{bmatrix} A_1 & 0 \\ B_d C_1 & A_d \end{bmatrix} \begin{bmatrix} X_1 \\ X_d \end{bmatrix} + \begin{bmatrix} B_1 \\ B_d D_1 \end{bmatrix} U_1 \\ Y_d &= \begin{bmatrix} D_d C_1 & C_d \end{bmatrix} \begin{bmatrix} X_1 \\ X_d \end{bmatrix} + D_d D_1 U_1 \end{aligned} \tag{3.71}$$

The *A, B, C* and *D* matrices for the connected system are,

$$\begin{aligned} A &= \begin{bmatrix} A_1 & 0 \\ B_d C_1 & A_d \end{bmatrix}, B = \begin{bmatrix} B_1 \\ B_d D_1 \end{bmatrix} \\ C &= \begin{bmatrix} D_d C_1 & C_d \end{bmatrix}, D = D_d D_1 \end{aligned} \tag{3.72}$$

By connecting the time-delay block with a delay-free system with uncertainties, the system shown in the Fig. 3.14 is used for robust controller synthesis that can handle time-delay uncertainty.

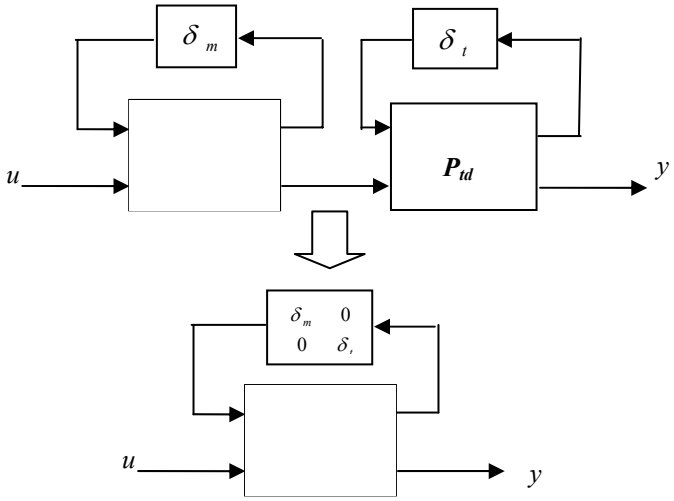

Fig. 3.14 System connection with the time-delay uncertainty block

3.8 Digital Environment

Digital environment is another issue should be considered in the design of wide-area damping controllers. Wide-area damping controllers are usually designed based on traditional continuous analog control concepts with the assumption that all measured stabilizing signals and control signals are continuous. In practice, most communication links use for control purposes are optical fibers. More and more stability controllers are digital ones. The performance and robustness of controllers designed with linear techniques in the continuous *s*-domain should be tested in digital environments.

The use of digital computers to calculate a control action for a continuous, dynamic system introduces the fundamental operation of sampling. If sample rates are fast enough, digital controllers can be made to closely match the performance of their continuous counterparts [86]. In the case of wide-area damping control system design, this becomes the problem of selecting suitable Phasor Measurement Units (PMU) data reporting rates. In other words, how fast these PMU measurements should be sent to the controller. From the viewpoint of control system performance, it's desirable to select sample rates as fast as possible. But the selection of sample rates is a compromise because it is limited by several factors such as the cost of hardware, bandwidth of communication links and capability of available instruments, etc. For the design of wide-area damping controller, the compromise choice is to select the slowest PMU data reporting rate that meets all performance specifications. Today's technologies make it possible to deploy PMUs at strategic locations of the grid and to deliver the signals at a speed of as high as 30 Hz data reporting rate to obtain a coherent picture of the entire network in real time [50].

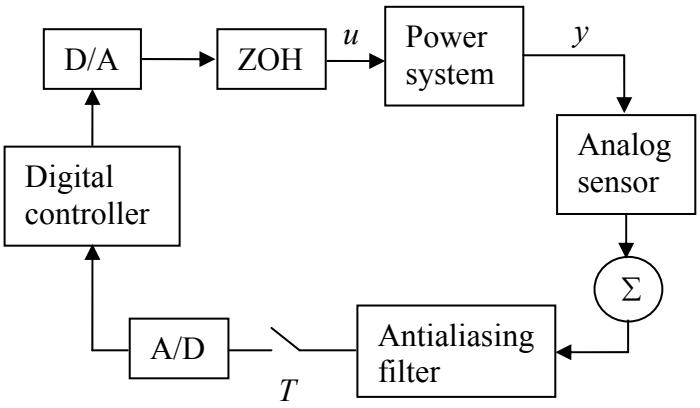

Fig. 3.15 Power systems with digital controllers

Fig. 3.15 is the block diagram showing a power system with digital controllers. The antialiasing filter is used to prevent the aliasing of the higher-frequency components of the signal. Analog measurements are sampled by the analog-to-digital (A/D) converter with the sample period *T*. The D/A converts the discrete control signal to an analog signal, and a zero-order hold (ZOH) maintains that same value throughout the sample period. The resulting control signal *u* is then applied to the actuator in precisely the same manner as the continuous implementation. The performance of a digital control system is depended very much on its sample rate (SR), ω_s . The SR required depends on the closed-loop bandwidth of the system (ω_b). Generally, sample rates should be faster than 30 times the bandwidth in order to assure that the digital controller can be made to closely match the performance of its continuous counterpart. It's desirable to make sample rates as fast as possible. But the selection of sample rates is limited by the cost of hardware, bandwidth of communication links, speed of digital controllers and A/D converters, and available instruments (PMU). The compromise choice is the slowest sample rate that meets all performance specifications.

The single most important impact of implementing a control system digitally is the delay associated with the hold. A delay in any feedback system degrades the stability and damping of the system. Because each value of *u(kT)* is held constant until the next value is available from the controller, the continuous value of *u(t)* consists of steps that, on the average, lag *u(kT)* by *T/2,* as shown by the dashed line in Fig.3. 16.

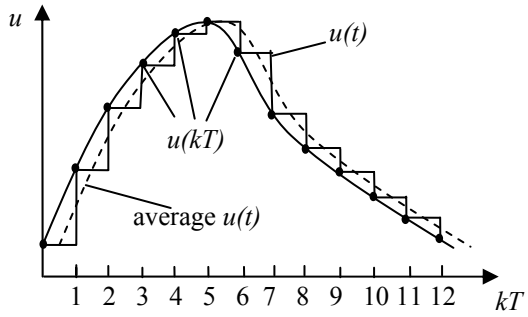

Fig. 3.16 The delay due to the hold operation

In this research, simulations based on discrete models derived from their continuous counterparts are conducted to test sample rate effects. It should be pointed out that neither the continuous model nor the discrete model is the correct one for simulations. Power systems are sampled-data systems where discrete signals appear in some places and continuous signals occur in other parts. The physical reality of power systems is that the digital controller operations are on discrete signals while the power system responses are in the continuous world and in order to consider the behavior of power systems between sample instants it is necessary to consider both the discrete actions of the digital controller and the continuous response of power systems. To do this, time domain simulations using a model that represents the realistic power system with all its nonlinearities is necessary.

Chapter 4. Case Studies

4.1 Two-area Four-machine System

The two-area four-machine system was created to exhibit the different types of oscillations that occur in both large and small interconnected power systems [87]. Detailed model descriptions are given in Appendix *A*. Fig. 4.1 shows the two-area four-machine system. All synchronous machines are modeled with static excitation system, governor and conventional PSS with two lead-lag compensation blocks. The system is stressed by increasing the load at bus 7 to 997 MW and load at bus 9 to 2077 MW. The exporting power P_{tie} from area 1 to area 2 through the tie line is 460 MW and chosen as nominal operating point. The exporting power P_{tie} from area 1 to area 2 is allowed to vary in the range [0-500] MW by varying the loads and generations in each area.

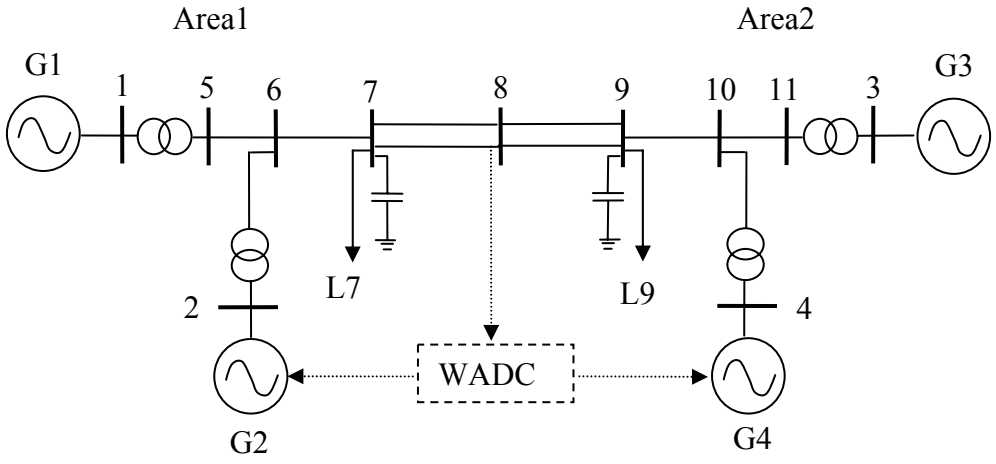

Fig. 4.1 Two-area four-machine test system

4.1.1 Wide-area Damping Controller Design

The design of wide-area damping controller includes the following steps:

1) Full-order Model and Small Signal Analysis: With detailed model, each generator has 9 states and the total order of the nonlinear model is 36. The nominal plant is selected as the power transfer between two areas is 460 MW. Then, the nonlinear model is linearized around this operating point. Small signal analysis shows that this system has a lightly damped inter-area mode $-0.057 \pm 2.9756i$ with frequency 0.4736 and damp ratio 0.0192. The objective of the wide-area damping controller is aimed at achieving acceptable damping for this mode.

2) Selection of Measurements and Control Device Locations: Geometric measures are used to evaluate the comparative strength of candidate signals and the performance of controllers at different locations with respect to this inter-area mode. The candidate input signals are real powers of tie-lines, generator rotor speeds and bus voltage angle difference and center-of-inertia (COI) difference between two areas. Table 4-1 shows the joint controllability/observability measures for all candidate signals and control locations.

Table 4.1: Joint controllability/observability measures (Two-area system)

	P_{6-7}	P_{7-8}	P_{8-9}	P_{9-10}	ω_1	ω_2	ω_3	ω_4	θ_{7-9}	δ_{a1-a2}
G1	0.181	0.193	0.193	0.181	0.042	0.042	0.021	0.021	0.265	0.104
G2	0.775	0.799	0.799	0.775	0.042	0.042	0.021	0.021	0.587	0.947
G3	0.422	0.441	0.441	0.422	0.084	0.024	0.043	0.043	0.315	0.547
G4	0.892	0.916	0.916	0.892	0.084	0.024	0.043	0.043	0.784	1.000

The rows of the table correspond to generators and the columns correspond to measurements. P_{i-j} denotes the real power of transmission line connecting bus *i* and *j*. ω_i denotes the rotor speed of generator *i*. θ_{7-9} denotes the voltage angle difference between bus 7 and 9. δ_{a1-a2} denotes the difference of center-of-inertia (COI) between two areas, which is defined as $\delta_{a1-a2}=\frac{\sum_{i=1}^{2}\delta_i H_i}{\sum_{i=1}^{2}H_i}-\frac{\sum_{j=3}^{4}\delta_j H_i}{\sum_{j=3}^{4}H_j}$, where δ_i and H_i are rotor angle and inertia constant of generator *i*. The results are normalized so that their values are in the range [0 1].

From the calculation results shown in Table 4-1, we have the following conclusions:

1) The most efficient generators for damping the inter-area mode are G4 and G2.
2) The most efficient stabilizing signal is δ_{a1-a2}, the difference of center-of-inertia (COI) between two areas.
3) Real tie-line powers are also suitable stabilizing signals because they have high joint controllability/observability measure.
4) None of single generator rotor speed is good choice for input signals of controller to damp the inter-area mode.

According to the above observation, we may choose generator 2 and generator 4 as our control locations and real power of tie-line from bus 7 to bus 8 as our stabilizing signal. What should be noticed here is that we don't choose the difference of center-of-inertia (COI) between two areas as input signal even though it has the highest measures of

controllability/observability with respect to the inter-area mode. We have several reasons to do so. First, generator states such as rotor angle are hard to obtain while system output like tie-line power are easily obtained by PMUs. This explains why output feedback control is more practical than state feedback in wide-area control system design for power grids. Second, to calculate COI, all generator rotor angles are needed. This increases the cost for measurement devices and communication channels compared to the only measurement of tie-line power. At last, even if we can obtain rotor angles easily and economically, they still need to be synchronized so that the time-delay may be larger than the measurement of tie-line power.

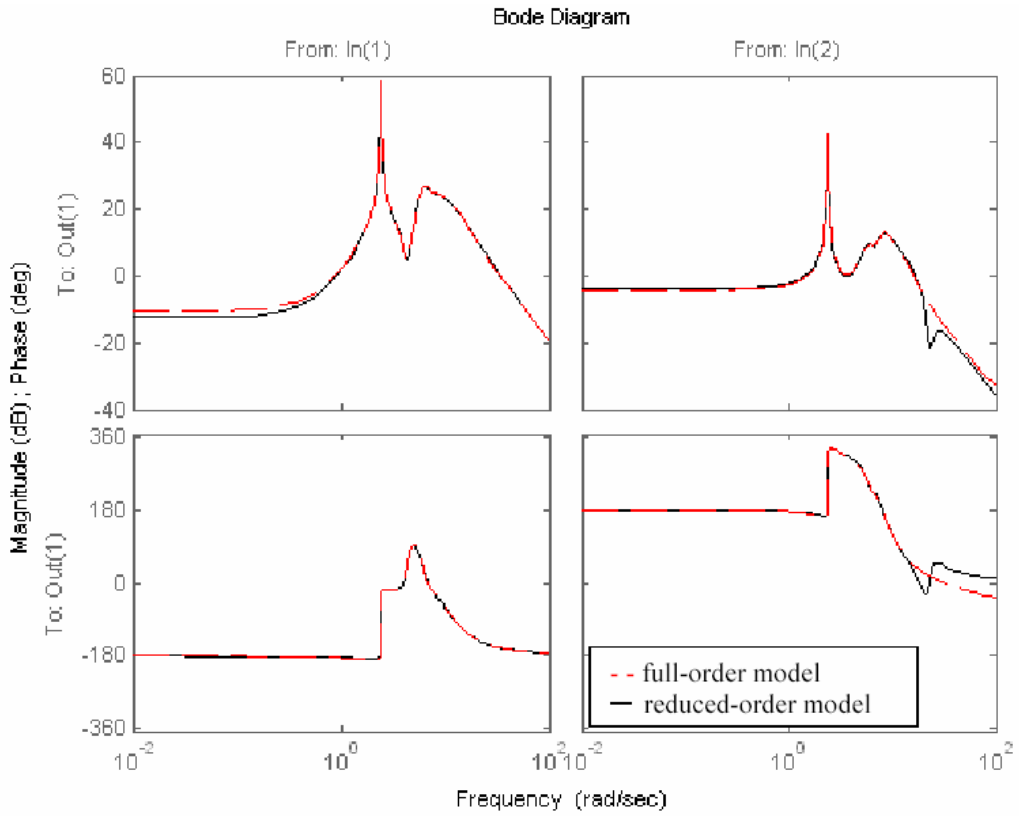

Fig. 4.2 Bode plots comparison of full-order model and reduced-order model (Two-area system)

3) Model Reduction: The order of the original linear model is 36. The LMI approach needs a large amount time for calculation. On the other hand, not all the states of the model are dominant. In fact, no more than a few states can contain the characteristics of this small system. Therefore, balanced model reduction is used to reduce the original high order model to an 8^{th}-order model. The frequency responses of the full-order model and reduced-order model are shown in Fig. 4.2. We can see that for the interested bandwidth, the reduced-order model is reliable for robust controller design.

4) Controller Synthesis: We are now ready to design our robust MIMO controller. The control input signal is real tie-line power $P_{7\text{-}8}$ and control locations are generator 2 and 4, as shown in Fig. 4.1 Two kinds of disturbances are considered. One is the change of the operating point, for example, changes of input mechanical power and voltage reference. The other is exogenous noise effecting on measured feedback signal give by remote phasor measurement units. For this mixed H_2/ H_∞ robust synthesis, H_∞ performance is evaluated by the difference of COI between two areas and H_2 performance is evaluated by the rotor speed of generator 1, which is dirtied by exogenous noise. The pole-placement constraint was specified in terms of a conic sector and two half planes as shown in Fig. 3.10. The inner angle of conic sector is $2\cos^{-1}(0.1)$, which ensures a minimum damping ratio of 0.1 for the inter-area mode. Also, the real part of the poles should large than -50 and less than -0.5. This constraint ensures a fast decay and at the same time a moderate controller gain. Weighting functions are given by:

$$W_1(s) = \frac{10}{s+10}, \quad W_2(s) = 2.0, \quad W_3(s) = \frac{20s+5}{s+20}$$

The *hinfmix* function available in the LMI Control Toolbox [24] was used to perform the necessary computations. After optimization, it is shown that the guaranteed closed-loop

RMS gain (H_∞ norm) is 0.1537 and guaranteed closed-loop H_2 norm is 0.3944. The order of the designed controller by solving the LMIs is the sum of the order of open-loop model and weighting function. Thus, a 12th-order controller is obtained. Balanced model reduction is used again to simplify this controller to an 8th order one. The controller parameters are listed in Appendix C. Fig. 4.3 shows the frequency response of the designed controller.

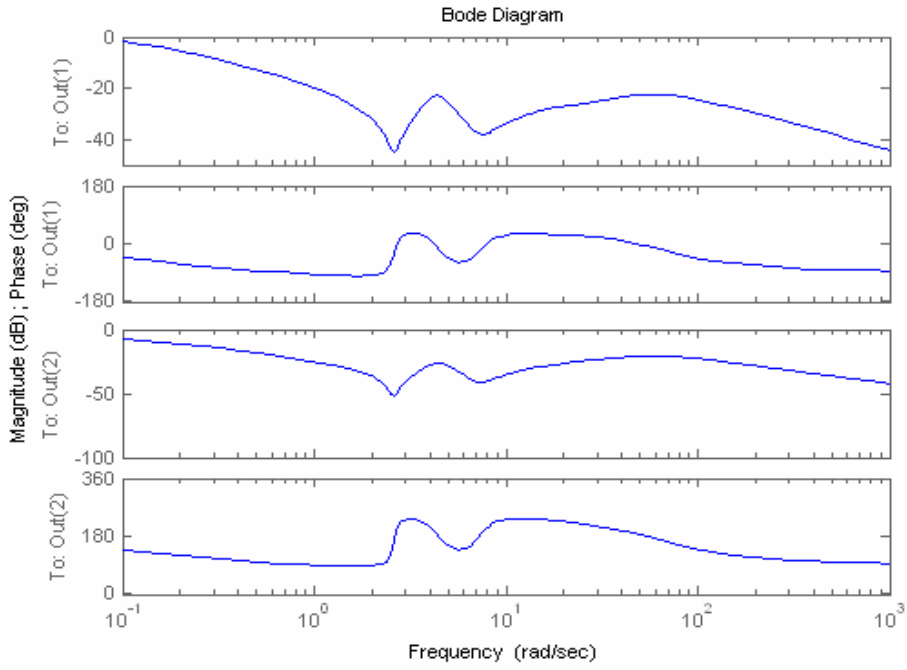

Fig. 4.3 Frequency response of the designed controller (Two-area system)

5) Closed-loop Verification and Nonlinear Time Domain Simulation: The resulting reduced-order controller is first verified by small signal analysis. The damping ratio the inter-area mode is improved to 0.146 under closed-loop conditions. Then, time response of linear closed-loop system is used to verify the performance of the controller. Fig. 4.4 shows the impulse response of the rotor speed deviation of generator 1 without and with

the controller. The impulse signal is added to the input mechanical torque of generator 1. It's seen that the wide-area controller improve the damping greatly.

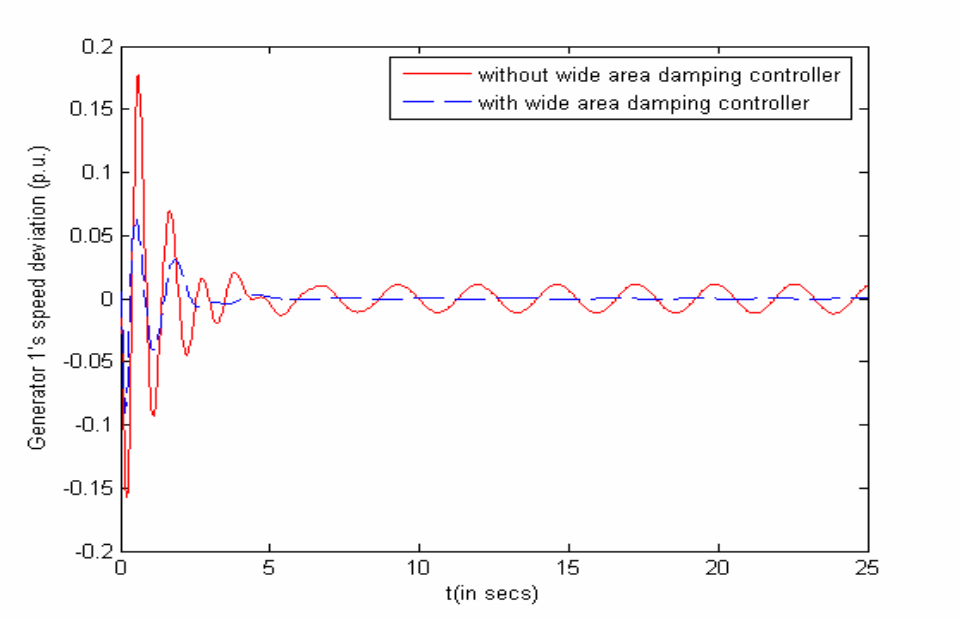

Fig. 4.4 The rotor speed response of generator 1 to impulse disturbance

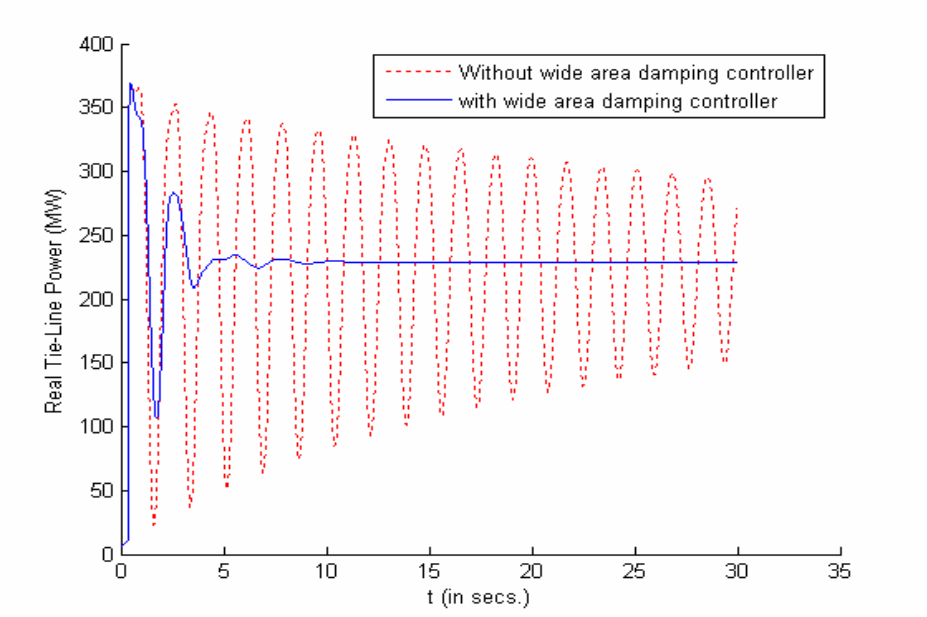

Fig. 4.5 Real tie-line power response to a three phase fault on line8-9

Nonlinear time domain simulations are carried out with TSAT to test the effectiveness, robustness and performance of the designed controller. A three phase short current fault is applied to the line 8-9 for 0.1 sec. Fig. 4.5 shows the real power of tie-line from bus 7 to bus 8 without and with the wide-area damping controller.

4.1.2 Controller Robustness

The robustness of the designed controller is tested by changing operating conditions and fault types. Fig 4.6 shows the real power of tie-line 8-9 response to a three phase fault on bus 8 with a duration of 4 cycles.

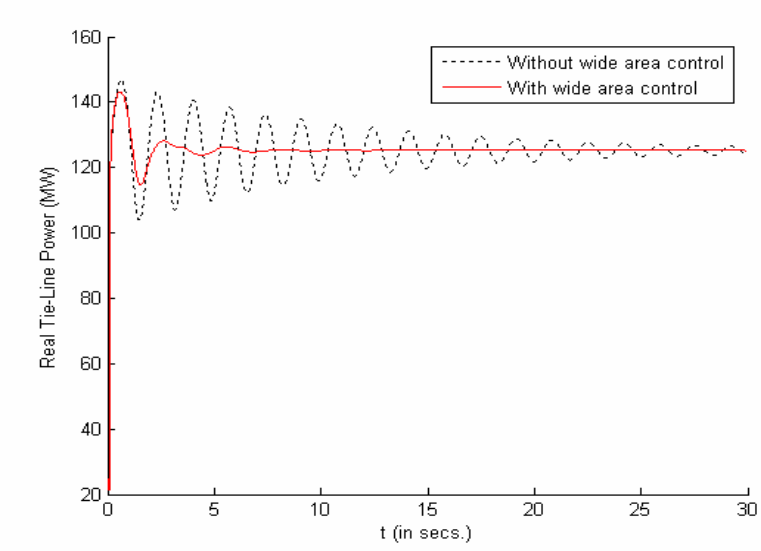

Fig. 4.6 Real power of tie-line 8-9 response to a three phase fault on bus 8

Table 4-2 shows the robustness of the designed controller against changing power flows. Table 4-3, 4-4, 4-5 shows the robustness of the designed controller against different load types with different tie-line flows. Table 4-6 shows the robustness of the controller against different tie-line strength.

Table 4.2: Robustness against different tie-line flows (Two-area system)

P_{79}	-243MW	-60MW	98MW	207MW	500MW	612MW
Frequency	0.607	0.591	0.611	0.603	0.595	0.582
Damping Ratio	2.71%	4.78%	8.56%	10.4%	12.7%	8.91%

Table 4.3: Robustness against different load types (Two-area system)

P_{79} = 500MW	Constant Impedance	Constant Current	Constant Power
Frequency	0.595	0.597	0.601
Damping Ratio	12.7%	12.9%	12.3%

Table 4.4: Robustness against different load types (Two-area system)

P_{79} = 207MW	Constant Impedance	Constant Current	Constant Power
Frequency	0.603	0.615	0.598
Damping Ratio	10.4%	10.7%	10.5%

Table 4.5: Robustness against different load types (Two-area system)

P_{79} = 612MW	Constant Impedance	Constant Current	Constant Power
Frequency	0.582	0.593	0.589
Damping Ratio	8.91%	8.93%	8.91%

Table 4.6: Robustness against different tie-line strength (Two-area system)

P_{79} = 500MW	One line7-8 open	Line7-9 +20%	One line8-9 open	Line8-9 +20%
Frequency	0.536	0.524		0.541
Damping Ratio	5.82%	7.83%	Transient unstable	4.97%

4.1.3 Effects of Time-Delays

The effect of time-delay is first demonstrated by linear simulation using MATLAB. Fig. 4.7 shows the impulse response of rotor speed deviation of generator 1 with wide-area damping controller that can't handle time-delays. Fig. 4.8 shows the impulse response of rotor speed deviation of generator 1 with wide-area damping controller that handles time-delays.

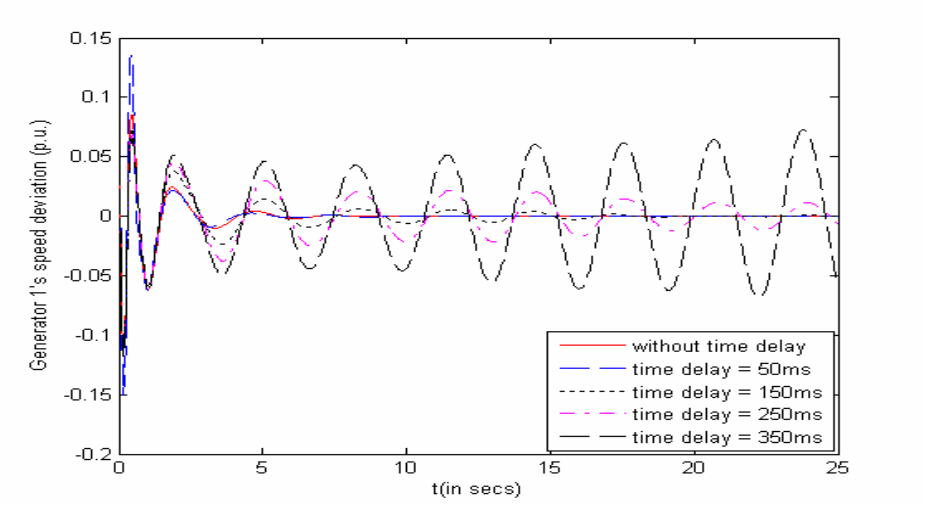

Fig. 4.7 Generator speed deviation with controllers that can't handle time-delays

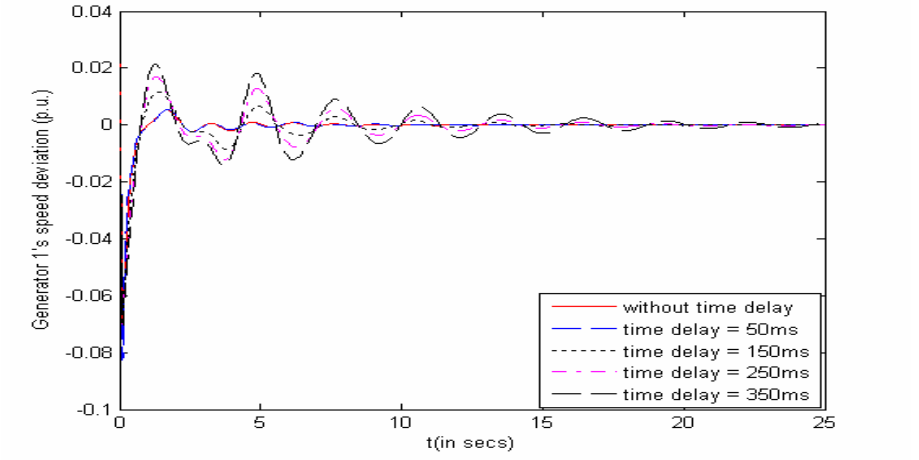

Fig. 4.8 Generator speed deviation with controllers that can handle time-delays

The effects of time-delay are also demonstrated by nonlinear simulation using TSAT. Fig. 4.9 and fig. 4.10 show the active power of tie-line 7-8 responses to a three-phase fault on line8-9 for 0.06s. Without modeling time-delays in the controller design procedure, the system is small signal unstable with a 250 ms time-delay. With the controller that taken time-delays into consideration, the system is small signal stable with a 350 ms time-delay.

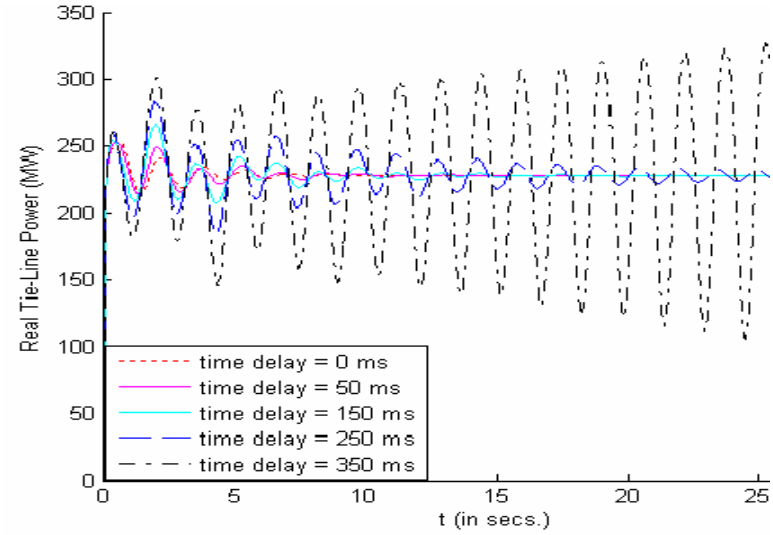

Fig. 4.9 Active tie-line power with controllers that can not handle time-delays.

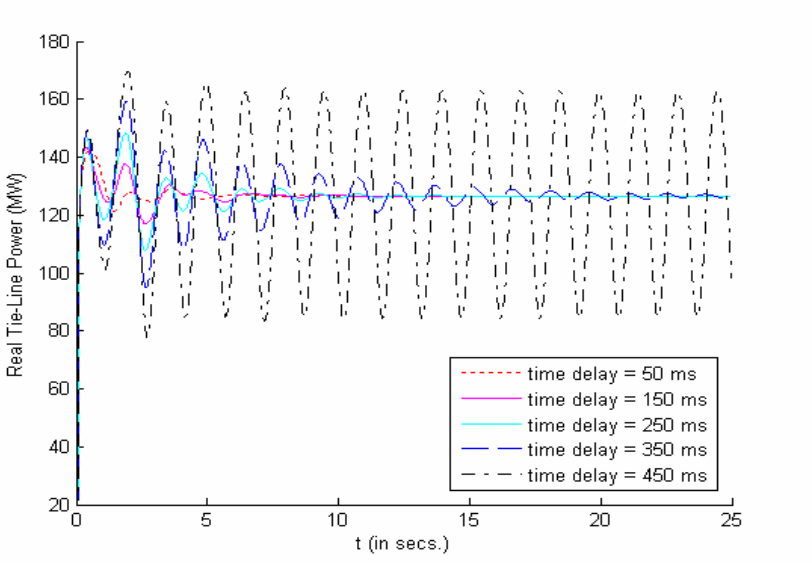

Fig. 4.10 Active tie-line power with controllers that can handle time-delays.

4.1.4 Selection of the Sample Rate for Digital Controller

Simulations using the continuous model can not reveal effects of sample rates of digital controllers. The continuous model is converted into its discrete counterpart for testing sample rate effects. It should be pointed out that neither the continuous model nor the discrete model is the correct one for simulations. Power systems are sampled-data systems where discrete signals appear in some places and continuous signals occur in other parts. The physical reality of power systems is that the digital controller operations are on discrete signals while the power system responses are in the continuous world and in order to consider the behavior of power systems between sample instants it is necessary to consider both the discrete actions of the digital controller and the continuous response of power systems. To do this, time domain simulations using a model that represents the realistic power system with all its nonlinearities is necessary.

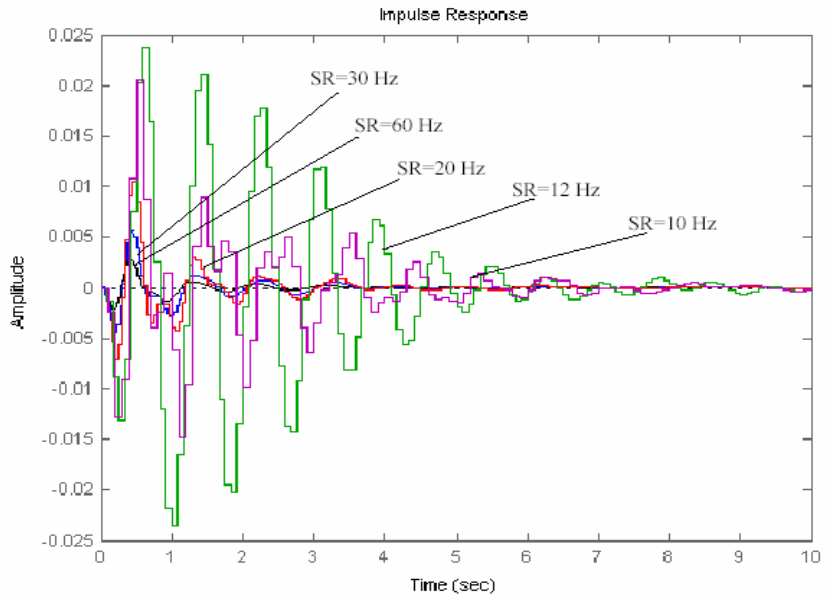

Fig. 4.11 Effects of different sample rates (Two-area system).

The discrete model is first derived from the continuous model used for the controller design. Then this model is used for testing sample rate effects. Fig. 4.11 shows the discrete counterpart of the rotor speed deviation of generator 1 to an impulse disturbance without time-delays. Even though the output generated is discrete, it still can be seen from the figure that the damping decreases as sample rate (SR) is decreased. Fig. 4.12 shows the same simulation with 200 ms time-delay. It can be seen in this figure that in order to achieve a satisfactory damping with such a large time-delay, the sample rate should be at least 30 Hz. Table 4-7 gives the lowest sample rates that ensure acceptable damping for different time-delays. When time-delay is larger than 500 ms, the system is unstable no matter how fast the sample rate is.

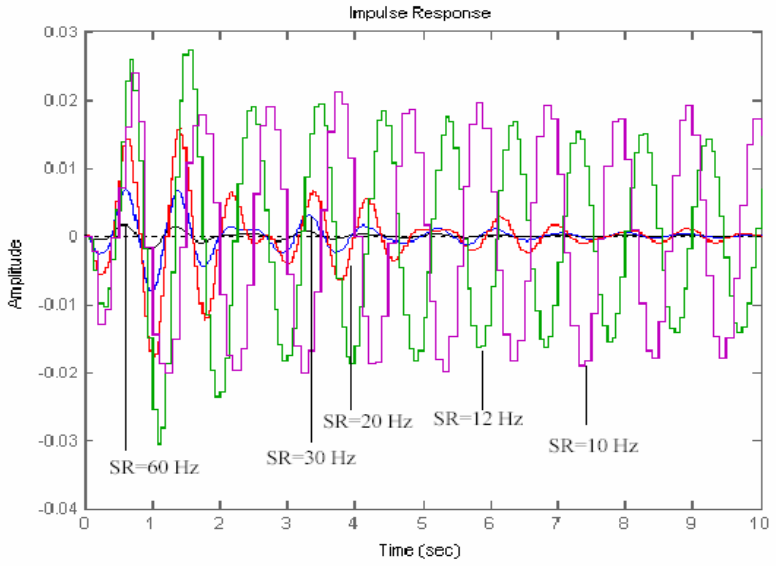

Fig. 4.12 Effects of different sample rates with 200 ms time-delay (Two-area system)

Table 4.7: Sample rates for different time-delays (Two-area system)

Time-delay (ms)	100	200	300	400	500
Sample rate (Hz)	15	20	30	60	--

4.2 New England 39-bus 10-machine System

In this section, a wide-area damping controller is designed for New England 39-bus 10-generator system, which is shown in Fig. 4.13. Detailed model descriptions and all parameters including network data and dynamic data for the generators, excitation systems, PSSs are given in Appendix B. All synchronous machines (except generator 1, which is an equivalent unit) are modeled with static excitation system, governor and conventional PSS with two lead-lag compensation blocks. The system is stressed by increasing the load and generation level.

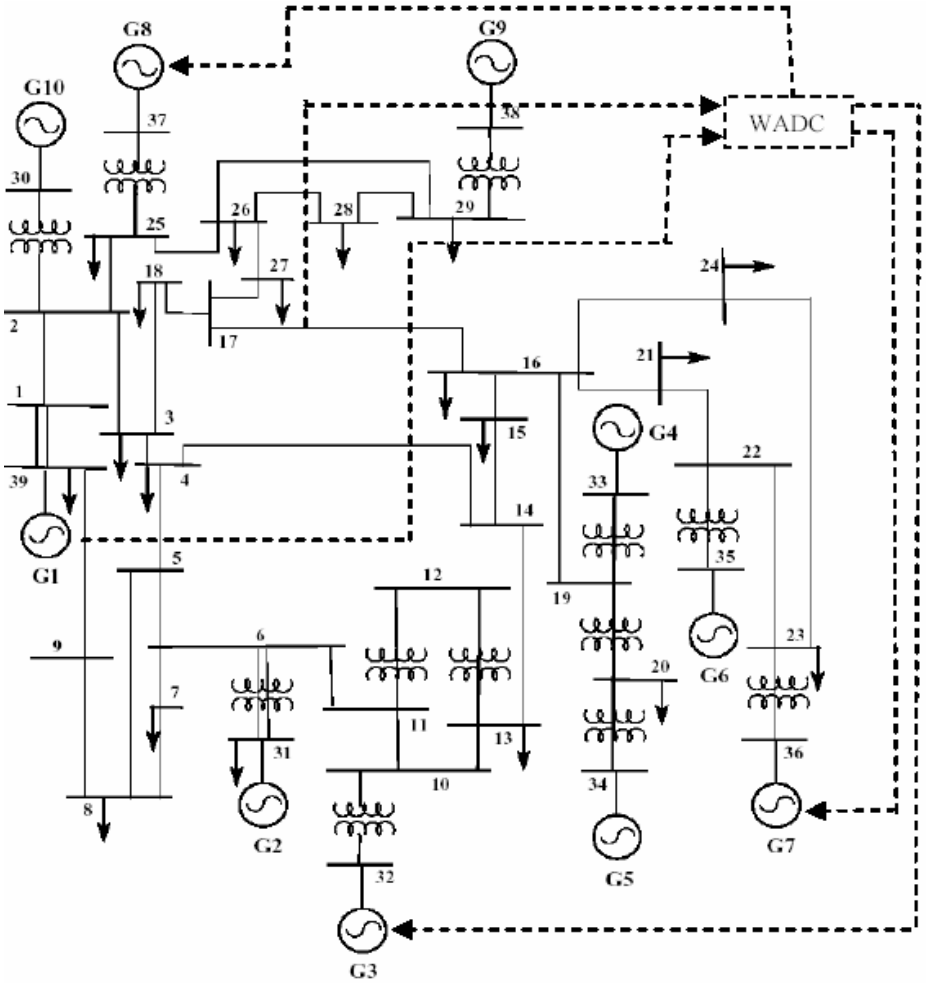

Fig. 4.13 New England 39-bus 10-generator system.

4.2.1 Wide-area Damping Controller Design

1) Full-order Model and Small Signal Analysis: All generators are represented by detailed model, i.e. two-axis model with exciter, governor and conventional PSS (except the equivalent unit G1). The nonlinear model is linearized around a nominal operating point. Small signal analysis shows that this system has several local and inter-area modes with damping ratios less than 10%, which is a widely accepted criterion for satisfactory damping. The classification of these lightly damped modes is shown in Table 4-8. From Table 4-8 we can see that though modes 4 to 8 are local ones. Even though their damping ratios are low, they won't last beyond 10s because of their relatively large frequency. Since an overall system settling time of 10-12 is acceptable, it is not necessary to provide supplemental damping to these modes. The modal graph is shown in Fig. 4.14

Table 4.8: Oscillatory modes for IEEE 39-bus system

Mode Index	Mode Type	Mode Shape	Freq.	Damping Ratio
1	Inter-area	1 vs. all others	0.4879	0.0238
2	Inter-area	(4,5,6,7) vs. (2,3),(8,9,10)	0.7353	0.0215
3	Inter-area	(2,3) vs. (8,9,10)	0.8056	0.0194
4	Local	4 vs. 5, 6, 7	1.4705	0.0443
5	Local	9 vs. 8, 10	1.0736	0.0409
6	Local	2 vs. 3	1.1873	0.0556
7	Local	5 vs. 6, 7	1.0922	0.0518
8	Local	6 vs. 7	1.4354	0.0497

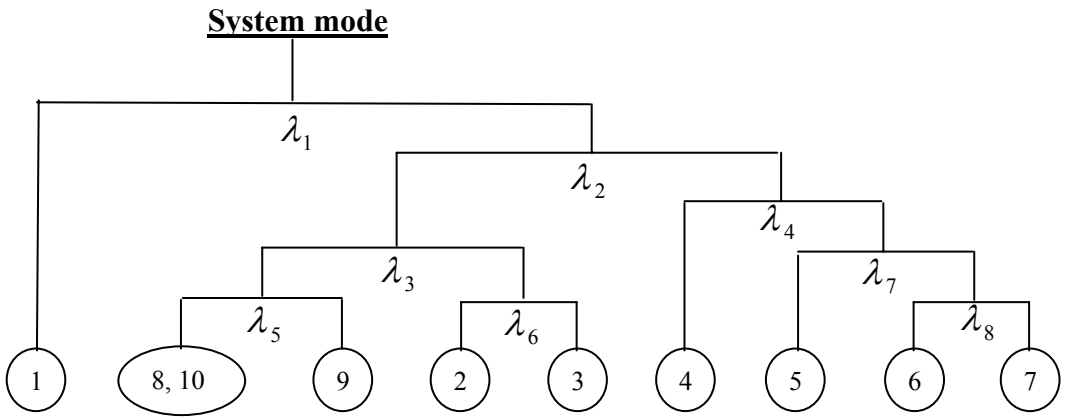

Fig. 4.14 Modal structure of 39-bus 10-generator system.

2) Selection of Measurements and Control Device Locations: From small signal analysis it is seen that the system has three coherent generator groups except the equivalent generator G1. (G2, G3), (G8, G9, G10) and (G4, G5, G6, G7) are nuclei of there groups correspondingly. Geometric measures are used again to evaluate the comparative strength of candidate signals and the performance of controllers at different locations with respect inter-area modes. Several kinds of input signals, such as real powers of transmission lines, generator rotor speeds and bus voltage angle difference and center-of-inertia (COI) difference between different areas, are compared. Table 4-9 shows the control locations with maximum controllability and signals with maximum observability with respect to different inter-area modes, where P_{i-j} denotes the real power of transmission line connecting bus *i* and *j*.

Table 4.9: Maximum controllability/observability measure (IEEE 39-bus system)

Mode Frequency	Maximum Controllability	Maximum Observability
0.4879	G8	$P_{9\text{-}39}$, $P_{1\text{-}2}$
0.7353	G7	$P_{15\text{-}16}$, $P_{16\text{-}17}$
0.8056	G3	$P_{4\text{-}5}$, $P_{9\text{-}39}$

According to Table 4-9, G3, G7 and G8 are selected as control locations. The selection of input signals is not so obvious. We don't want to choose so many measurements as controller inputs because this will increase possible interaction between control loops and the cost for communication links. We choose $P_{16\text{-}17}$ as input signal for mode 2. Since $P_{9\text{-}39}$ has good observability for both mode 1 and mode 3, it is also chosen. As shown in simulation, these two signals are enough for controller inputs to damp inter-area modes. Each tie-line power contains information of all inter-area modes in different levels. In fact, $P_{16\text{-}17}$ itself contains enough information for all three inter-area modes and could be the only input signals for the controller with the cost of higher gain and a little bit worse but still acceptable damping effects.

3) Model Reduction: The original linear model order is 88. It is reduced to a 12^{th} -order model by the method of balanced model reduction. The frequency responses of the full-order model and reduced-order model are shown in Fig. 4.15. We can see that for the interested bandwidth, the reduced-order model is reliable for robust controller design.

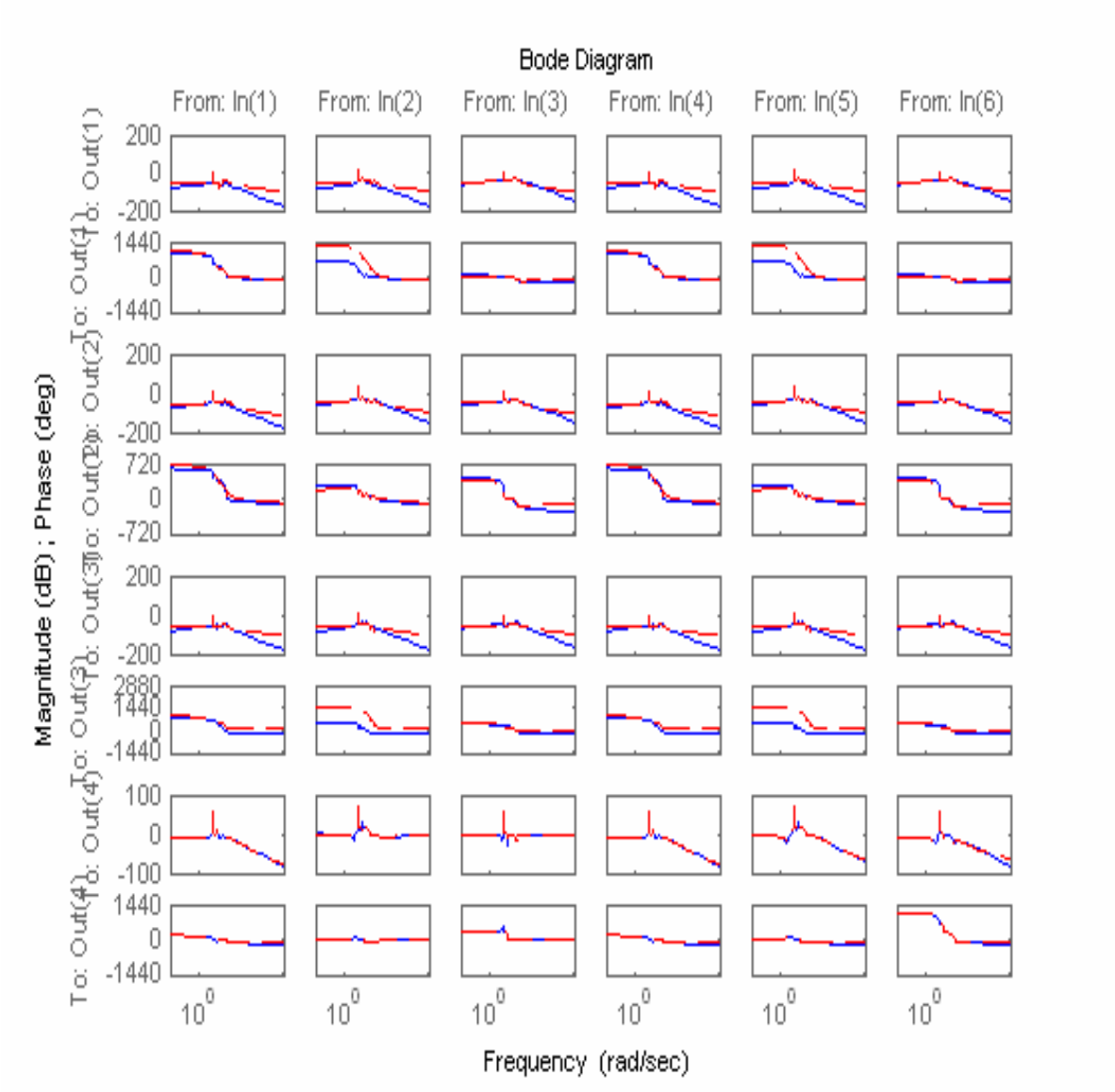

Fig. 4.15 Bode plots comparison of full-order model and reduced-order model.

4) Controller Synthesis: With the control input signals selected as tie-line power $P_{15\text{-}16}$ and $P_{9\text{-}39}$ and control locations are G3, G7 and G8, we may design the wide-area damping controller now. We designed two controllers. The first one has two input signals, $P_{16\text{-}17}$ and $P_{9\text{-}39}$. The second one only has $P_{16\text{-}17}$ as its input. Other design considerations are similar to the controller designed for two-area system.

For the first controller (C1), the guaranteed closed-loop RMS gain (H_∞ norm) is 0.4971 and guaranteed closed-loop H_2 norm is 0.5758. For the second controller (C2), the guaranteed closed-loop RMS gain (H_∞ norm) is 0.7316 and guaranteed closed-loop H_2 norm is 0.8259. The order of the controller is 14, the sum of orders of weighting function and reduced-order model. Balanced model reduction is used again to simplify this controller to a 10th order one. Weighting functions are given by $W_1(s) = \frac{50}{s+50}, \quad W_2(s) = 1.0, \quad W_3(s) = \frac{80s}{s+80}$. The controller parameters are as listed in Appendix C.

The frequency response of controller C1 and C2 are shown in Fig. 4.16 and Fig. 4.17.

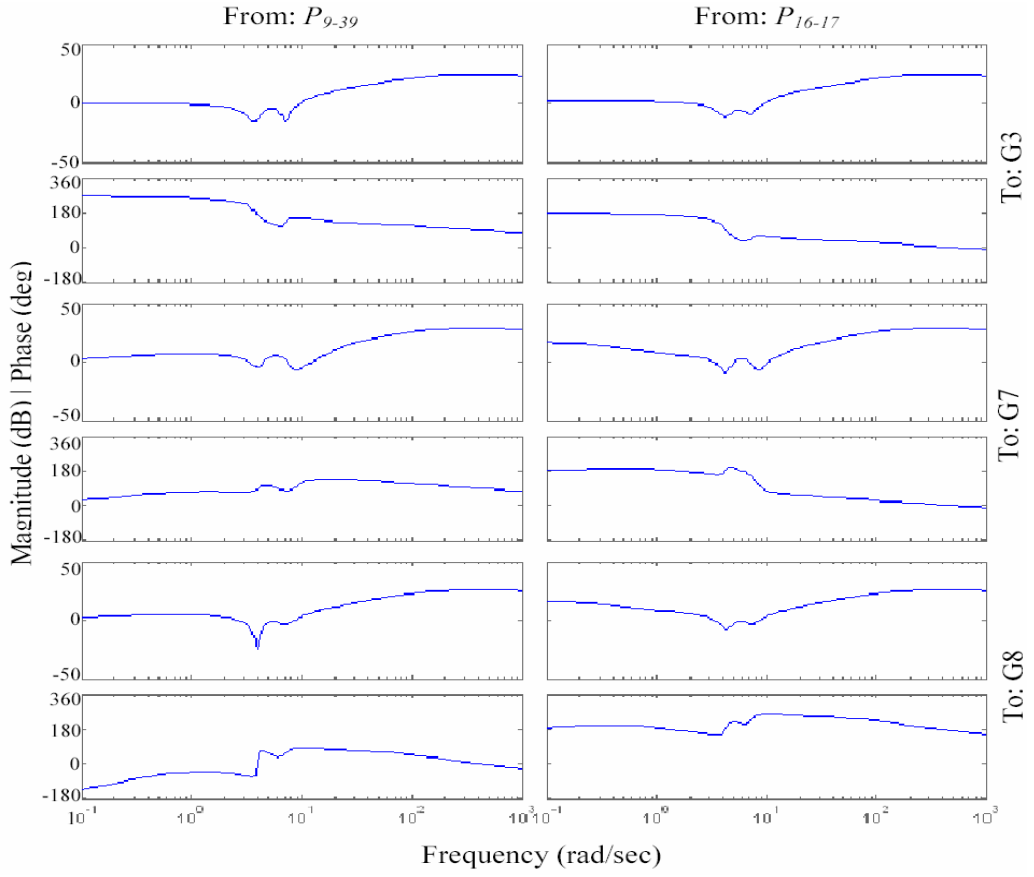

Fig. 4.16 Frequency response of controller C1.

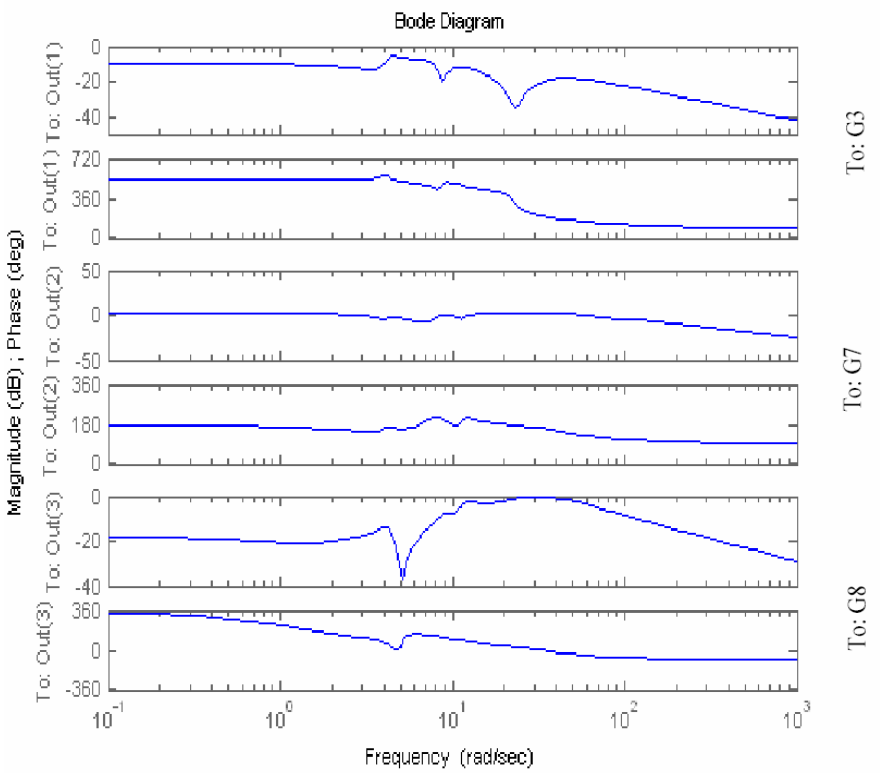

Fig. 4.17 Frequency response of controller C2.

5) Closed-loop Verification and Nonlinear Time Domain Simulation: The resulting reduced-order controllers are first verified by small signal analysis. Table 4-10 shows the improved damping of inter-area modes with wide-area damping controllers.

Table 4.10: Improved damping of inter-area mode (IEEE 39-bus system)

Mode Frequency	Open-loop damping ratio	Closed-loop damping ratio (C1)	Closed-loop damping ratio (C2)
0.4879	0.0238	0.1351	0.1046
0.7353	0.0215	0.2187	0.1842
0.8056	0.0194	0.1893	0.1375

Time response of linear closed-loop system is used to verify the performance of the controller. Fig. 4.18 shows the impulse response of the rotor speed deviation of generator 5 without and with the controllers. The impulse signal is added to the input mechanical torque of generator 5.

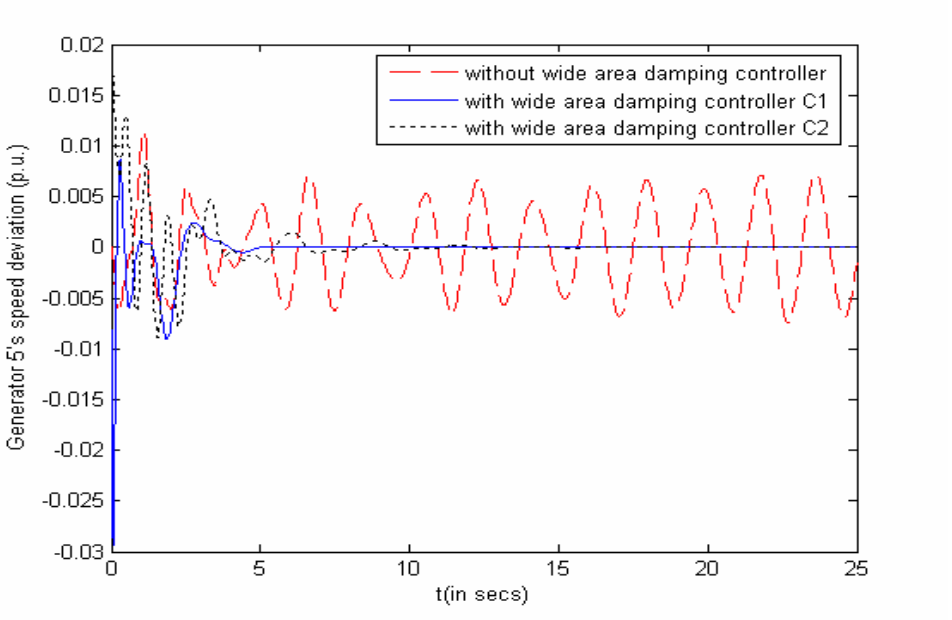

Fig. 4.18 The rotor speed response of generator 5 to impulse disturbance.

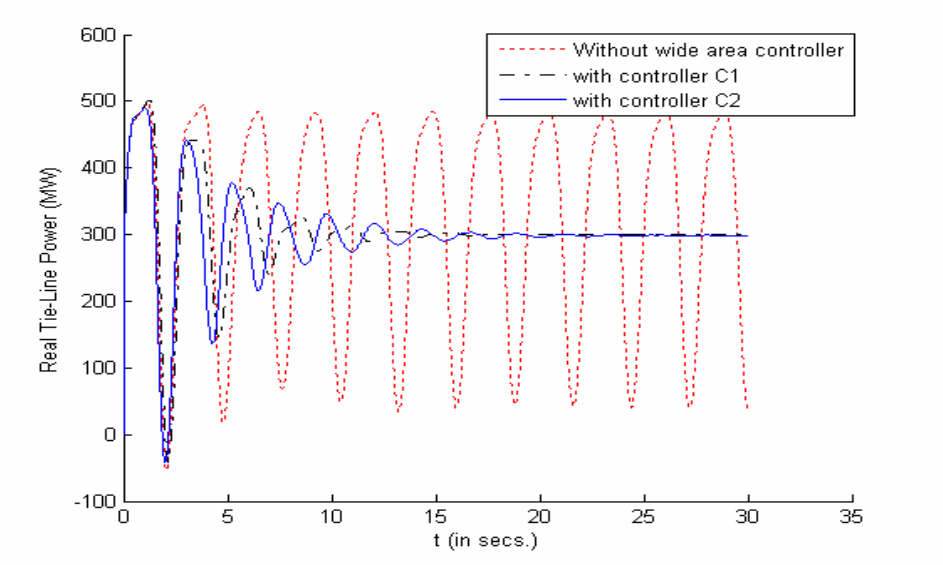

Fig. 4.19 Real power of tie-line 16-17 response to a three phase fault on bus 16.

Nonlinear time domain simulations are carried out with TSAT to test the performance of the designed controllers. A three phase short current fault is applied to the bus 16 for 0.05 sec. Fig. 4.19 shows the real power of tie-line 16-17 without and with the wide-area damping controller.

4.2.2 Controller Robustness

The eigen-analysis of the system was carried out for different operating points to verify the robustness of the designed controller. Table 4-11 displays the robustness of the controller C1 in case of the outage of different heavily loaded lines. Table 4-12 shows the performance of the controller C1 for different tie-line flows between the area containing generator G4, G5, G6 and G7 and the rest part of the system. Same analysis conducted for the system with controller C2 showed that controller C2 also improved the damping of the inter-area modes satisfactorily.

Table 4.11: Damping ratios and frequencies of inter-area modes for different line outages (IEEE 39-bus system)

Line outage	Mode 1		Mode 2		Mode 3	
	ξ	f(Hz)	ξ	f(Hz)	ξ	f(Hz)
16-24	0.1165	0.4252	0.0622	0.7513	0.0583	0.8011
15-16	0.1003	0.4295	0.0597	0.7244	0.0526	0.7972
16-17	0.0947	0.4137	0.0581	0.7396	0.0574	0.7935

Table 4.12: Damping ratios and frequencies of inter-area modes for different power flows (IEEE 39-bus system)

Power flow (MW)	Mode 1		Mode 2		Mode 3	
	ξ	f(Hz)	ξ	f(Hz)	ξ	f(Hz)
300	0.1136	0.4042	0.0523	0.7139	0.0613	0.7832
400	0.1098	0.4153	0.0597	0.7241	0.0604	0.7879
500	0.1072	0.4286	0.0619	0.7169	0.0597	0.7935
600	0.0903	0.4257	0.0606	0.7292	0.0568	0.7798
700	0.0947	0.4145	0.0594	0.7235	0.0541	0.7801

To evaluate the performance and robustness of the designed controllers in different fault scenarios, nonlinear time domain simulations are conducted using TSAT. Controller output limits are $\pm 10\%$ of the synchronous machine terminal voltage.

Two types of faults are simulated. The first type is a three phase short current fault applied to buses for 4 cycles. Several critical buses connected with heavily loaded transmission lines were tested. The second fault type is a three phase short current fault applied to transmission lines for 4 cycles. The fault was cleared by taking out the faulted line. Several critical heavily loaded transmission lines were tested. The two controllers achieved satisfactory damping effects for all of these scenarios.

Fig. 4.20 shows the transient response of the active power of line 16-17 to a three phase fault applied to bus 16. Fig. 4.21 shows the transient response of the active power of line 15-16 to a three phase fault applied to line 16-24. Fig. 4.22 shows the transient response of the active power of line 15-16 to a three phase fault applied to line 16-17. Fig. 4.23 shows the transient response of the active power of line 15-16 to a three phase fault

applied to line 3-18. Fig. 4.24 shows the transient response of the active power of line 15-16 to a three phase fault applied to line 13-14. It can be seen that the damping effect of controller C1 is a little bit better than controller C2. This may be explained as the benefits brought by more measurements, which provide more system dynamic information.

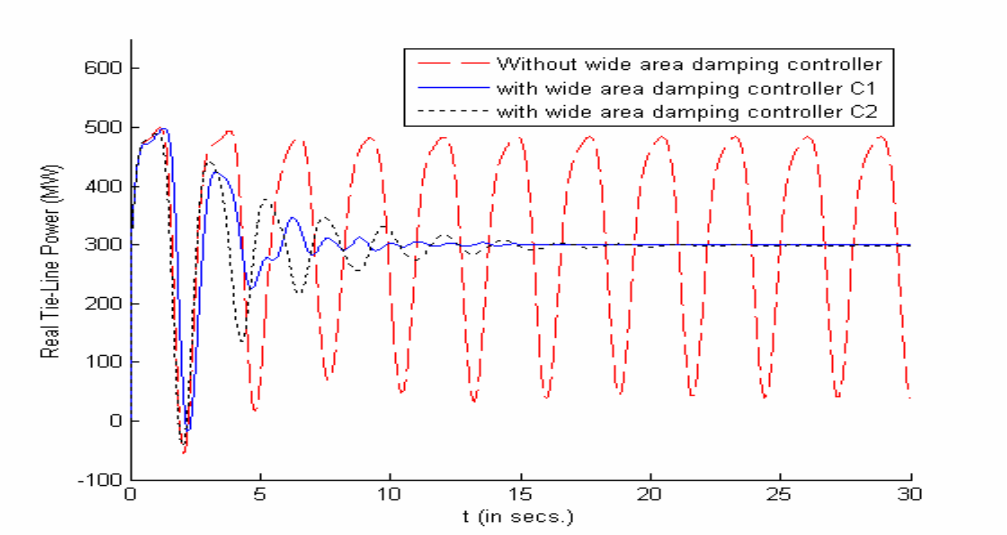

Fig. 4.20 Active power of line 16-17 response to a three phase fault on bus 16.

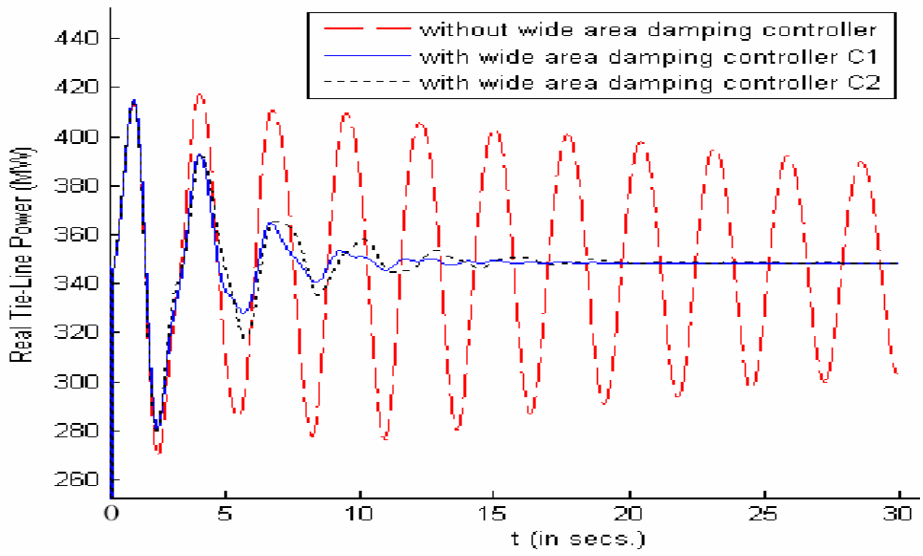

Fig. 4.21 Active power of line 15-16 response to a three phase fault on line 16-24.

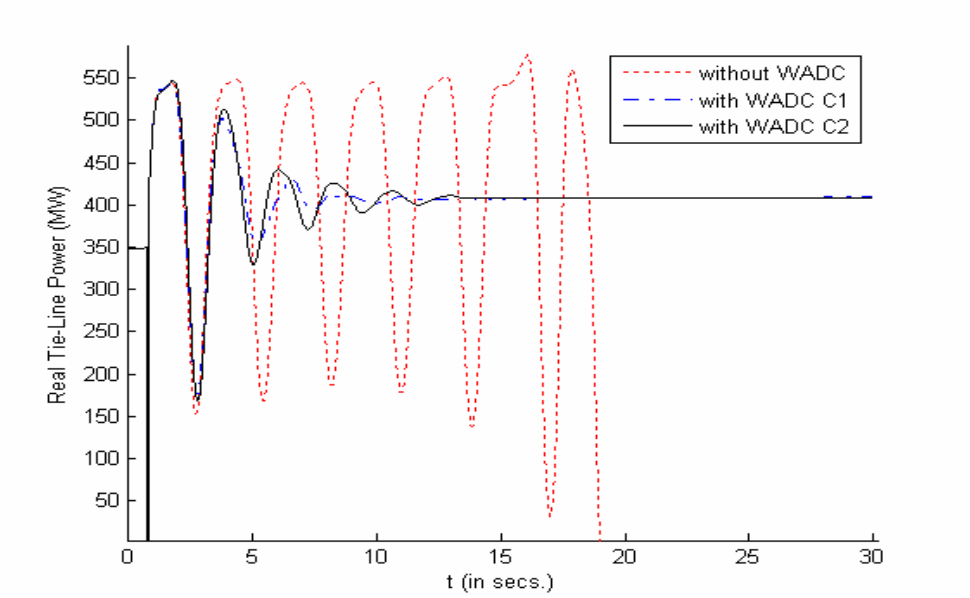

Fig. 4.22 Active power of line 15-16 response to a three phase fault on line 16-17.

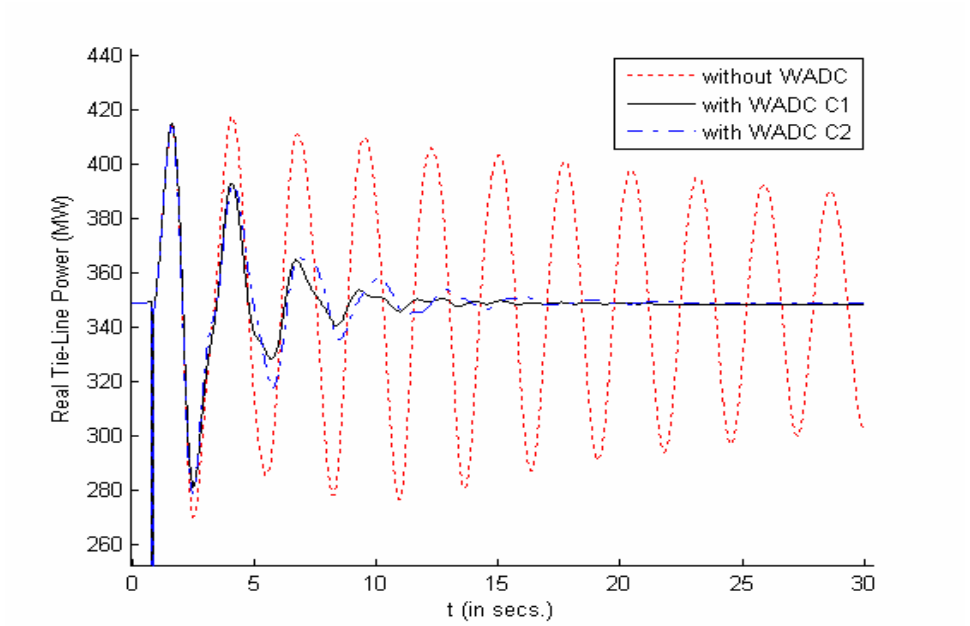

Fig. 4.23 Active power of line 15-16 response to a three phase fault on line 3-18.

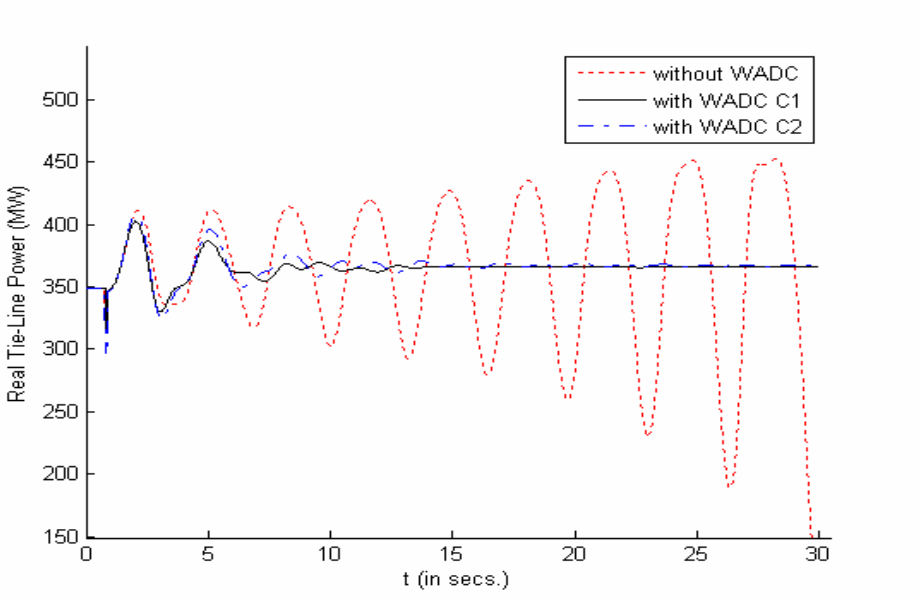

Fig. 4.24 Active power of line 15-16 response to a three phase fault on line 13-14.

4.2.3 Effects of Time-Delays

The effect of time-delays is first demonstrated by linear simulation using MATLAB. Fig. 4.25 shows the impulse response of rotor speed deviation of generator 5 with wide-area damping controller that can't handle time-delays. Fig. 4.26 shows the impulse response of rotor speed deviation of generator 5 with wide-area damping controller that handles time-delays. Without modeling time-delays in the controller design procedure, the system is unstable when time-delays are equal to or larger than 150 ms. While with time-delays modeled in the design procedure, the resulting controller can handle a 350 ms time-delay.

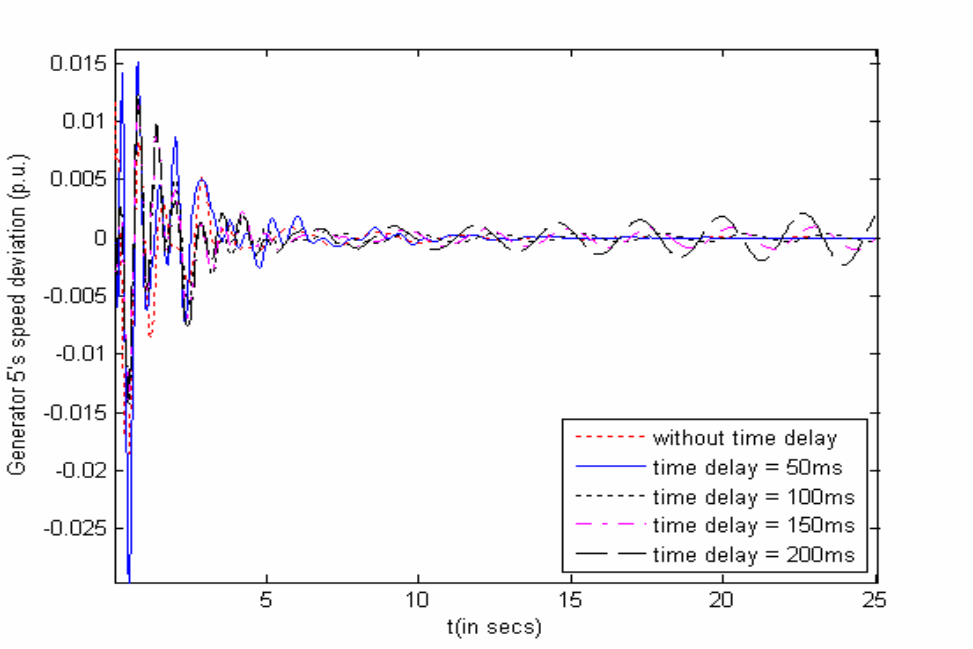

Fig. 4.25 Generator 5' speed deviation with controllers that can't handle time-delays.

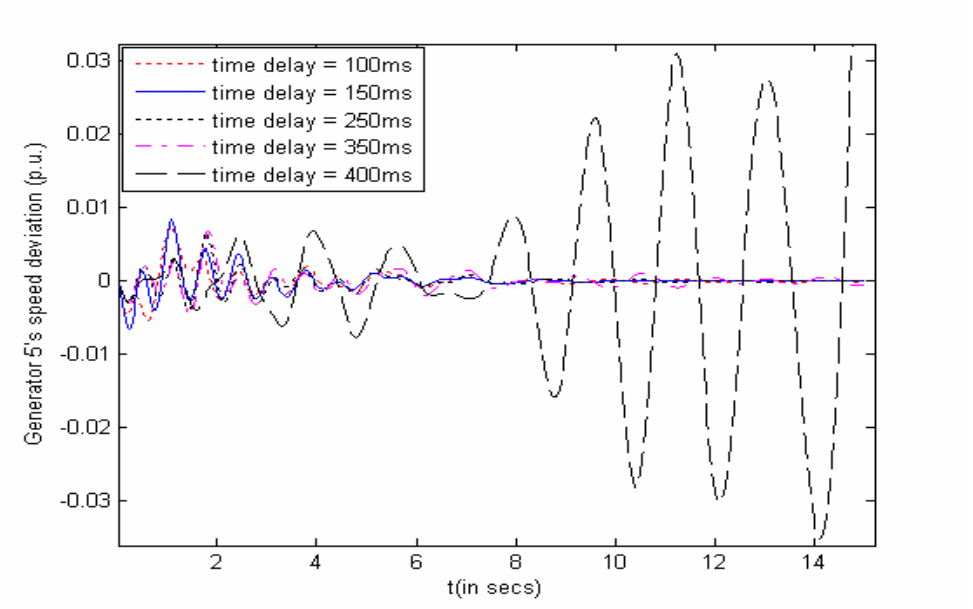

Fig. 4.26 Generator 5' speed deviation with controllers that can handle time-delays.

The effects of time-delays are also demonstrated by nonlinear simulation using TSAT. Fig. 4.27 and Fig. 4.28 show the active power of tie-line 16-17 responses to a three-phase

fault on bus 16 for 0.05s. Without modeling time-delays in the controller design procedure, the damping is unacceptable with a time-delay of 150 ms. With the controller that taken time-delays into consideration, the system is small signal stable with a time-delay as large as 300ms.

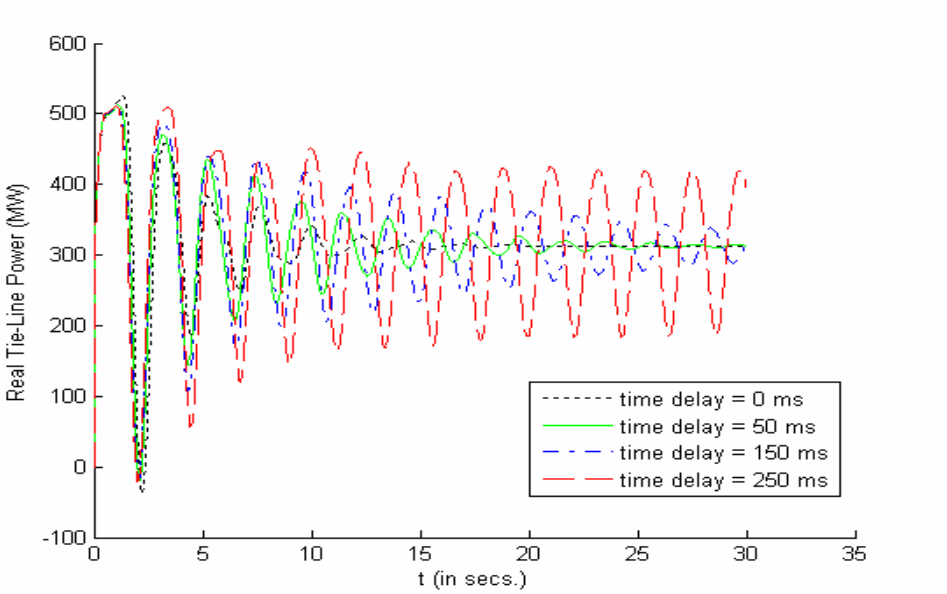

Fig. 4.27 Active power of tie-line 16-17 with controllers that can not handle time-delays

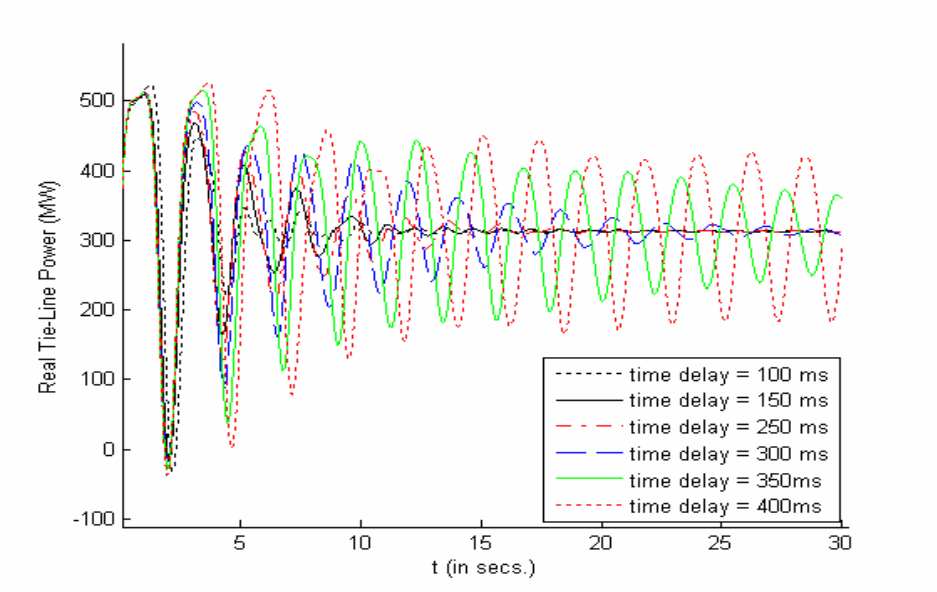

Fig. 4.28 Active power of tie-line 16-17 with controllers that can handle time-delays.

4.2.4 Selection of the Sample Rate for Digital Controller

The discrete model is first derived from the continuous model used for the controller design. Then this model is used for testing sample rate effects. Fig. 4.29 shows the discrete counterpart of rotor speed deviation of generator 5 to an impulse disturbance without time-delays. Even though the output generated is discrete, it still can be seen from the figure that the damping decreases as sample rate is decreased.

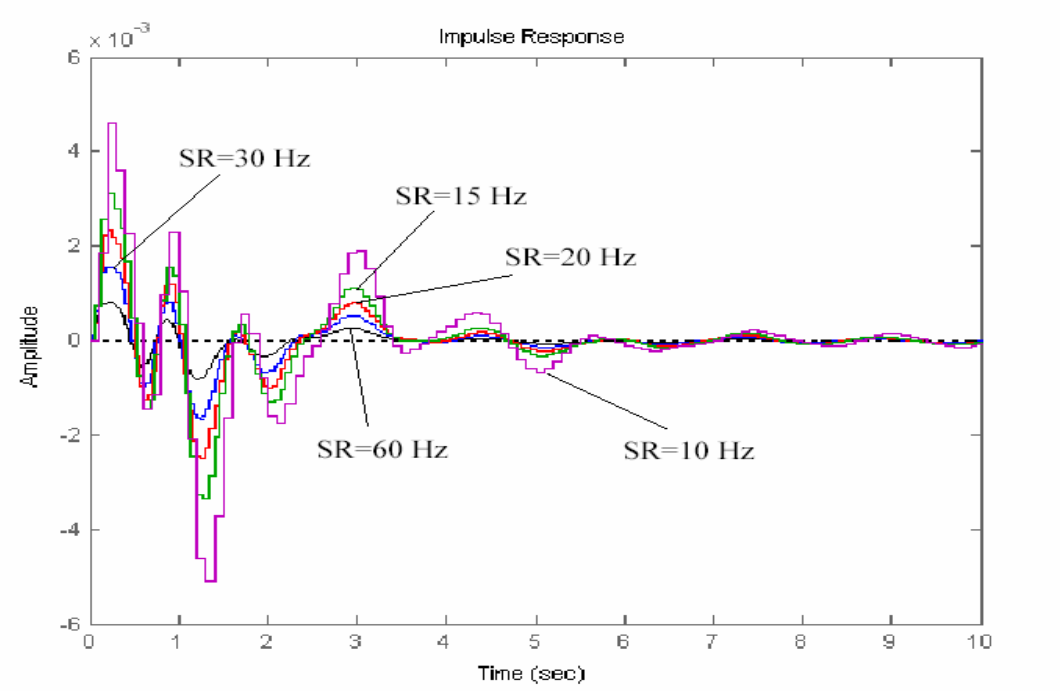

Fig. 4.29 Effects of different sample rates (IEEE 39-bus system).

Time-delay is the most important factor affecting the selection of sample rate. Large time-delays necessitate higher sample rates to achieve acceptable performance. Fig. 4.30 shows the counterpart in the *z*-domain of rotor speed deviation of G5 to an impulse disturbance under different sample rates with a 200 ms time-delay. It can be seen in this

figure that in order to achieve a satisfactory damping with such a large time-delay, the sample rate should be at least 30 Hz.

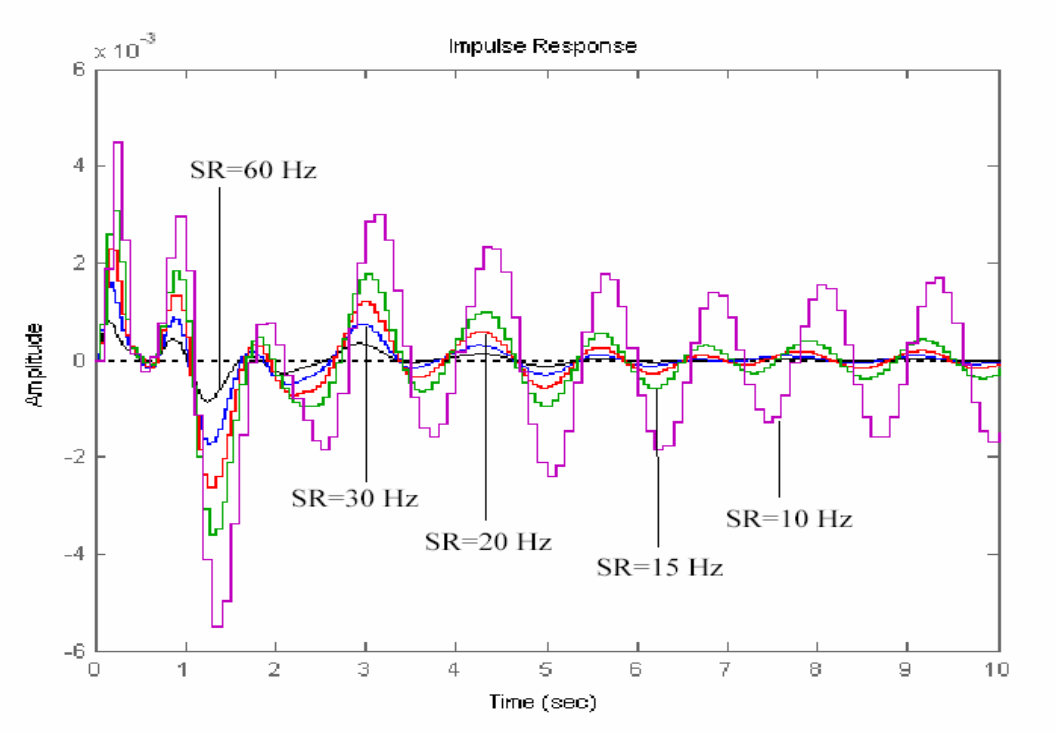

Fig. 4.30 Effects of different sample rates with a 200 ms time-delay (IEEE 39-bus system)

Table 4-13 gives the lowest sample rates that ensure acceptable damping for different time-delays. When time-delay is larger than 300 ms, the system is unstable no matter how fast the sample rate is.

Table 4.13: Sample rates for different time-delays (IEEE 39-bus system)

Time-delay (ms)	50	100	150	200	250	300
Sample rate (Hz)	15	15	30	30	60	120

4.3 WECC 29-generator 179-bus System

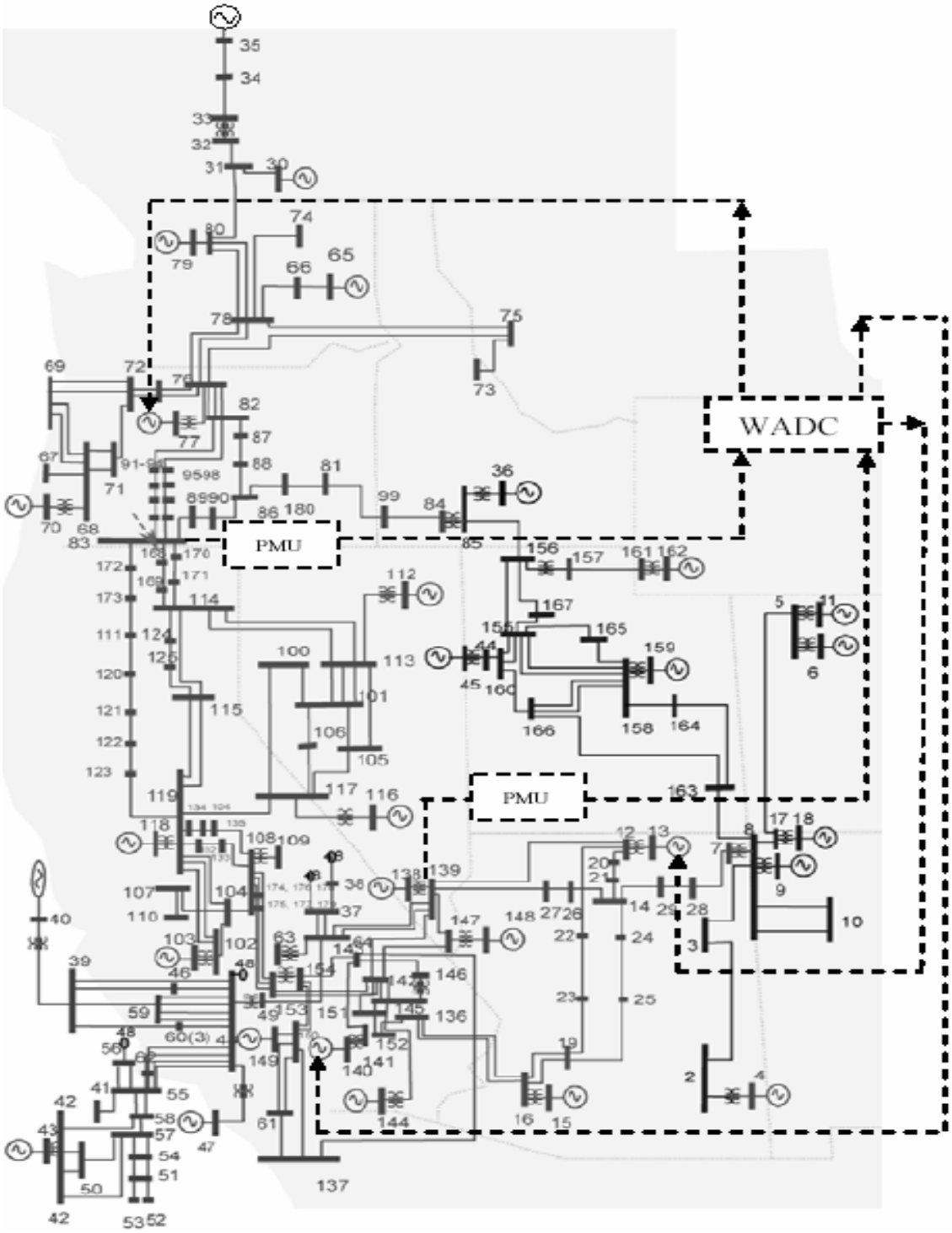

Fig. 4.31 WECC 29-generator 179-bus system one-line diagram.

The 29-generator 179-bus study system, shown in Fig. 4.31, is a reduced order model of the Western Electricity Coordinating Council (WECC) system, which serves 13 U.S. Western states, portions of western Canada and northern Mexico. All 29 generators are equipped with conventional, local power system stabilizers (PSS).

The heavy power transfers from the Pacific Northwest and Arizona into California cause two troublesome modes in the WECC system. The first one is associated with the Pacific AC Intertie (PACI) which transmits hydro generation from the Pacific Northwest and Canada to Central and Southern California. This mode is the source of unstable oscillations around 0.3 Hz, including the one broke up the WECC system on August 10, 1996 [89]. The second one is the source of undamped oscillations around 0.7 Hz when there are high power transfers from Arizona to California [90].

4.3.1 Wide-area Damping Controller Design

1) Full-order Model and Small Signal Analysis*:* All generators are represented by the detailed model, i.e. the two-axis model with exciter, governor and conventional PSS. The model is linearized around a nominal operating point. At this operating point, the system has a total generation of 61650 MW and 12448 MVAR, with 3153 MW transferred from Pacific Northwest to California through PACI and 3652 MW transferred from Arizona to California through California-Arizona corridor. Small signal analysis shows that at this operating point, both PACI mode (0.3 Hz mode) and California/Arizona mode (0.7 Hz mode) are poorly damped, as shown in Table 4-14.

Table 4.14: Inter-area modes of the study system (WECC system)

Mode	Frequency (Hz)	Damping ratio
PACI	0.287	0.042
California/Arizona	0.695	0.023

2) Selection of Measurements and Control Device Locations: Geometric measures of modal controllability/observability are used to select measurements and control sites. The results are shown in Table 4-15. The active power on the intertie connecting bus #83 and #170 has the maximum observability for the PACI mode and the active power on the intertie connecting bus #12 and #139 has the maximum observability for the California/Arizona mode. They are selected as the input signals. The selection of control sites takes some practical considerations, like generator types and locations, into account. Generator at bus #15 can't be chosen as control sites because it's a nuclear plant. Generator at bus #30 isn't selected because its location is far away and large time-delay will be caused in control signal transmissions. Generators at bus #13, #77 and #140 are chosen as control sites. Thus, the designed wide-area damping controller has two inputs and three outputs, as shown in Fig. 4.31.

Table 4.15: Maximum controllability and observability measures for WECC system

Mode	Maximum Controllability	Maximum Observability
PACI	Generators at bus #30, #77	$P_{83\text{-}170}$
California/Arizona	Generators at bus #15, #140 and #13	$P_{12\text{-}139}$

3) Model Reduction: The order of the original linear model is 376. It is reduced to a 24^{th} -order model by the method of balanced model reduction via the Schur method provided by the robust control toolbox in Matlab.

4) Controller Synthesis: The synthesis of the damping controller is defined as a problem of mixed H_2/H_∞ output-feedback control with regional pole placement and is resolved by the LMI approach. The *hinfmix* function available in the LMI Control Toolbox of Matlab was used to perform the necessary computations.

5) Closed-loop Verification and Nonlinear Time Domain Simulation: The performance of the designed controller is verified by eigenvalue analysis of the closed-loop system and linear simulations. Table 4-16 shows the improved damping of inter-area modes with the wide-area damping controller. Fig. 4.32 shows the impulse response of the rotor speed deviation of generator at bus #15 without and with the wide-area damping controller. Nonlinear time domain simulations are carried out with TSAT to test the performance of the designed controller. A three phase short current fault is applied to the bus #83 for 0.05 sec. Fig. 4.33 shows the real power of tie-line 83-170 (PACI) without and with the wide-area damping controller.

Table 4.16: Frequencies and damping ratios of the inter-area modes (WECC system)

Mode	Open-loop		Closed-loop	
	f(Hz)	ξ	f(Hz)	ξ
PACI	0.287	0.042	0.294	0.113
California/Arizona	0.695	0.023	0.702	0.154

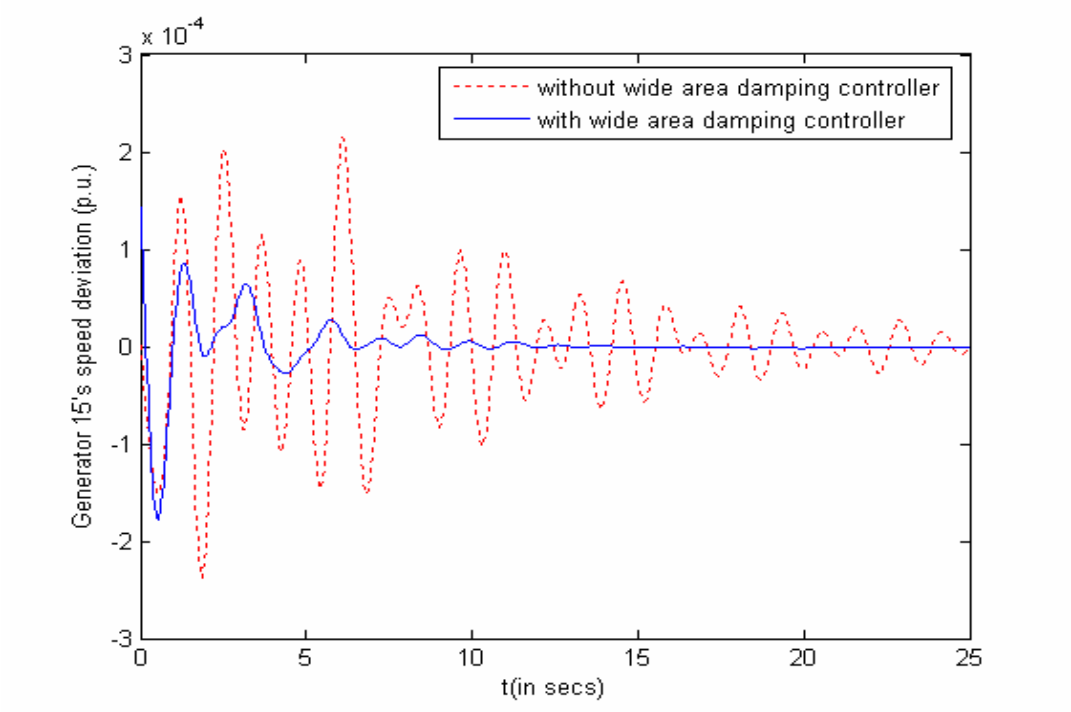

Fig. 4.32 The rotor speed response of generator 15 to impulse disturbance.

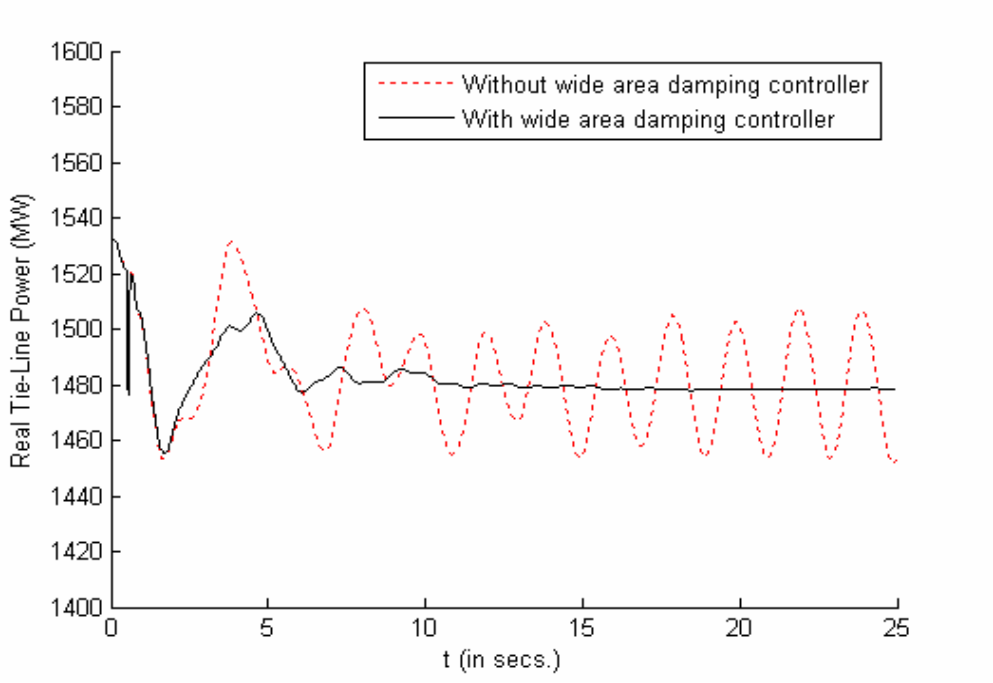

Fig. 4.33 Active power of line 83-170 response to a three phase fault on bus #83.

4.3.2 Controller Robustness

The eigen-analysis of the system was carried out for different operating points to verify the robustness of the designed controller. Table 4-17 displays the robustness of the controller in case of the outage of different heavily loaded lines. Table 4-18 shows the performance of the controller for different PACI flows with 3652 MW transferred from Arizona to California through California-Arizona corridor. Table 4-19 shows the performance of the controller for different flows between California and Arizona with 3153 MW transferred from Pacific Northwest to California through PACI.

Table 4.17: Damping ratios of inter-area modes for different line outages (WECC)

Line outage	PACI mode		California/Arizona mode	
	f(Hz)	ξ	f(Hz)	ξ
16-136	0.279	0.106	0.691	0.132
48-59	0.291	0.111	0.704	0.143
76-78	0.285	0.107	0.683	0.127
115-128	0.274	0.102	0.697	0.125

Table 4.18: Damping ratios and frequencies of inter-area modes for different PACI power flows

PACI power flow (MW)	PACI mode		California/Arizona mode	
	f(Hz)	ξ	f(Hz)	ξ
2975	0.312	0.114	0.711	0.145
3107	0.304	0.111	0.704	0.156
3453	0.293	0.102	0.708	0.154
3769	0.285	0.097	0.707	0.152
3980	0.278	0.083	0.703	0.147

Table 4.19: Damping ratios and frequencies of inter-area modes for different California/Arizona corridor power flows

California/Arizona power flow (MW)	PACI mode		California/Arizona mode	
	f(Hz)	ξ	f(Hz)	ξ
3415	0.306	0.103	0.711	0.141
3659	0.294	0.112	0.702	0.152
3823	0.297	0.111	0.699	0.143
4196	0.289	0.108	0.694	0.127
4370	0.288	0.105	0.685	0.118

Nonlinear time domain simulations are conducted using TSAT to show the robustness of the designed controller for different fault scenarios. Fig. 4.34 shows the transient response of the active power of line 27-139 to a three phase fault applied to line 16-136. Fig. 4.35 shows the transient response of the active power of line 12-139 to a three phase fault applied on bus #139 for 4 cycles. Fig. 4.36 shows the transient response of the active power of line 15-16 to a three phase fault applied to one of the double circuit line 76-78 for 4 cycles. The fault is cleared by taking out the faulted circuit.

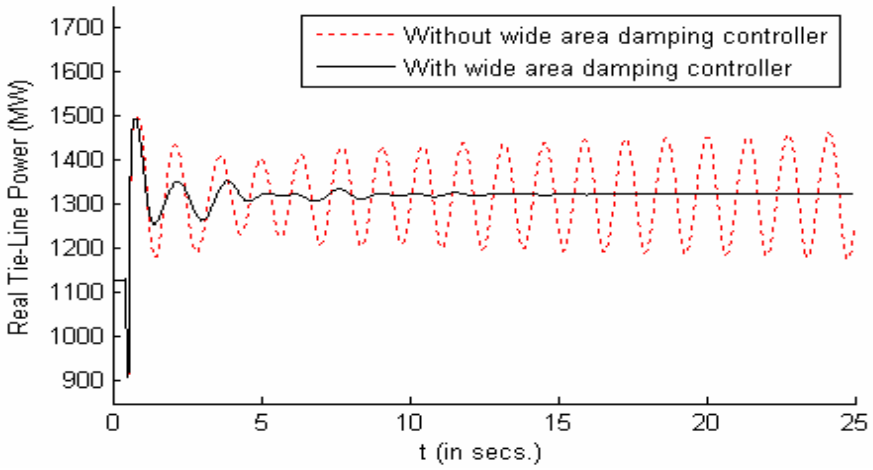

Fig. 4.34 Active power of line 27-139 response to a three phase fault on line 16-136.

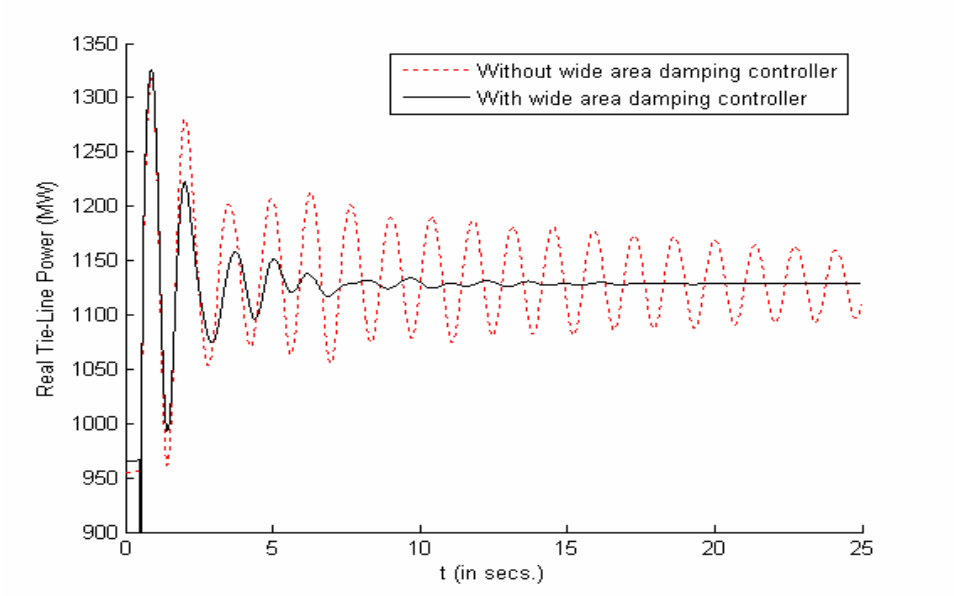

Fig. 4.35 Active power of line 12-139 response to a three phase fault on bus #139.

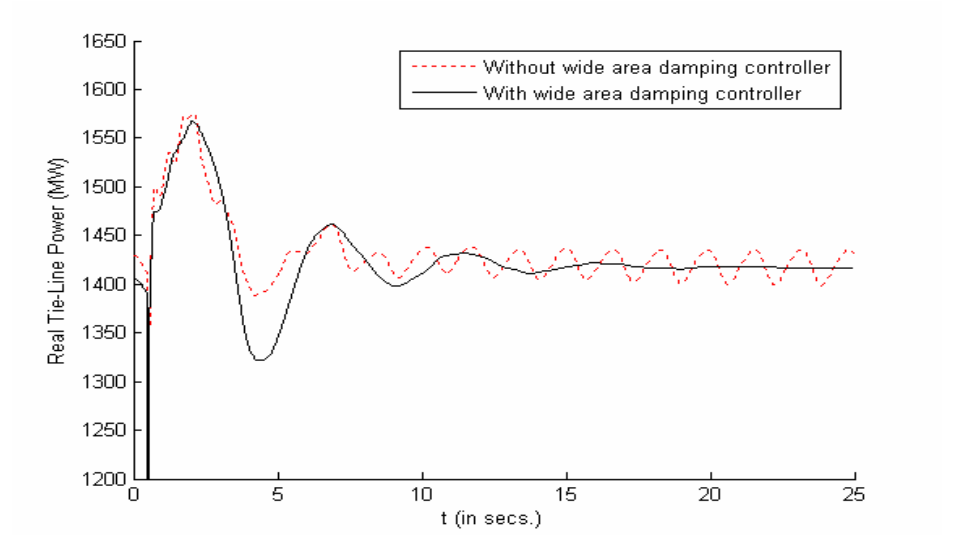

Fig. 4.36 Active power of line 83-172 response to a three phase fault on line 76-78

4.3.3 Effects of Time-Delays

The effect of time-delays is first demonstrated by linear simulation using MATLAB. Fig. 4.37 shows the impulse response of rotor speed deviation of generator 15 with wide-area

damping controller that can't handle time-delays. Fig. 4.38 shows the impulse response of rotor speed deviation of generator 15 with wide-area damping controller that handles time-delays. Without modeling time-delays in the controller design procedure, the system is unstable when time-delays are equal to or larger than 100 ms. While with time-delays modeled in the design procedure, the resulting controller can handle a 300 ms time-delay.

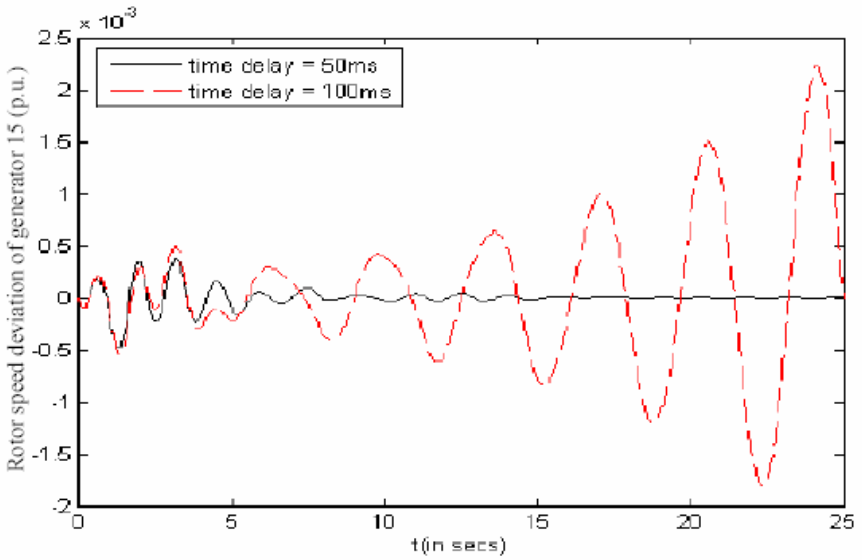

Fig. 4.37 Time-delay effects without time-delays considered in controller design (WECC).

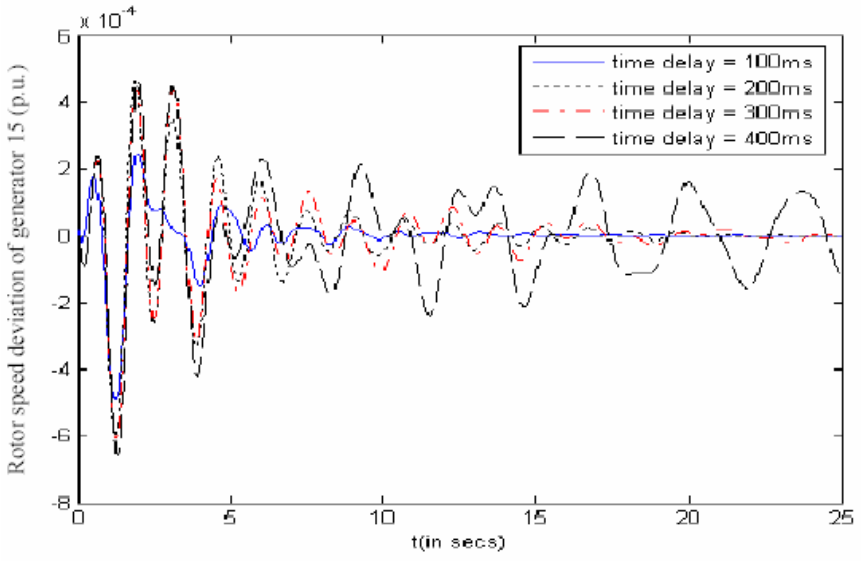

Fig. 4.38 Time-delay effects with time-delays considered in controller design (WECC).

The controller was tuned and its performance in the actual nonlinear power system was evaluated by time domain simulation using TSAT. Fig. 4.39 shows PACI tie-line flow for three phase fault on bus #83 with different time-delays. Fig. 4.40 shows active power flow of line 27-139 for three phase fault on line 16-136 with different time-delays. From the simulations we can see that the wide-area damping controller can handle time-delays as large as 300ms. The system is unstable when the time-delay is larger than 400ms.

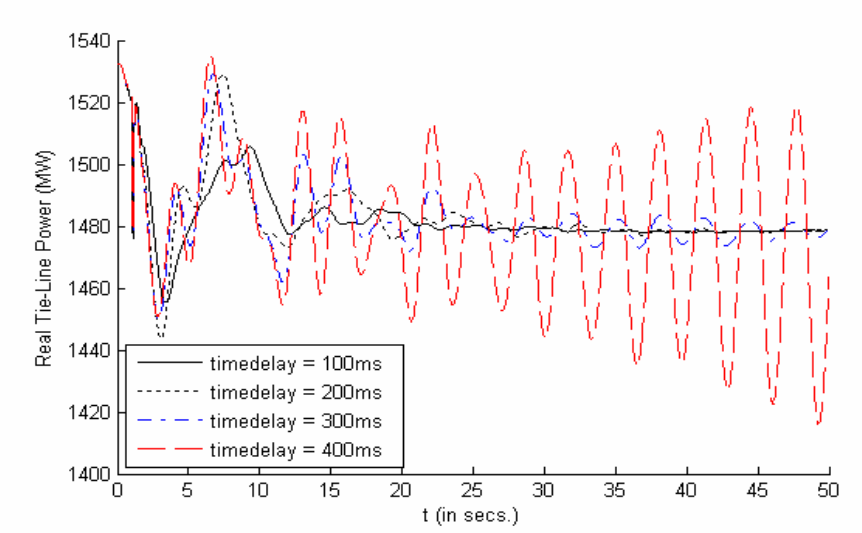

Fig. 4.39 Active power of line 83-170 response to a three phase fault on bus #83 with different time-delays

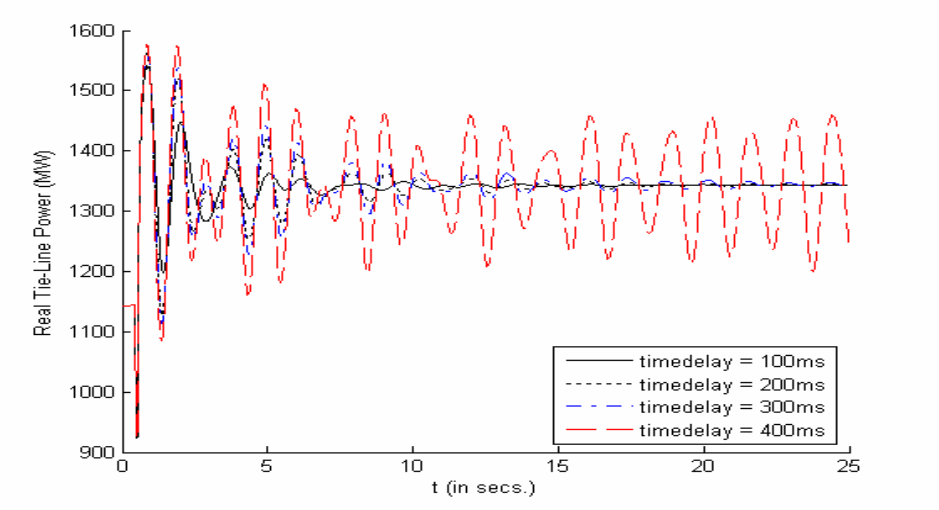

Fig. 4.40 Active power of line 27-139 response to a three phase fault on line 16-136 with different time-delays.

4.3.4 Selection of the Sample Rate for Digital Controller

The discrete model is first derived from the continuous model used for the controller design. Then this model is used for testing sample rate effects. Fig. 4.41 shows the discrete counterpart of rotor speed deviations of generator 15 to an impulse disturbance without time-delays. Fig. 4.42 shows the discrete counterpart of rotor speed deviations of generator 15 to an impulse disturbance with a 100ms time-delay. Fig. 4.43 shows the discrete counterpart of rotor speed deviations of generator 15 to an impulse disturbance with a 200ms time-delay. Base on linear simulations, we find the lowest sample rates that ensure system stability for different time-delays, which is shown in Table 4.20. When time-delays are larger than 350 ms, the system is unstable no matter how fast the sample rate is.

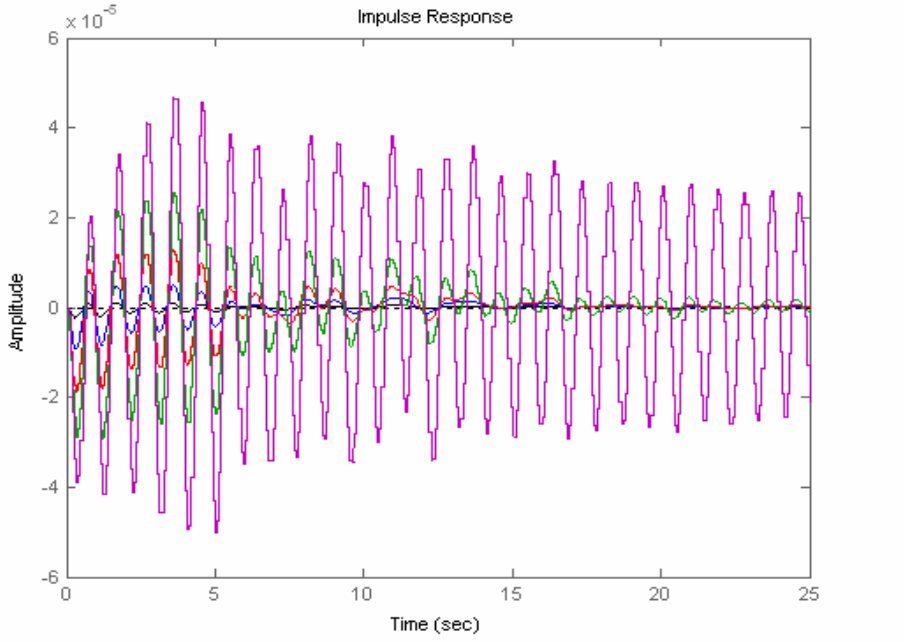

Fig. 4.41 Damping effects for different sampling rates without time-delays.

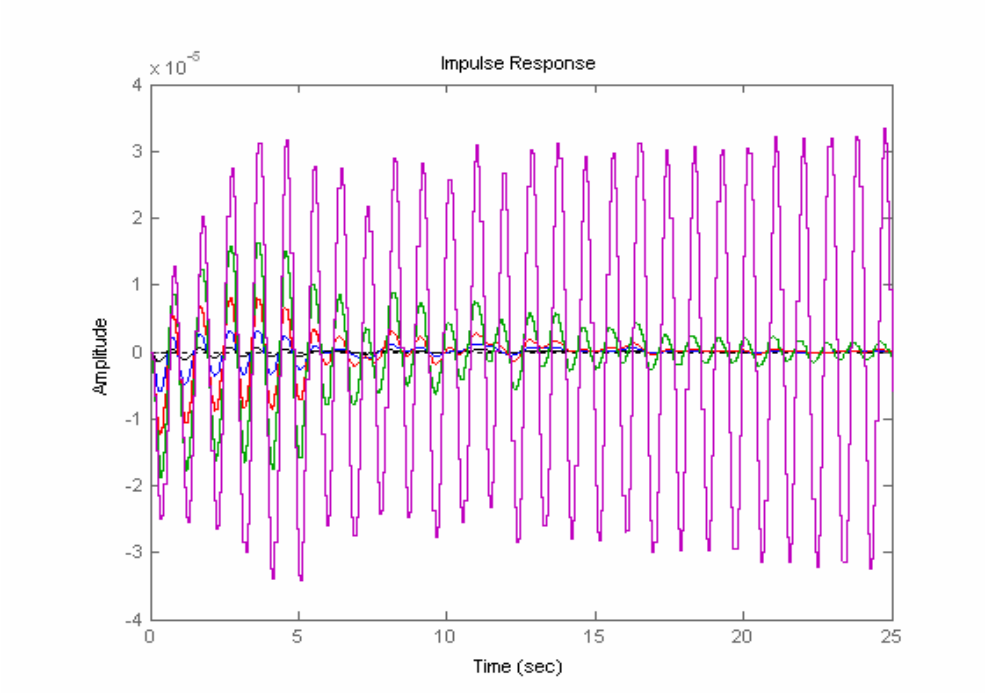

Fig. 4.42 Damping effects for different sampling rates with a 200ms time-delay.

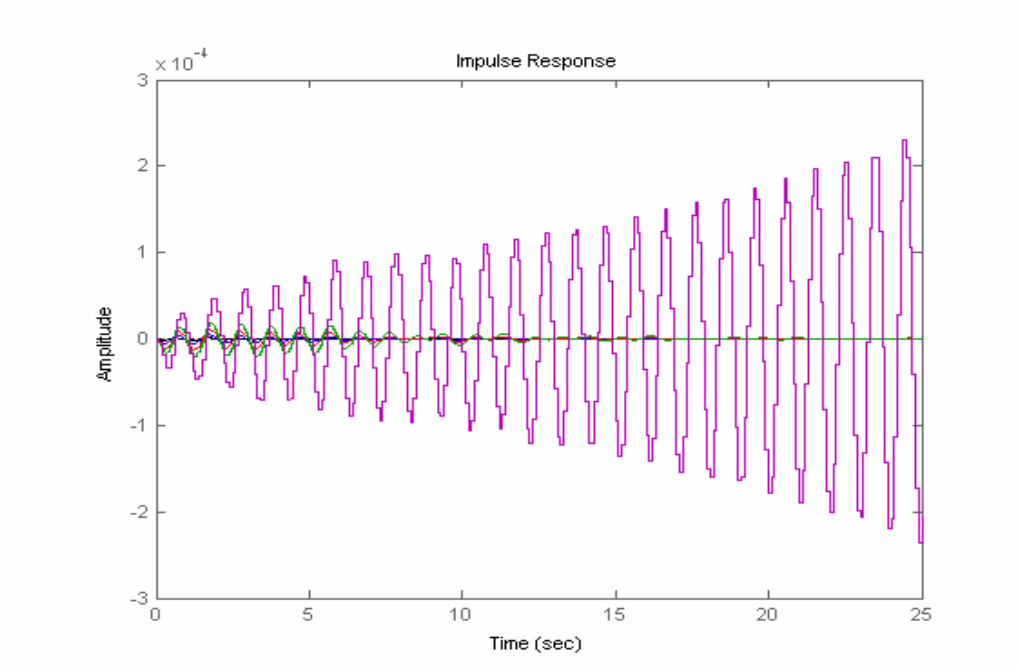

Fig. 4.43 Damping effects for different sampling rates with a 300ms time-delay.

Table 4.20: Desirable sample rates for different time-delays (WECC system)

Time-delay (ms)	200	250	300	350	larger
Sample rate (Hz)	20	30	60	120	--

Nonlinear simulations using TAST based on a model that represents the realistic power system with all its nonlinearities are conducted to verify the results of linear simulation. Fig. 4.44 shows active power flow of California/Arizona corridors for three phase fault on line 16-136 without time-delays. Fig. 4.45 shows active power flow of line 27-139 for three phase fault on line 16-136 with a 100ms time-delay. Table 4.21 lists the damping ratios for the PACI mode and California/Arizona mode when there is no time-delay. Table 4.22 lists the damping ratios for PACI mode and California/Arizona mode when there is a 100ms time-delay.

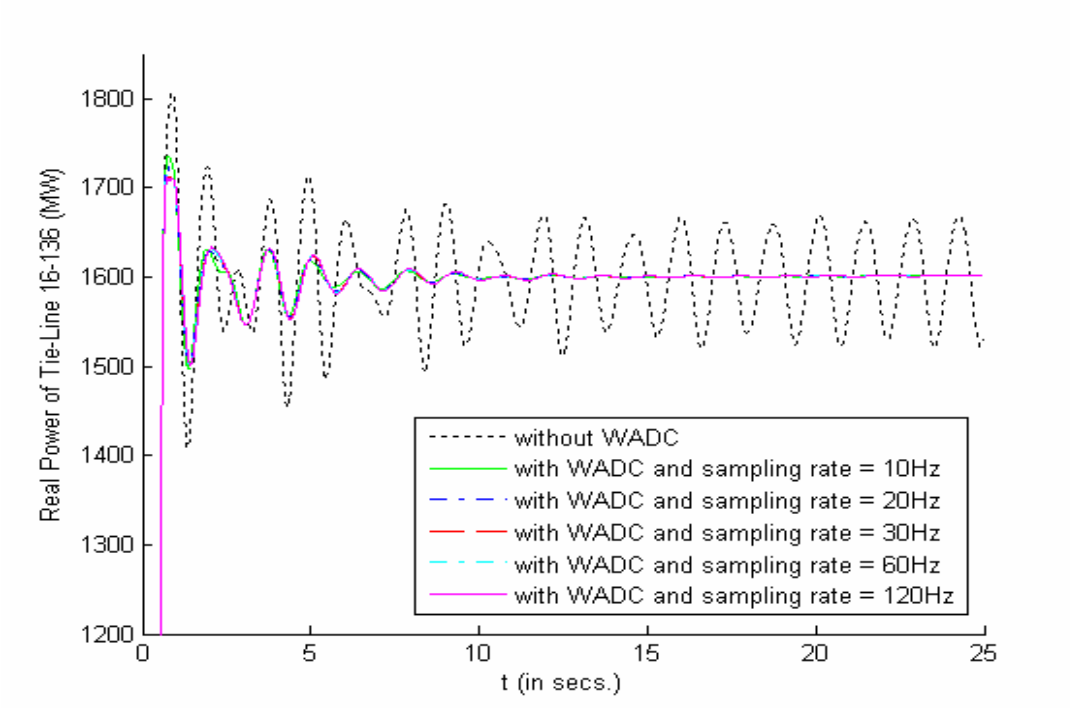

Fig. 4.44 Active power flow of California/Arizona corridors for three phase fault on line 16-136 without time-delays.

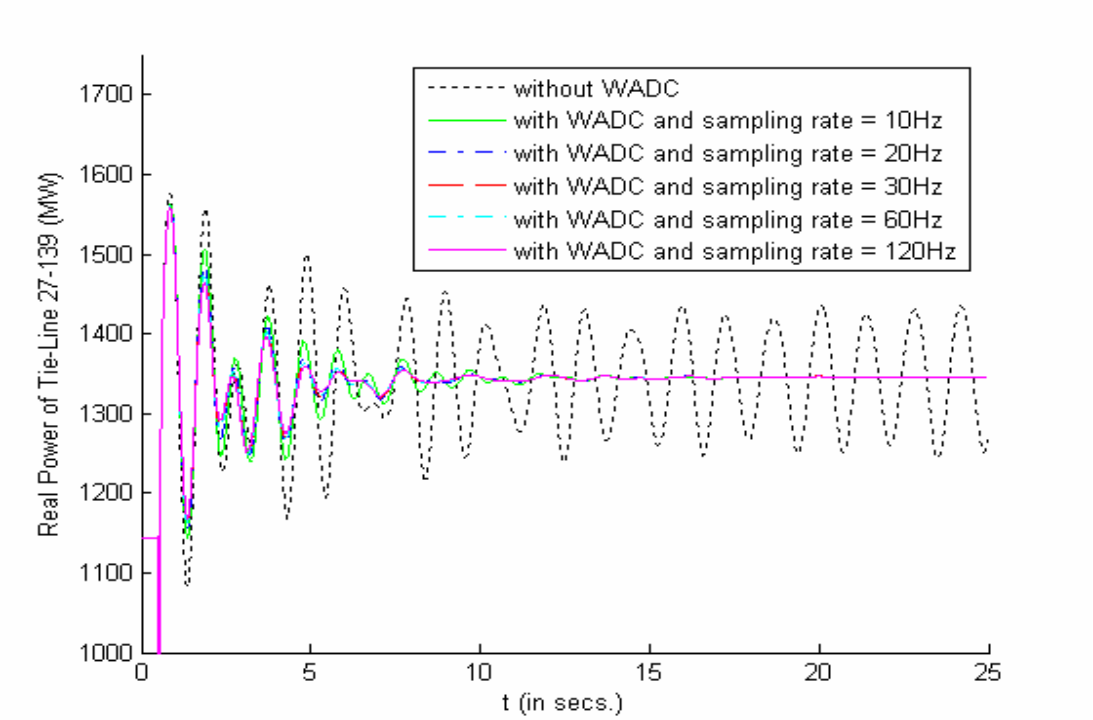

Fig. 4.45 Active power flow of line 27-139 for three phase fault on line 16-136 with a 100ms time-delay.

Table 4.21: Damping ratios for different sampling rates without time-delays

Sample rate (Hz)	10	20	30	60	120
Damping ratio for 0.3 Hz mode (%)	12.36	12.72	13.04	13.22	13.95
Damping ratio for 0.7 Hz mode (%)	7.46	7.97	8.23	8.47	8.78

Table 4.22: Damping ratios for different sampling rates with a 100ms time-delay

Sample rate (Hz)	10	20	30	60	120
Damping ratio for 0.3 Hz mode (%)	10.65	10.82	10.91	11.02	11.15
Damping ratio for 0.7 Hz mode (%)	6.81	7.24	7.33	7.54	7.56

From the above results we can see that when the time-delay is less than 200 ms, 10 Hz sampling rate is good enough for ensuring acceptable damping effects. Increasing sampling rate only improves damping ratio slightly.

Fig. 4.46 shows active power flow of line 27-139 for three phase fault on line 16-136 with a 300ms time-delay. Fig. 4.47 shows active power flow of line 27-139 for three phase fault on line 16-136 with a 350ms time-delay. We can see from these simulations that for time-delays equal to or larger than 250ms, the sampling rates that ensure the acceptable damping ratios increase as time-delays increase. When time-delays are larger than 350 ms, the system is unstable no matter how fast the sampling rate is. The results are shown in Table 4.23.

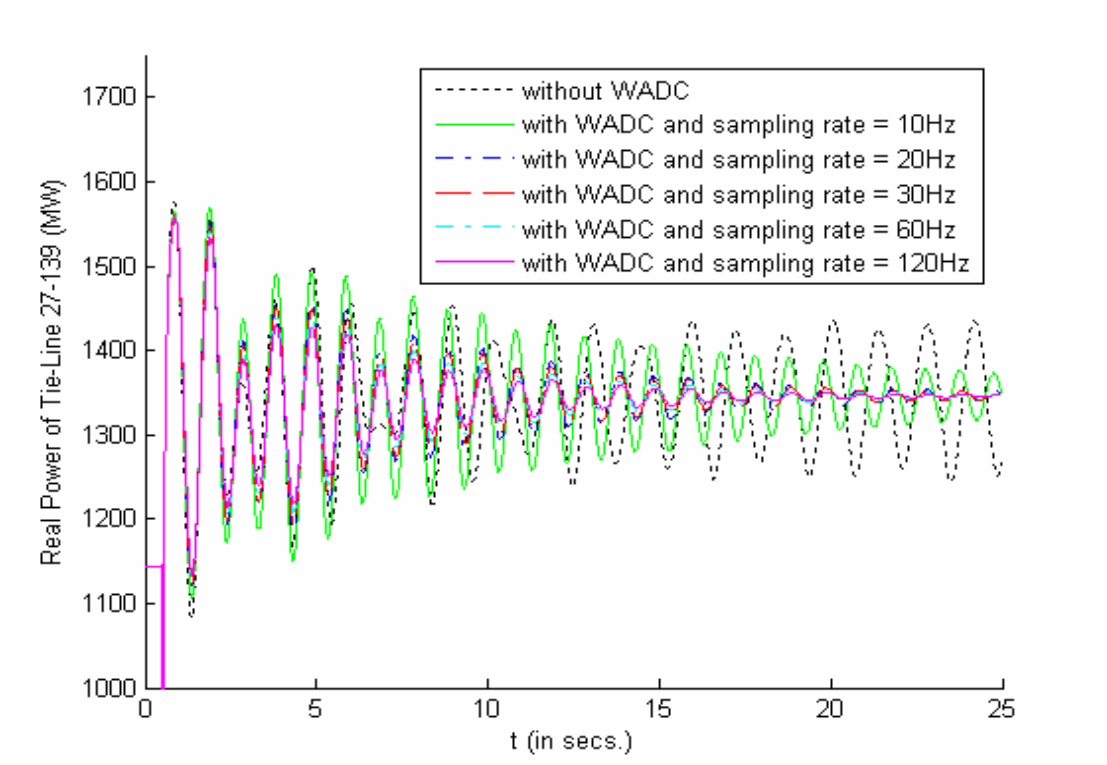

Fig. 4.46 Active power flow of line 27-139 for three phase fault on line 16-136 with a 300ms time-delay.

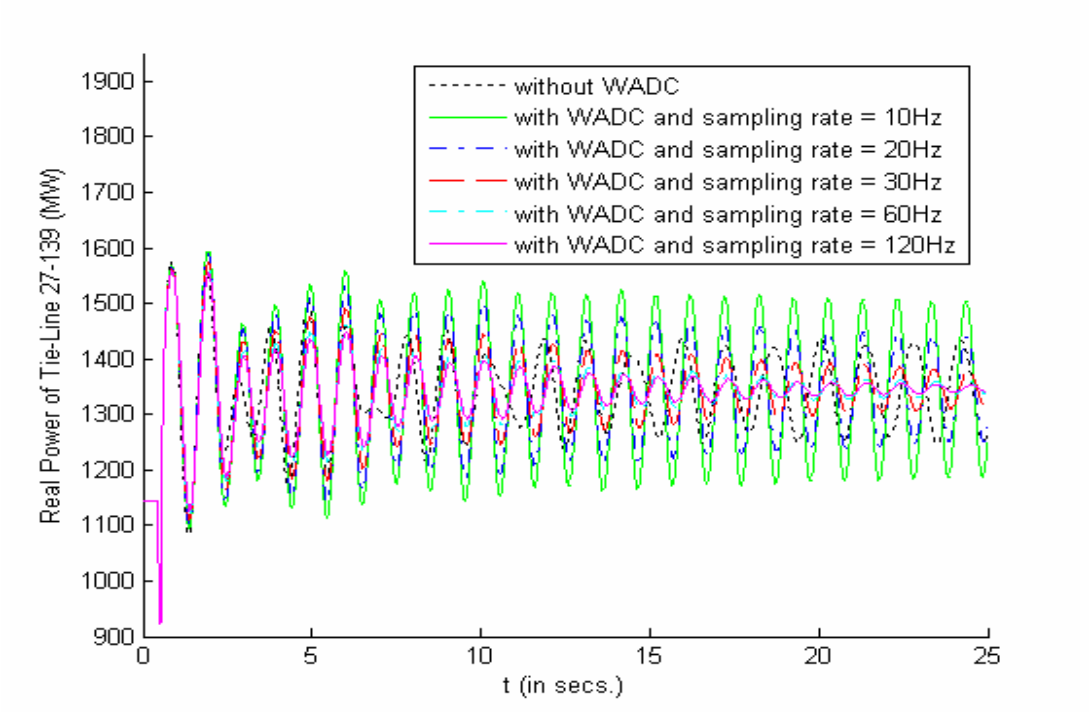

Fig. 4.47 Active power flow of line 27-139 for three phase fault on line 16-136 with a 350ms time-delay.

Table 4.23: Desirable sample rates for large time-delays (WECC system)

Time-delay (ms)	250	300	350	larger
Sample rate (Hz)	30	60	120	--

We can see from linear and nonlinear simulations that they give different conclusions for the selection of PMU data reporting rates. The different results between linear and nonlinear simulations justify the necessity of testing the performance and robustness of designed controller with linear techniques in practical nonlinear environments. Usually, a tuning process is necessary to improve the performance of designed controllers.

Chapter 5. Conclusions and Future Work

5.1 Conclusions

In this paper, the design procedure of a wide-area damping controller for inter-area oscillations is described. A centralized structure is proposed for such a controller. The comparative strength of candidate stabilizing signals and the performance of controllers at different locations with respect to inter-area modes are evaluated by geometric measures of controllability/observability. Time-delay is modeled as an uncertainty in the controller design procedure so that the resulting controller can handle a range of time-delays. The synthesis of the robust MIMO controller is defined as a problem of mixed H2/H∞ output-feedback control with regional pole placement and is resolved by the LMI approach. The design method is tested on three study systems. Linear analyses and nonlinear simulations demonstrated the robustness and efficiency of the designed controllers. The effects of time-delays on controller robustness and selection of data reporting rates of PMUs are studied. From the simulation results, the following conclusions can be drawn:

- Geometric measures of controllability/observability are effective in evaluating the comparative strength of candidate stabilizing signals of widely differing types.

- Active powers and current magnitudes on tie-lines are good choices for stabilizing signals with respect to critical inter-area oscillation modes.

• For the small size system considered, one stabilizing signal is enough for the input of a WADC. Multiple inputs improve the control performance only slightly for such small systems but are expected to be necessary for acceptable control performance in large systems.

• Mixed H2/H∞ output-feedback control with regional pole placement can be applied to the wide-area damping controller synthesis with good results which cannot be obtained by only using either one.

• Nonlinear simulation using a typical transient stability program like TSAT is required to show that such a design of a wide-area controller is effective in a practical implementation. Such a step is shown for the controllers in three examples.

• Time-delays reduce the damping of control systems. It's necessary to model time-delays in the controller design procedure so that the designed controller can handle time-delays introduced into wide-area control systems.

• The controller designed with continuous techniques should be tested in digital environments to establish its efficiency. The selection of PMU data reporting rates for digital control systems is affected by time-delays. The larger the time-delay is, the higher the rates are necessary to ensure an acceptable damping performance.

5.2 Future Work

Although this research achieved promising results in applying wide- area measurements and robust control techniques to the design of wide-area control systems for the damping of power system oscillations, the work doesn't end here. The following aspects should be studied further:

1. Application of FACTS devices in the design of wide-area damping control systems: The approach used in this research is to design wide-area measurements based controllers that provide control actions through generator excitation systems supplemental to the action of local PSSs. For inter-area oscillations, FACTS devices may be preferred because they can change the power flow on tie-lines directly and thus damp power oscillations more efficiently.

2. Decentralized control: The control system proposed in this research has a centralized architecture. The designed centralized controller collects several remote measurements and sends control signals to several control devices simultaneously. There are several disadvantages in this approach. For example, this centralized approach increased time-delays caused by collecting measurements to control center and re-routing them or control signals to control sites, increased investments for communication network and central computers, and the interactions between control loops. By contrast, a decentralized approach has less time-delays, less investment for hardware, and reduced interactions between control loops. The design of a decentralized wide-area damping control

system is an approach not yet addressed for the problem of power system oscillations.

3. Coordination with protection and other control systems: In present day transient stability programs, the existing protection systems and other control systems like SPS/RAS are not modeled. Therefore, the interactions between the designed control system and existing protection and other control systems were not studied in this research. In practice, coordination of all kinds of protection and control systems is an important and difficult task. Poor coordination between all control systems may result in undesirable actions. The reliability of the transmission network can be jeopardized by unintentional and unexpected control system actions and loss of facilities caused by maloperation or poorly coordinated control systems. To study the coordination between wide-area control systems and existing protection and other control systems, modeling all these systems in the design procedure is desirable.

4. Robustness: By applying robust control techniques into the design procedure, the resulting controller is robust for a range of operating conditions. The achieved robustness of designed controllers is very much dependent on the method for modeling all kinds of uncertainty. The more realistic the uncertainty modeled, the more robustness is achieved. Thus, to ensure the performance of the designed controller in a larger operating range, more complex uncertainty models should be used in the controller design procedure.

5. Controller tuning: When implemented in the actual nonlinear system, the controller designed with linear techniques may not have as good performance and robustness as in linear simulation because of the loss of some system properties in model linearization and model reduction. It's necessary to tune the controller parameters and verify its effectiveness with nonlinear simulations. In our design process, controller parameters like gains, zeros and poles are manually modified (tuned) from observation of the controller performance in nonlinear simulations. This method is time consuming and has no guarantee for finding the optimal settings. It's desirable to propose a systematic tuning method so that the controller designed by linear techniques work well in practical nonlinear environments.

Bibliography

[1] P. Kundur, Power System Stability and Control. New York: McGraw-Hill, 1994

[2] E.V. Larsen and J. H. Chow, SVC control design concepts for system dynamic performance, in IEEE Special Publications: Application of Static VAR Systems for System Dynamic Performance, pp. 36–53, 1987.

[3] M. Aboul-Ela, A. Sallam, J. McCalley, and A. Fouad, "Damping controller design for power system oscillations using global signals," IEEE Trans. Power Syst., vol. 11, pp. 767–773, May 1996.

[4] M. Klein, L.X. Le, G.J. Rogers, S. Farrokhpay and N.J. Balu, "H∞ damping controller design in large power systems", IEEE Trans. on Power systems, Vol.10, No.1, pp. 158-166, Feb.1995.

[5] R. A. Ramos, L. F. C. Alberto, and N. G. Bretas, "A New Methodology for the Coordinated Design of Robust Decentralized Power System Damping Controllers", IEEE Transactions on Power Systems, vol. 19, no.1, pp. 444-454, February 2004.

[6] Z. Chuanjiang, M. Khammash, V. Vittal, and Q. Wenzheng, "Robust power system stabilizer design using H∞ loop shaping approach", IEEE Transactions on Power Systems, vol. 18 , no.2, pp. 810-818, May 2003.

[7] George E. Boukarim, Shaopeng Wang, Joe H. Chow, Glauco N. Taranto and Nelson, Martins, "A Comparison of Classical, Robust, and Decentralized Control Designs for Multiple Power System Stabilizers," IEEE Trans. on Power System, Vol. 15, No. 4, pp. 1287-1292, November 2000.

[8] W.A. Mittelstadt, PE. Krause, P.N. Overholt, J.F. Hauer, R.E. Wilson, D.T. Rizy, "The DOE Wide-area Measurement System (WAMS) Project - Demonstration of Dynamic Information Technology for Future Power System," Fault and Disturbance Analysis & Precise Measurements in Power Systems, Arlington, VA, Nov, 1995.

[9] A. G. Phadke, "Synchronized phasor measurements - a historical overview," In Proc. IEEE/PES Transmission and Distribution Conference and Exhibition, pp. 416-479, 2002.

[10] I. Kamwa, J. Beland, G. Trudel, R. Grondin, C. Lafond, and D. McNabb, "Wide-Area Monitoring and Control at Hydro-Québec: Past, Present and Future," in Proc. IEEE PES Summer Meeting, pp.1-12, 18-22 June 2006.

[11] I. Kamwa, A. Heniche, G. Trudel, M. Dobrescu, R. Grondin and D. Lefebvre, "Assessing the technical value of FACTS-based wide-area damping control loops," IEEE/PES General Meeting, Vol. 2, pp.1734 –1743, 12-16 June, 2005.

[12] I. Kamwa, R. Grondin, Y. Hebert, "Wide-area measurement based stabilizing control of large power systems—A decentralized/ hierarchical approach," IEEE Trans. Power Syst., vol. 16, no. 1, pp. 136–153, Feb. 2001.

[13] H. Ni, G. T. Heydt, and L. Mili, "Power system stability agents using robust wide-area control," IEEE Trans. Power Syst., vol. 17, pp. 1123–1131, Nov. 2002.

[14] J. Chow, J. Sanchez-Gasca, H. Ren, and S. Wang, "Power system damping controller design using multiple input signals," IEEE Contr. Syst. Mag., vol. 20, pp. 82–90, Aug. 2000.

[15] A. F. Snyder et al., “Delay-input wide-area stability control with synchronized phasor measurements,” in Proc. IEEE PES Summer Meeting, vol. 2, pp. 1009–1014, 2000.

[16] J. Quintero and V. Venkatasubramanian, “A Real-Time Wide-Area Control Framework for Mitigating Small-Signal Instability in Large Electric Power Systems,” in Proc. of the 38th Annual Hawaii International Conference on System Sciences, 03-06 Jan. 2005.

[17] B. Chaudhuri, B. C. Pal, A. C. Zolotas, I. M. Jaimoukha, and T. C. Green, “Mixed-Sensitibity Approach to H∞ Control of Power System Oscillations Employing Multiple FACTS Devices,” IEEE Trans. Power Syst., vol. 18, NO. 3, August 2003.

[18] Peter W. Sauer, M. A. Pai Power System Dynamics and Stability, Prentice Hall 1997.

[19] Miroslav Begovic, Borka Mirosevic, Damir Novosel, “A Novel Method for Voltage Instability Protection”, Proceeding of the 35th Hawaii International Conference on System Sciences, 2002.

[20] Perez-Arriaga, I. J., G. C. Verghese and F. C. Schweppe (1982), "Selective Modal Analysis with Applications to Electric Power Systems, Part I: Heuristic Introduction," IEEE T-PAS, Vol. 101, No. 9, pp 3117-3125.

[21] Porter, B. and R. Crossley, Modal Control – Theory and Applications, Taylor & Francis, 1972.

[22] M. Tarokh, “Measures for controllability, observability and fixed modes,” IEEE Trans. on Automatic Control, 37(8), August, 1992 pp.1268-1273.

[23] X. Yang, A. Feliachi, R. Adapa, "Damping Enhancement in the Western Power System," IEEE Trans. on Power Systems, PWRS-10(3), August 1995, pp.1271-1278.

[24] P.Gahinet et al. LMI Control Toolbox, The MathWorks, Inc., 1995.

[25] J.J. Sinchez-Gasca and J.H. Chow, "Power System Reduction to Simplify the Design of Damping Controllers for Inter-area Oscillations," IEEE Trans. on Power System, vol. 11, no. 3, pp 1342-1349, August 1996.

[26] R. Y. Chiang and M. G. Sofonov, Robust Control Toobox for UFC with Matlab: The Math Works Inc., 1996.

[27] TSAT Version 4.1 User's manual, Powertech Labs Inc., September 2004.

[28] A. M. A. Hamdan and A. M. Elabdalla, "Geometric measures of modal controllability and observability of power systems models," Electric Power System Research, vol. 15, pp. 147–155, 1988.

[29] K. Tomsovic, D.E. Bakken, V. Venkatasubramanian, Anjan Bose, "Designing the next generation of real-time control, communication, and computations for large power systems," Proc. IEEE Vol. 93, Issue 5, pp. 965-979, May 2005.

[30] B. Chaudhuri, B.C. Pal, "Robust damping of inter-area oscillations through controllable phase shifters using global signals," IEEE PES General Meeting, Vol. 3, pp.1673-1679, 13-17 July 2003.

[31] V. Arcidiacono, E. Ferrari, R. Marconato, J. DosGhali, D. Grandez, "Evaluation and Improvement of Electramechanical Oscillation Damping by Means of Eigenvalue-Eigenvector Analysis. Practical Results in the Central Peru Power System," IEEE

Trans. on power apparatus and Systems, Vol. PAS-99, pp. 769-778, March/April 1980.

[32] N. Martins and L. T. G. Lima, "Determination of suitable locations for power system stabilizers and Static VAR Compensators for damping electromechanical oscillations in large scale power systems," IEEE Trans. Power Syst., vol. 5, pp. 1455–1469, Nov. 1990.

[33] H. F. Wang, F. J. Swift, and M. Li, "Selection of installing locations and feedback signals of FACTS-based stabilisers in multimachine power systems by reduced-order modal analysis," Proc. Inst. Elect. Eng., Gen. Transm. Dist., vol. 144, no. 3, pp. 263–269, May 1997.

[34] P. Zhang, A. R. Messina, A. Coonick, and B. J. Cory, "Selection of locations and input signals for multiple SVC damping controllers in large scale power systems," in Proc. IEEE Power Eng. Soc. Winter Meeting, 1998, Paper IEEE-0-7803-4403-0, pp. 667–670.

[35] A. M. A. Hamdan, "An investigation of the significance of singular value decomposition in power system dynamics," Int. J. Elect. Power Energy Syst., vol. 21, no. 6, pp. 417–424, 1999.

[36] E.V. Larsen and J. H. Chow, SVC control design concepts for system dynamic performance, in IEEE Special Publications: Application of Static VAR Systems for System Dynamic Performance, pp. 36–53, 1987.

[37] I. Kamwa, L. Gerin-Lajioe, G. Trudel, "Multi-Loop Power System Stabilizers Using Wide-Area Synchronous Phasor Measurements," Proceedings of the American Control Conference, Philadephia, Pennsylvania, June 1998, pp. 2963-2967.

[38] P. Pourbeik and M. J. Gibbard, "Damping and synchronizing torques induced on generators by FACTS stabilizers in multimachine power systems," IEEE Trans. Power Syst., vol. 11, pp. 1920–1925, Nov. 1996.

[39] S. E. M. De Oliveira, "Synchronizing and damping torque coefficients and power system steady-state stability as affected by static VAR compensators," IEEE Trans. Power Syst., vol. 9, pp. 109–119, Feb. 1994.

[40] B. T. Ooi, M. Kazerani, R. Marceau, Z. Wolanski, F. D. Galiana, D. McGillis, and G. Joos, "Mid-point siting of FACTS devices in transmission lines," IEEE Trans. Power App. Syst., vol. 100, pp. 3933–3939.

[41] H. F.Wang, F. J. Swift, and M. Li, "Indices for selecting the best location of PSS's or FACTS-based stabilisers in multimachine power systems: a comparative study," Proc. Inst. Elect. Eng., Gen. Transm. Dist., vol. 144. no. 2, pp. 155–159, Mar. 1997.

[42] S. Lee and C. C. Liu, "An output feedback static var controller for the damping of generator oscillations," Elect. Power Syst. Res., vol. 25, no. , pp. 9–16, 1994.

[43] E. Z. Zhou, "Application of static var compensators to increase power system damping," IEEE Trans. Power Syst., vol. 8, pp. 655–661, May 1993.

[44] Innocent Kamwa and L. Gerin-Lajoie, "State-Space System Identification-Toward MIMO Models for Modal Analysis and Optimization of Bulk Power Systems," IEEE Trans. on Power Systems, Vol. 15, No.1, FEB. 2000.

[45] Carson W. Taylor, Dennis C. Erickson, Kenneth E. Martin, Robert E. Wilson and V. Venkatasubramanian, "WACS—Wide-Area Stability and Voltage Control System: R&D and Online Demonstration," Proceedings of the IEEE, Vol. 93, No. 5, MAY 2005.

[46] N. Martins, A. A. Barbosa, J.C.R. Ferraz, M.G. dos Santos, A.L.B. Bergamo, C.S. Yung, V.R. Oliveira, N.J.P. Macedo, "Retuning Stabilizers for the North-South Brazilian Interconnection," IEEE PES Summer Meeting, 18-22 July 1999, Vol. 1, pp. 58-67.

[47] H.Breulman, E. Grebe, M. Losing, W. Winter, R. Witzman, P. Dupuis, M. P. Houry, T. Margotin, J. Zerenyi, J. Duzik, J. Machowski, L. Martin, J. M. Rodrigues, E. Urretavizcaya, "Analysis and Damping of Inter-Area Oscillations in the UCTE/CENTREL Power System," CIGRE 2000 in Paris, Paper 38-113.

[48] U.S.-Canada Power System Outage Tack Force: Final Report on the August 14, 2003 Blackout in the United States and Canada (on line): http://www.pserc.wisc.edu/BlackoutFinal-Web.pdf.

[49] A. Heniche and I. Kamwa, "Using global control and SMES to damp inter-area oscillations: An exploratory assessment," in Proc. 2000 IEEE Power Engineering Society Summer Meet., pp. 1872–1876.

[50] G. Heydt, C. Liu, A. Phadke, and V. Vittal, "Solutions for the Crisis in Electric Power Supply," IEEE Computer Applications to Power Systems, vol. 14, pp. 22–30, July 2001.

[51] T. Smed, "Feasible Eigenvalue Sensitivity for Large Power Systems," IEEE T-PWRS, Vol. 8, No. 2, pp 555-563.

[52] Wei Xuan, J.H.Chow, J.J. Sanchez-Gasca, "On the Sensitivity of Network Variables for FACTS Device Damping Control," 2002 IEEE Power Engineering Society Winter Meeting, Vol.2, 27-31 Jan. 2002, pp.1188-1193.

[53] A. Heniche, I. Kamwa, "Control Loops Selection to Damp Inter-Area Oscillations of Electrical Networks," IEEE Trans. on Power Systems, 17(2), May 2002, pp.378-384.

[54] F. L. Pagola, I. J. Perez-Arriaga, G. C. Verghese, "On the Sensitivities, Residues and Participation. Application to Oscillatory Stability Analysis and Control", IEEE Trans. Power Systems, Vol. 4, No.1, Feb, 1989, pp. 278-285.

[55] D. R. Ostojic, "Stabilization of Multi-modal Electromechanical Oscillation by Coordinated Application of Power System Stabilizers", IEEE Trans. Power Systems, pp 1439-1445, 1991.

[56] Richard C. Dorf, Modern Control Systems, Addison-Wesley Publishing Company, 1992.

[57] G. Rogers, Power System Oscillations. Norwell, MA: Kluwer, 2000.

[58] J.H. Chow, L.P. Harris, M.A. Kale, H.A. Othman, J.J. Sanchez-Gasca and G.E. Terwilliger, 'Robust control design of power system stabilisers using multi variable frequency domain techniques', Proc. of the 29th Conference of Decision and Control, Honolulu, Hawaii, Dec. 1990.

[59] U. Kiffmeier and U. Keuchel, 'Comparison of classical PID and modern H∞ control concepts for frequency and voltage control of power plants', IFAC Control of Power Plants and Power Systems, Munich, Germany, 1992.

[60] S. Chen and O.P. Malik, 'H∞ optimisation based power system stabiliser design', IEE Proc. -Gener. Transm. Distrib., Vol. 142, No.2, pp 179-184, March 1995.

[61] S.S. Ahmed, L. Chen, and A. Petroianu, 'Design of suboptimal H∞ excitation controllers', IEEE Trans. on power systems, Vol.11, No.1, Feb 1996.

[62] R. Asgharian, 'A Robust H∞ Power System Stabiliser with no adverse effect on shaft torsional modes', IEEE Trans. on Energy Conversion, Vol 9, No.3, Sept. 1994.

[63] G. Zames, "Feedback and optimal sensitivity: Model reference transformations, multiplicative seminorms and approximate inverses," IEEE Trans. Automatic Control, Vol. AC-26, No.2, pp 301-320, April 1981.

[64] K. Glover, "Robust stabilisation of linear mutli-variable system: Relations to approximation," Int. journal of control, Vol 43, No.3, pp 741-766, 1986.

[65] k. Zhou, John C. Doyle, Essentials of Robust Control, Prentice Hall, 1998.

[66] Vijay Vittal, Mustafa Khammash, Chuanjiang Zhu, Wenzheng Qiu, "Robust Control of Large Scale Power Systems," Project Report, PSERC Publication 02-43, November 2002.

[67] J.C. Doyle and G.Stein, "Multivariable Feedback Design: Concepts for Classical/Modern Synthesis," IEEE Trans. Automatic Control, Vol. AC-26, pp 4-16, 1981.

[68] C. Scherer, P. Gahinet, and M. Chilali, "Multiobjective output-feedback control via LMI optimization," IEEE Trans. on Automatic Control, vol. 42, no. 7, pp. 896–911, Jul. 1997.

[69] B. C. Pal, A. H. Coonick, B. J. Cory. "Linear matrix inequality versus Root-locus approach for damping inter-area oscillations in power systems," Electrical Power and Energy Systems, vol. 23, No. 6, pp. 48149, Aug, 2001.

[70] J.C. Doyle, K. Glover, P.P. Khargonekar and B. A. Francis, "State-space solutions to H2 and H∞ control problems," IEEE Trans. Automatic Control, Vol. 34, No.8, pp 831-848, Aug. 1989.

[71] J. Sefton and K. Glover, "Pole/zero cancellations in the general H∞ problem with reference to a two block design," Systems and Control Letters, vol. 14, pp. 295–306, 1990.

[72] B. Pal, A. Coonick, I. Jaimoukha, and H. Zobaidi, "A linear matrix inequality approach to robust damping control design in power systems with superconducting magnetic energy storage device," IEEE Trans. on Power System., vol. 15, pp. 356–362, Feb. 2000.

[73] P. Gahinet and P. Apkarian, "A linear matrix inequality approach to H∞ control," Int. J. Robust and Non-linear Control, vol. 4, pp. 421–448, 1994.

[74] S. Boyd, L. EI Ghaoui, E.Feron, and V. Balakrishnan. Linear Matrix Inequalities in System and Control Theory, volume 15 of Studies in Applied Mathematics. SIAM, Philadelphia, PA, June 1994.

[75] Scherer, C., Gahinet, P., and Chilali, M. "H∞ design with pole placement constraints: an LMI approach," IEEE Trans. Autom. Control, 1996, 41, (3), pp. 358–367.

[76] R. Majumder, B. Chaudhuri, H. El-Zobaidi, B.C. Pal and I.M. Jaimoukha, "LMI approach to normalized H∞ loop-shaping design of power system damping controllers," IEE Proc.-Gener. Transm. Distrib., Vol. 152, No. 6, November 2005.

[77] Jaw-Kuen Shiau; Taranto, G.N.; Chow, J.H.; Boukarim, G., "Power swing damping controller design using an iterative linear matrix inequality algorithm", IEEE Trans. on Control Systems Technology, Volume 7, Issue 3, May 1999 Page(s):371 – 381.

[78] R.A. Ramos, L.F.C. Alberto and N.G. Bretas., "LMI-based controller design with feedback inearisation: application to power systems," IEE Proc.-Control Theory Appl., Vol. 150, No. 5, September 2003.

[79] Gahinet, P., "Explicit Controller Formulas for LMI-based H∞ Synthesis," Proc. Amer. Contr. Conf., 1994, pp. 2396–2400.

[80] P. Shrikant Rao and I. Sen, "Robust Pole Placement Stabilizer Design Using Linear Matrix Inequalities," IEEE Trans. Power Syst., vol. 15, no. 1, pp. 313-319, February 2000.

[81] Biju Naduvathuparambil, Matthew C. Valenti, and Ali Feliachi, "Communication Delays in Wide-area Measurement Systems," Proceedings of the Thirty-Fourth Southeastern Symposium on System Theory, pp.118- 122, 2002.

[82] Hongxia Wu, Konstantinos S. Tsakalis and G. T. Heydt, "Evaluation of Time Delay Effects to Wide-Area Power System Stabilizer Design," IEEE Trans. on Power Syst., Vol. 19, NO. 4, pp 1935-1941, Nov. 2004.

[83] Balarko Chaudhuri, Rajat Majumder and B. C. Pal, "Wide-Area Measurement-Based Stabilizing Control of Power System Considering Signal Transmission Delay," IEEE Trans. on Power Syst., Vol. 19, NO. 4, pp 1971-1979, Nov. 2004.

[84] Rajat Majumder, Balarko Chaudhuri, B. C. Pal and Qing-Chang Zhong, "A Unified Smith Predictor Approach for Power System Damping Control Design Using Remote Signals," IEEE Trans. on Power Syst., Vol. 13, NO. 6, Nov. 2005.

[85] K. Hirayama et al., "Digital AVR Application to Power Plants," IEEE Trans. on Energy Conversion, Vol. 8, no. 4, pp 602-609, December, 1993.

[86] Gene F. Franklin, J. David Powell, and Michael L. Workman, Digital Control of Dynamic Systems, Addison-Wesley, 1997.

[87] P. Kundur, M. Klein, G. J. Rogers, and M. Zwyno, "Applications of power system stabilizers for enhancement of overall system stability," IEEE Trans. on Power Syst., vol. 4, pp. 614–622, May 1989.

[88] L. D. Philipp. Ausif Mahmood, B. L. Philipp, "An improved refinable rational approximation to the ideal time delay," IEEE Trans. Circuits and Systems, vol. 46, pp. 637-640, May 1999.

[89] D. N. Kosterev, C. W. Taylor, and W. A. Mittelstadt, "Model validation for the August 10, 1996 WSCC system outage," IEEE Trans. Power Syst., vol. 14, no. 3, pp. 967-979, August 1999.

[90] J. F. Hauer, "Robustness issues in stability control of large electric power systems," The 32nd IEEE conference on decision and control, San Antonio, TX, December 15-17, 1993.

[91] R. L. Cresap, D. N. Scott, W. A. Mittelstadt, and C. W. Taylor, "Damping of pacific AC intertie oscillations via modulation of the parallel pacific HVDC intertie," *CIGRE* 14-05, 19

Appendix A

Two-area four-machine system parameters

The system consists of two similar areas connected by a weak tie. Each area consists of two coupled units, each having a rating of 900 MVA and 20 kV. The generator parameters in per unit on the rated MVA and kV base are as follows:

X_d = 1.8

X_q =1.7

$X_d^{'}$ = 0.3

$X_q^{'}$ =0.55

Ra = 0.0025

$T_d^{'}$ = 8.0s

$T_q^{'}$ = 0.4s

H = 6.5 for G1 and G2

H = 6.175 for G3 and G4

K_D = 0

Each step-up transformer has an impedance of 0+j0.15 per unit on 900 MVA and 20/30 kV base, and has an off-nominal ratio of 1.0.

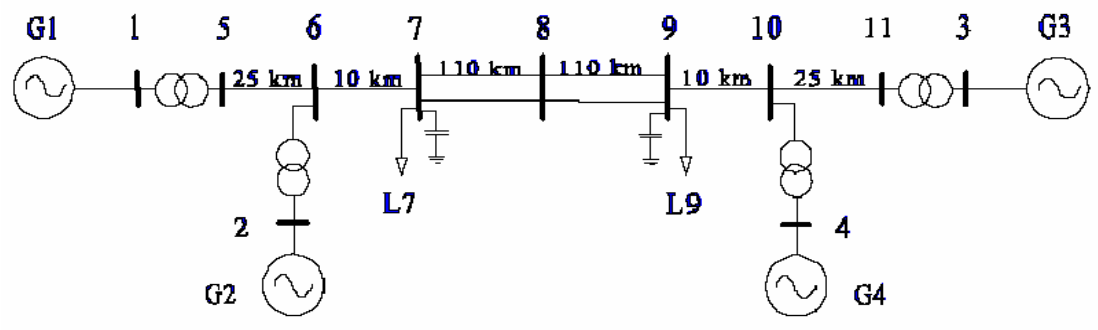

Fig. A.1 two-area four-machine test system.

The transmission system nominal voltage is 230 kV. The line lengths are identified in Fig. A.1. The parameters of the lines in per unit on 100 MVA, 230 kV base are:

R = 0.0001 pu/km

X_l = 0.001 pu/km

Bc = 0.00175 pu/km

The system is operating with area 1 exporting 400 MW to area 2, and the generating units are loaded as follows:

G1: P = 700 MW, Q = 185 MVAr, Et = $1.03\angle 20.2^0$

G2: P = 700 MW, Q = 235 MVAr, Et = 1.01/10.5

G3: P = 719 MW, Q = 176 MVAr, Et = 1.03/-6.8

G4: P = 700 MW, Q = 202 MVAr, Et = 1.01/-17.0

The loads and reactive power supplied (Qc) by the shunt capacitors at buses 7 and 9 area as follows:

Bus 7: P_l = 976 MW, Q_l = 100 MVAr, Qc = 200 MVAr

Bus 9: P_l = 1767 MW, Q_l = 100 MVAr, Qc = 350 MVAr

Self-excited dc exciter

$K_A = 20.0$

$T_A = 0.055$

$T_E = 0.36$

$K_F = 0.125$

$T_F = 1.8$

$A_{ex} = 0.0056$

$B_{ex} = 1.075$

$T_R = 0.05$

Appendix B

IEEE 39-bus system parameters

Power Flow Data

The power flow data for this system is divided in:

- Bus Data
- Load Data
- Generation Data
- Branch Data

Bus Data

Table A-1 represents the bus data. The nomenclature for the table headings is:

Bus Number	Number of the bus
Bus Name	Alphabetic identifier for each bus
Bus BaskV	Bus base voltage, in KV
Bus Type	Bus type code:
	(1) Load Bus, PQ bus
	(2) Generator Bus, PV bus
	(3) Swing Bus

Bus G_L	Real component of shunt admittance to ground, in MW
Bus B_L	Reactive component of shunt admittance to ground, in Mvar
Bus Voltage	Voltage magnitude, in per unit
Bus Angle	Voltage angle, in degrees

Table A.1: IEEE 39-Bus Test System: Bus Data

Bus Number	Bus Name	Bus BaskV	Bus Type	Bus G_L	Bus B_L	Bus Voltage (pu)	Bus Angle
1	BUS1	345	1	0.0	0.0	1.04814	-9.4266
2	BUS2	345	1	0.0	0.0	1.05050	-6.8854
3	BUS3	345	1	0.0	0.0	1.03411	-9.7286
4	BUS4	345	1	0.0	0.0	1.01161	-10.5291
5	BUS5	345	1	0.0	0.0	1.01647	-9.3765
6	BUS6	345	1	0.0	0.0	1.01725	-8.6816
7	BUS7	345	1	0.0	0.0	1.00668	-10.8417
8	BUS8	345	1	0.0	0.0	1.00570	-11.3376
9	BUS9	345	1	0.0	0.0	1.03220	-11.1509
10	BUS10	345	1	0.0	0.0	1.02346	-6.3140
11	BUS11	345	1	0.0	0.0	1.02012	-7.1235
12	BUS12	345	1	0.0	0.0	1.00721	-7.1351
13	BUS13	345	1	0.0	0.0	1.02066	-7.0184
14	BUS14	345	1	0.0	0.0	1.01808	-8.6628
15	BUS15	345	1	0.0	0.0	1.01937	-9.0593
16	BUS16	345	1	0.0	0.0	1.03457	-7.6558
17	BUS17	345	1	0.0	0.0	1.03648	-8.6478

Table A.2: IEEE 39-Bus Test System: Bus Data (continue)

Bus Number	Bus Name	Bus BaskV	Bus Type	Bus G_L	Bus B_L	Bus Voltage (pu)	Bus Angle
18	BUS18	345	1	0.0	0.0	1.03427	-9.4855
19	BUS19	345	1	0.0	0.0	1.05086	-3.0390
20	BUS20	345	1	0.0	0.0	0.99142	-4.4475
21	BUS21	345	1	0.0	0.0	1.03373	-5.2570
22	BUS22	345	1	0.0	0.0	1.05085	-0.8181
23	BUS23	345	1	0.0	0.0	1.04588	-1.0161
24	BUS24	345	1	0.0	0.0	1.03986	-7.5361
25	BUS25	345	1	0.0	0.0	1.05869	-5.5136
26	BUS26	345	1	0.0	0.0	1.05359	-6.7740
27	BUS27	345	1	0.0	0.0	1.03990	-8.7842
28	BUS28	345	1	0.0	0.0	1.05091	-3.2666
29	BUS29	22	2	0.0	0.0	1.05048	-0.5097
30	BUS30	22	2	0.0	0.0	1.04750	-4.4697
31	BUS31	22	3	0.0	0.0	0.98200	0.0000
32	BUS32	22	2	0.0	0.0	0.98310	1.6325
33	BUS33	22	2	0.0	0.0	0.99720	2.1762
34	BUS34	22	2	0.0	0.0	1.01230	0.7415
35	BUS35	22	2	0.0	0.0	1.04930	4.1386
36	BUS36	22	2	0.0	0.0	1.06350	6.8297
37	BUS37	22	2	0.0	0.0	1.02780	1.2652
38	BUS38	22	2	0.0	0.0	1.02650	6.5515
39	BUS39	22	2	0.0	0.0	1.03000	-10.9566

Load Data

Table A-2 represents the load data. The nomenclature for the table headings is:

Bus Number	Number of the Bus
P_L	Real component of the load, in MW
Q_L	Reactive component of the load, in Mvar

Table A.2: IEEE 39-bus Test System: Load Data

Bus Number	P_L (MW)	P_Q (MVAR)
3	322.0	2.4
4	500.0	184.0
7	233.8	84.0
8	522.0	176.0
12	8.5	88.0
15	320.0	153.0
16	329.4	32.3
18	158.0	30.0
20	680.0	103.0
21	274.0	115.0
23	247.5	84.6
24	308.6	-92.2
25	224.0	47.2
26	139.0	17.0
27	281.0	75.5
28	206.0	27.6
29	283.5	126.9
31	9.2	4.6
39	1104.0	250.0

Generation Data

Table A-3 represents the generation data. The nomenclature of the table headings is:

Bus Number Number of the bus

P_G Generator real power output, in MW

P_Q Generator reactive power output, in Mvar

Table A.3: IEEE 39-bus Test System: Generation Data

Bus Number	P_G (MW)	P_Q (MVAR)
29	0.00	100.00
30	250.00	136.20
31	572.87	170.34
32	650.00	175.90
33	632.00	103.34
34	508.00	164.39
35	650.00	204.84
36	560.00	96.88
37	540.00	-4.43
38	830.00	19.38
39	1000.00	68.45

Branch Data

Table A.4 represents the branch (transmission lines and transformers) data. The nomenclature for the table headings is:

Number Number of the branch

From Bus Branch starting bus number

To Bus Branch ending bus number

Resistance (pu) Branch resistance, in per unit

Reactance (pu) Branch reactance, in per unit

Susceptance (B) Branch total charging susceptance, in per unit

Branch Tap Transformer off-norminal turns ratio

Table A.4: IEEE 39-bus Test System: Branch Data

Branch Number	From Bus	To Bus	Resistance (pu)	Reactance (pu)	Susceptance (pu)	Branch Tap
1	1	2	0.0035	0.0411	0.6987	0.000
2	1	39	0.0020	0.0500	0.3750	0.000
3	1	39	0.0020	0.0500	0.3750	0.000
4	2	3	0.0013	0.0151	0.2572	0.000
5	2	25	0.0070	0.0086	0.1460	0.000
6	3	4	0.0013	0.0213	0.2214	0.000
7	3	18	0.0011	0.0133	0.2138	0.000
8	4	5	0.0008	0.0128	0.1342	0.000
9	4	14	0.0008	0.0129	0.1382	0.000
10	5	6	0.0002	0.0026	0.0434	0.000
11	5	8	0.0008	0.0112	0.1476	0.000
12	6	7	0.0006	0.0092	0.1130	0.000
13	6	11	0.0007	0.0082	0.1389	0.000
14	7	8	0.0004	0.0046	0.0780	0.000
15	8	9	0.0023	0.0363	0.3804	0.000
16	9	39	0.0010	0.0250	1.2000	0.000
17	10	11	0.0004	0.0043	0.0729	0.000
18	10	13	0.0004	0.0043	0.0729	0.000
19	13	14	0.0009	0.0101	0.1723	0.000
20	14	15	0.0018	0.0217	0.3660	0.000
21	15	16	0.0009	0.0094	0.1710	0.000
22	16	17	0.0007	0.0089	0.1342	0.000
23	16	19	0.0016	0.0195	0.3040	0.000
24	16	21	0.0008	0.0135	0.2548	0.000

Table A.4: IEEE 39-bus Test System: Branch Data (continue)

Branch Number	From Bus	To Bus	Resistance (pu)	Reactance (pu)	Susceptance (pu)	Branch Tap
25	16	24	0.0003	0.0059	0.0680	0.000
26	17	18	0.0007	0.0082	0.1319	0.000
27	17	27	0.0013	0.0173	0.3216	0.000
28	21	22	0.0008	0.0140	0.2565	0.000
29	22	23	0.0006	0.0096	0.1846	0.000
30	23	24	0.0022	0.0350	0.3610	0.000
31	25	26	0.0032	0.0323	0.5130	0.000
32	26	27	0.0014	0.0147	0.2396	0.000
33	26	28	0.0043	0.0474	0.7802	0.000
34	26	29	0.0057	0.0625	1.0290	0.000
35	28	29	0.0014	0.0151	0.2490	0.000
36	2	30	0.0000	0.0181	0.0000	1.025
37	6	31	0.0000	0.0500	0.0000	1.070
38	6	31	0.0000	0.0500	0.0000	1.070
39	10	32	0.0000	0.0200	0.0000	1.070
40	12	11	0.0016	0.0435	0.0000	1.006
41	12	13	0.0016	0.0435	0.0000	1.006
42	19	20	0.0007	0.0138	0.0000	1.060
43	19	33	0.0007	0.0142	0.0000	1.070
44	20	34	0.0009	0.0180	0.0000	1.009
45	22	35	0.0000	0.0143	0.0000	1.025
46	23	36	0.0005	0.0272	0.0000	1.000
47	25	37	0.0006	0.0232	0.0000	1.025
48	29	38	0.0008	0.0156	0.0000	1.025

Dynamic Data

The dynamic data are classified as:

- Generator Dynamic Data
- Exciter Data
- Governor Data

Generator Dynamic Data

Table A.5 represents the generator dynamic data. The nomenclature for the table headings is:

$X_d, X_d^{'}$ Generator direct-axis synchronous and transient reactance, in p.u.;

$X_q, X_q^{'}$ Generator quadrature-axis synchronous and transient reactance, in p.u.;

R_a Generator armature resistance, in p.u.;

$T_d^{'}, T_q^{'}$ Direct and quadrature axis transient field winding time constants;

H Generator inertia constant;

K_D Damping coefficient;

Table A.5: IEEE 39-bus Test System: Generator Dynamic Data

Gen	30	31	32	33	34	35	36	37	38	39
X_d	1.8200	0.9050	0.8650	0.8650	2.0700	0.8650	0.9308	0.9308	1.2356	1.9500
X_d'	0.3420	0.4370	0.2740	0.2740	0.2800	0.2740	0.3503	0.3503	0.2290	0.3400
X_q	1.7910	0.6300	0.5800	0.5800	1.9900	0.5800	0.6706	0.6706	1.2221	1.8700
X_q'	0.5500	0.4400	0.2120	0.2120	0.4900	0.2120	0.2652	0.2652	0.3630	0.4275
R_a	0.0015	0.0068	0.0113	0.0113	0.0046	0.0113	0.0024	0.0024	0.0013	0.0020
T_d'	5.30	6.00	7.40	7.40	4.10	7.40	8.00	8.00	4.55	8.00
T_q'	1.500	0.067	0.050	0.050	0.560	0.050	0.040	0.040	0.480	1.500
H	3.5452	3.8554	3.1617	3.1617	2.3186	3.1617	3.0317	3.0317	3.5031	5.3906
K_D	0.0	0.0	0.0	0.0	0.0	0.0	0.0	0.0	0.0	0.0

Exciter Data

Table A.6 represents the exciter data. The nomenclature for the table headings is:

K_A Amplifier gain, in per unit

T_A Amplifier time constant, in second

T_E Exciter time constant, in second

K_F Regulator gain, in per unit

T_F Regulator time constant, in second

A_{EX}, B_{EX} Derived saturation constants for rotating exciters

V_{Rmax} Regulator maximum output, in per unit

V_{Rmin} Regulator minimum output, in per unit

E_{fdmax} Maximum field voltage, in per unit

E_{fdmin} Minimum field voltage, in per unit

Table A.6: IEEE 39-bus Test System: Exciter Data

Gen	30	31	32	33	34	35	36	37	38	39
K_A	40	19.5768	15.5969	40	20	40	25	25	30	8.5
T_A	0.03	0.0166	0.0487	0.05	0.03	0.05	0.02	0.02	0.01	0.05

The following exciter parameter values were common for all the generators:

T_E 0.36

K_F 0.12

T_F	0.36
A_{EX}	0.0056
B_{EX}	1.07
V_{Rmax}	8.0
V_{Rmin}	-8.0
E_{fdmax}	8.85
E_{fdmin}	-8.85

Governor Data

Table A.7 represents the governor data. The nomenclature for the table headings is:

R	Trubine droop setting, in %
T_G	Governor time constant, in second

Table A.7: IEEE 39-bus Test System: Governor Data

Gen	30	31	32	33	34	35	36	37	38	39
R	3.5452	3.8554	3.1617	3.1617	2.3186	3.1617	3.0317	3.0317	3.5031	5.3906
T_G	1.8200	6.6667	5.0000	5.0000	20.000	5.0000	2.0000	2.0000	10.000	25.000

Appendix C

Controller Matrices

1. Controller for two-area four machine system

$$A_k = \begin{bmatrix} -114.6 & 199.7 & -144.5 & -85.12 & 294.8 & -193.2 & 62.88 & 6.113 \\ -7.9 & 3.737 & -2.578 & 1.12 & -0.848 & 2.927 & -5.6 & 0.2506 \\ 37.18 & -62.91 & 47.48 & 34.54 & -97.03 & 62.48 & -20.6 & -1.669 \\ 119.1 & -204.9 & 147.9 & 70.58 & -320.7 & 211 & -67.1 & -4.421 \\ 36.12 & -51.07 & 39.38 & 23.54 & -91.13 & 52.67 & -16.88 & -1.277 \\ 14.38 & -13.61 & 11.49 & 10.46 & -39.5 & 4.565 & -4.613 & -0.4484 \\ 11.27 & -22.18 & 16.77 & 7.987 & -32.31 & 23.76 & -7.22 & -0.00938 \\ 15.04 & -23.27 & 16.11 & 12.14 & -31.57 & 24.62 & -18.28 & -1.834 \end{bmatrix}$$

$$B_k = \begin{bmatrix} -0.017 & -0.0019 & 0.0025 & -0.00058 & -0.00041 & -0.0004 & 0.00072 & 0.0125 \end{bmatrix}^T$$

$$C_k = \begin{bmatrix} 709.1 & -1347 & 1027 & 493.6 & -2024 & 1408 & -440 & -28.3 \\ -795 & 1057 & -828 & -535.1 & 1933 & -863 & 350.4 & 28.85 \end{bmatrix}$$

$$D_k = \begin{bmatrix} 0 & 0 \end{bmatrix}^T$$

2. Controller C1 for IEEE 39-bus 10-machine system

$$A_k = \begin{bmatrix} -469.5 & 1706 & -393.6 & -1144 & 291.7 & 560.4 & -317.2 & 833.2 & -581.6 & 375.2 \\ 1718 & -6608 & 1572 & 4432 & -1151 & -2308 & 1054 & -3294 & 2030 & -1480 \\ -66.75 & 299.4 & -79.55 & -207.1 & 51.76 & 110.9 & -30.31 & 152.2 & -60.2 & 69.01 \\ 1011 & -3905 & 939.1 & 2618 & -679.3 & -1364 & 609.2 & -1949 & 1181 & -875.9 \\ 413.8 & -1551 & 356.2 & 1040 & -277.2 & -345.9 & -562.5 & 257.2 & -777 & 515.9 \\ 49.61 & -213.4 & 52.89 & 140.6 & -35.11 & -90.7 & 18.92 & -111.9 & 55.44 & -49.99 \\ -807.6 & 3096 & -737.7 & -2074 & 540.5 & 1084 & -496.8 & 1543 & -950.9 & 693.3 \\ -364.1 & 1361 & -326.8 & -915.4 & 235.3 & 456.2 & -240.7 & 660.2 & -429.1 & 302.6 \\ 444.7 & -1713 & 410.1 & 1149 & -298 & -596.5 & 270.6 & -852.8 & 518.5 & -386.3 \\ -394.8 & 1470 & -344.8 & -987.6 & 253.4 & 497.6 & -254.8 & 726.6 & -472.7 & 326.6 \end{bmatrix}$$

$$B_k = \begin{bmatrix} 780.3 & -3038 & 139.7 & -1797 & -709.3 & -97.88 & 1424 & 627.1 & -788.4 & 675.3 \\ -784.6 & 3034 & -135.7 & 1792 & 713.6 & 97.18 & -1421 & -625.6 & 786.1 & -676.6 \end{bmatrix}^T$$

$$C_k = \begin{bmatrix} -1.003 & 0.00168 & -0.582 & 0.066 & 2.029 & 0.675 & -2.75 & -2.91 & -2.004 & 0.0437 \\ 5.284 & 0.6428 & -1.925 & 1.271 & 1.878 & 8.257 & 11.77 & 3.903 & 12.01 & 3.222 \\ -4.026 & -1.235 & -1.208 & -0.459 & -2.822 & -15.7 & -8.399 & -7.47 & -1.966 & -0.6502 \end{bmatrix}$$

$$D_k = \begin{bmatrix} 0 & 0 \\ 0 & 0 \\ 0 & 0 \end{bmatrix}$$

3. Controller C2 for IEEE 39-bus 10-machine system

$$A_k = \begin{bmatrix} 1.685 & -6.808 & 0.288 & -0.1698 & 0.898 & 5.446 & 2.026 & 0.1445 & 4.474 & 0.205 \\ 17.33 & -29.99 & 11.77 & 9.567 & -2.453 & 0.785 & -23.84 & 20.41 & 74.36 & 5.342 \\ -17.24 & 20.83 & -4.697 & -4.033 & -8.404 & -39.45 & -11.23 & -12.98 & -65.3 & -6.11 \\ 32.51 & -25.05 & 20.42 & -16.91 & -2.766 & 36.98 & 19.3 & 20.07 & 108.1 & -75.96 \\ -36.88 & 23.3 & 0.4285 & 25.64 & -9.925 & -66.67 & -35.53 & -17.78 & -103.4 & 15.59 \\ 7.221 & -18.29 & 8.65 & 5.873 & -5.233 & -13.64 & -21.54 & 11.24 & 47.35 & -9.237 \\ -1.95 & 0.8974 & 1.89 & 2.77 & -4.436 & -12.86 & -10.42 & 14.52 & 2.344 & 3.136 \\ 9.452 & -14.68 & 3.563 & -1.311 & -1.232 & 4.18 & -12.76 & 2.376 & -35.23 & 2.236 \\ -7.892 & 8.274 & -1.233 & 2.465 & -0.234 & -10.4 & -3.201 & -4.992 & 54.11 & -36.13 \\ 2.759 & -3.143 & 0.6265 & -0.733 & -0.567 & 2.957 & 0.515 & 1.902 & -2.457 & 6.296 \end{bmatrix}$$

$$B_k = \begin{bmatrix} -0.034 & -0.381 & 0.322 & -0.1316 & 0.0939 & -0.1637 & 0.008 & 0.093 & -0.0787 & -0.0242 \end{bmatrix}^T$$

$$C_k = \begin{bmatrix} -17.19 & 50.23 & 21.71 & 19.08 & -22.28 & -117.7 & -88.11 & 85.54 & 89.39 & -23.45 \\ -107.1 & -7.46 & 103.5 & -24.17 & 39.83 & 65.3 & -41.02 & 33.07 & -389.5 & 80.06 \\ -134.1 & 38.89 & 30.6 & 120.1 & -74.01 & -288.8 & -263.3 & -14.04 & -294.5 & 61.88 \end{bmatrix}$$

$$D_k = \begin{bmatrix} 0 \\ 0 \\ 0 \end{bmatrix}$$